analytical chemistry

Review

pubs.acs.org/ac

Atomic Spectroscopy

Nicolas H. Bings,*[,†] Annemie Bogaerts,[‡] and José A. C. Broekaert[§]

[†]Institute of Inorganic and Analytical Chemistry, Johannes Gutenberg-University Mainz, Duesbergweg 10-14, 55128 Mainz, Germany

[‡]Department of Chemistry, University of Antwerp, Universiteitsplein 1, B-2610 Wilrijk-Antwerp, Belgium

[§]Institute of Inorganic and Applied Chemistry, University of Hamburg, Martin-Luther-King-Platz 6, 20146 Hamburg, Germany

CONTENTS

Atomic Absorption Spectrometry 670
- Flame Atomic Absorption Spectrometry 670
- Graphite Furnace Atomic Absorption Spectrometry 671
- Direct Solids Sampling Atomic Absorption Spectrometry 671
- Vapor Generation Atomic Absorption Spectrometry 671
- Continuum Source Atomic Absorption Spectrometry 672

Atomic Fluorescence Spectrometry 672
Atomic Emission Spectrometry 673
- Arcs and Special Sources 673
- Inductively Coupled Plasmas 673
- Microwave Induced Plasmas 675
- Microplasmas 675

Laser Induced Breakdown Spectrometry 676
- Fundamental Studies 676
- Applications 677
- Outlook 677

Glow Discharge Optical Emission and Mass Spectrometry 678
- Fundamental Studies 678
- Methodological Studies and Applications of GD-OES and GDMS 680
- New GD Sources for Novel Applications and Combined GD-LA Systems 683

Inductively Coupled Plasma Mass Spectrometry 686
- Fundamental Studies 687
- Instrumental Developments and Applications 689
  - Elemental Speciation, Analysis of Biological Samples and Nanomaterials 689
  - Laser Ablation for Direct Solid Sampling 692
  - Collision and Reaction Cells 696
  - Time-of-Flight Instruments 697
  - High Resolution and Multicollector Instruments 697

Author Information 698
- Corresponding Author 698
- Notes 698
- Biographies 698

References 699

In the field of atomic spectrometry, innovation in atomic absorption, atomic emission, atomic fluorescence and atomic mass spectrometry especially was communicated in the journals *Analytical Chemistry*, *Analytical and Bioanalytical Chemistry*, *Analytica Chimica Acta*, *Analytical Sciences*, *Applied Spectroscopy*, *International Journal of Environmental Analytical Chemistry*, *Journal of Analytical Atomic Spectrometry*, *Journal of Environmental Monitoring*, *Microchemical Journal*, *Microchimica Acta*, and *Spectrochimica Acta, Part B*. Except otherwise stated in the respective subsections, further journals were not considered in this review, in which especially the trends in the method development are emphasized. As in the former issues of this review series,[1−5] an always somewhat arbitrary choice had to be made, which was done in view of citing work from the prominent groups working in the field and in view of illustrating the trends discussed. Apart from the journals to be considered it should be mentioned that prominent meetings in the field of atomic spectrometry took place during the period considered, which extended from January 2010 to June 2012. Here especially the Winter Conferences in 2010 in Fort Myers (U.S.), in 2011 in Zaragoza (Spain), and in 2012 in Tucson (U.S.) as well as the XXXVII Colloquium Spectroscopicum Internationale in Buzios (Brazil), the yearly PittCon and FACSS meetings and meetings like the 2012 International Symposium on Environmental Analytical Chemistry in Antwerp (Belgium), the Euro-Mediterranean Symposium on Laser Induced Spectroscopy (EMSLIBS) which in 2011 took place in Çeşme-Izmir (Turkey), and the European Symposium on Atomic Spectrometry (ESAS), of which the 2010 meeting was held in Wroclaw (Poland), have also to be mentioned.

Topics of general interest in atomic spectrometry deal with all parts of the spectrometric system from the sources over the types of spectrometers to the detectors used as well as with topics like optimization and calibration. A compact wide-range spectrometer with an image intensifier was described which may be of great use for work with many types of sources for diagnostic as well as for analytical purposes, e.g., ref 6. Further methodology for sample introduction, which is of use for all types of atomic spectrometries and sources dealing with liquids, such as thermal inkjet-based aerosol generation for microvolume sample introduction in atomic spectrometry is to be mentioned here.[7] The topic of calibration needs especially to include considerations on the error on the calibration itself as discussed in a tutorial review by Mermet.[8]

ATOMIC ABSORPTION SPECTROMETRY

Flame Atomic Absorption Spectrometry. In flame atomic absorption research certainly centered on the use of commercial equipment for problem-solving work. Some methodological work nevertheless was reported. Porenta et al.[9] reported on the use of a nitrogen plasma as an atom reservoir

Special Issue: Fundamental and Applied Reviews in Analytical Chemistry 2013

Published: November 7, 2012

   dx.doi.org/10.1021/ac3031459 | *Anal. Chem.* 2013, 85, 670−704

for the determination of Cu and obtained a detection limit of 0.25 μg mL^{-1}. Most work centered on the combination of suitable online preconcentration methods with FAAS to obtain the detection limits and accuracy required in a number of application areas. Exemplarily, liquid-phase microextraction[10] here has to be mentioned as well as approaches such as the use of liquid carbon dioxide. With the latter preconcentration of copper 8-hydroxyquinoline complex in a C18 mini column by a factor of 24 could be realized.[11] Also generally known ion-exchange column separation can be tailored for suitable combinations with FAAS, which especially is of use for water analysis.[12] For trace levels thermospray flame furnace approaches, known since longer still can be optimized and allow determinations of ng amounts of Cd, e.g., in collected cigarette smoke samples.[13] The online sample preconcentration methods also are of use for speciation work, as it was shown at the example of chromium speciation by combining cloud point extraction after a complexation of Cr(III) with DDTC and with Triton X-100 as extractand.[14]

Graphite Furnace Atomic Absorption Spectrometry. In graphite furnace atomic absorption spectrometry, theoretical considerations further dealt with the thermochemical processes occurring in the atom reservoir. Here Lvov[15] published an interesting treaty on the mechanism of congruent dissociative vaporization of a solid with simultaneous condensation of the supersaturated vapor of low-volatility products, which may be relevant for the processes in an analytical graphite furnace. Katskov and Darangwa[16] described simulations of the transient sample vapor composition and release rate during electrothermal vaporization and in a second part of their work verified the models developed with investigations on the atomization of Ag and Cu.[17] Donati and Jones[18] investigated atomic cloud generation in a tungsten coil atomizer being of use as an absorption reservoir but also as an emission source. In the case of the use of platforms, research also was done on the species deposited on graphite and on tungsten in the case of Be and the presence of Al or Si matrixes.[19]

Also in graphite furnace AAS, much work was done on online preconcentration. Liquid-phase microextraction was proposed by several groups. It was used successfully for the determination of Hg in tap water.[20] Another work on the preconcentration in a single microdroplet by liquid−liquid extraction after complexation dealt with Cu.[21] The features of electrochemical deposition on a gold-coated porous carbon electrode were shown for the determination of traces of As with a detection limit down to 0.004 μg mL^{-1}.[22] Such preconcentration principles also were applied in the case of a flame furnace, as shown for Pb.[23]

A further field of methodological work in graphite furnace AAS is the use of matrix modifiers. Pd salts also with a second component such as Fe were shown to be of use for the determination of Cd and attempts were made to explain the influence of variations of the ratio of Pd to Fe on the Cd signals.[24] For the determination of Si, the use of methane/argon mixtures as a gaseous modifier were shown to improve the signals shape for the Si and enabled it to obtain a detection limit of 0.2 μg L^{-1}.[25] Further, the use of Au nanoparticles as an effective modifier for the determination of As and Sb by graphite furnace AAS was described.[26]

The use of W furnaces for electrothermal atomization remains a topic of research. When combined with online preenrichment,[27] a detection limit of 4 ng mL^{-1} for Pb can be obtained. With solid-phase extraction and metal furnace atomization, Cr(II) and Cr(VI) in river water can be determined down to the 10 pg level.[28]

Direct Solids Sampling Atomic Absorption Spectrometry. A further feature of graphite furnace atomization is the ease for direct solids sampling. Exemplarily, the determination of Cr, Cu, Fe, K, Mn, Sb, and Zn in powdered aluminum nitride down to 0.05 (Zn) and 80 ng g^{-1} for Fe has been described.[29] For these types of refractory matrixes, the use of modifiers also may be useful, as shown in the examples of the determination of Cr and Mn in alumina by slurry nebulization under the use of NbC and NaF as the modifier.[30] Other applications of slurry sampling under the use of modifiers were the determination of Sn in marine sediments under the use of Ir/W/Nb mixtures as a permanent modifier[31] and the determination of Zn in marine sediments under the use of Pd/Mg mixtures as a permanent modifier and slurry sampling.[32] For the aim of matrix modification also, electrodeposition on a platform can be successful. This was shown in the example of the electrodeposition of Pd and an Ir/Au mixture on graphite platforms for the determination of Hg in environmental samples, such as soils, sediments, and plants by direct solids sampling graphite furnace AAS.[33]

Vapor Generation Atomic Absorption Spectrometry. As advantages for this approach, the complete isolation of the analytes from the sample matrix and the increased sampling efficiency especially as compared to nebulization in the case of liquid samples are well-known. For this approach, innovation especially lies in the better understanding of the mechanisms for these techniques but also in the extension of the applicability of these techniques to more and more elements by the use of appropriate chemical reactions.

The mechanism of hydrogen transfer in arsane generation by solutions of tetrahydridoborate, as studied with gas chromatography mass spectrometry under the investigation of isotopic distributions, informed on the role of nanoparticles and colloids arising from the interaction of metals and the tetrahydridoborate−As complex as well as its deuterated analogue.[34] The role of spectral interferences of oxygen and water molecules in hydride generation atomic absorption spectrometry with quartz atomizers in the case of the determination of As and Se showed that for the lines As 193.7 nm and Se 196.0 nm, limitations of the power of detection may occur, which can be decreased by optimizing the atomizer temperature and the carrier-gas flows.[35]

UV photochemical generation of a volatile molecular Cd species from an acetic acid medium could be realized under the use of a thin film generator comprising a 20 W low pressure UV source and Cd determinations could be realized with a quartz tube atomizer brought at 900 C, provided a 10% hydrogen/argon mixture was used as the transport gas.[36] For the case of Au, one was successful in obtaining volatile species through the use of a special mixing apparatus and a gas−liquid separator design in the presence of surfactants (Triton X-100, Antifoam B) and diethyldithiocarbamate. At a carrier gas flow of 600 mL min^{-1}, a detection limit of 17 ng mL^{-1} was obtained in the case of a quartz tube atomizer and transmission electron microscopy could prove the presence of Au nanoparticles with a diameter of approximately 10 nm and smaller transported to the atomizer.[37] A similar approach could be used for chemical vapor generation in the case of Ag, and here a detection limit of 1 ng mL^{-1} for Ag could be obtained. With the aid of the ^{111}Ag radioactive indicator, the transport efficiency could be optimized.[38] For the case of Cu thin film, hydride generation was proposed as a new approach. Here, a single device integrated the functions of the hydride generator and gas liquid separator, and a graphite furnace was used as an atomizer. Solutions of the sample containing 0.0005% (m/v) phenanthroline and 1% formic acid were merged with

dx.doi.org/10.1021/ac3031459 | Anal. Chem. 2013, 85, 670−704

tetrahydroborate reductant to yield a thin film wetting a reaction surface from which product vapor was efficiently liberated and transported into the heated furnace, resulting in a detection limit of 100 pg mL^{-1} for Cu.[39] For the case of Co, volatile species can be generated when a buffer system of formic acid and formiate containing Co(II) is exposed to UV radiation and a detection limit of 0.08 ng mL^{-1} in the case of atomic fluorescence detection was reported.[40] Hydride generation can directly be combined with direct extraction from solids as shown in the case of sediments. Here As and Sb could be extracted with deionized water, phosphate buffer (pH = 6) and hydrochloric acid (2 mol L^{-1}) as extractants and directly analyzed for As and Se by chemical hydride generation AAS and a differentiation between the water leachable, exchangeable and acid leachable fractions can be made.[41]

Vapor generation AAS becomes very sensitive when combined to preenrichment methods and then can be used species sensitive. Here trapping methods were shown to be very useful. Indeed for Te hydride trapping on a platinum-coated tungsten coil could be successfully applied.[42] The potential of online coupled hydride generation AAS was also shown for the case of As preconcentration via solid phase extraction and speciation by HPLC-gradient hydride generation AAS.[43]

Continuum Source Atomic Absorption Spectrometry. The number of applications of continuum source atomic absorption spectrometry since the commercial availability of instrumentation constantly increases. The easy background correction through the availability of the complete direct spectral environment of the analytical lines and the wide range of lines and molecular bands that can be selected not only for atomic but also for molecular absorption measurements here open new ways.

For direct determinations of metals in biodiesel, where the spectral background may be structured, the approach is very useful and the detection limits for Al, Cu, Fe, and Mn in the case of graphite furnace atomization were at the ng g^{-1} level.[44] As an interesting topic, the use of atomizers with a small diameter and internal volume was investigated. It was found that all radiation of the xenon arc lamp in the case of 2 mm instead of 5.8 mm diameters for the graphite tube still could be used and that the smaller internal volume which resulted hereof leads to improvements in sensitivity of a factor of 6 to 12.[45]

Much work was done on the determination of nonmetals through the use of molecular absorption measured at the band spectra, which became feasible through the high spectral resolution which is indispensable to isolate the analytical wavelengths in the case of a continuum primary radiation source. For the case of P, the PO band and the nonresonant P line at 213.6 nm, which is interfered by NO and PO bands, can be used. Here Zeeman background correction in the case of line sources as well as continuum sources is effective but remains limited in dynamic range.[46] The molecular absorption of NO can also be used for the determination of nitrate, when using an air−acetylene flame and high-resolution continuum source AAS. However, it was found that hydrochloric, sulfuric, and phosphoric acids as well as metal salts, which can form acids by hydrolysis, such as Al, Cr, Cu, Fe, and Mn, show strong effects and reduce the NO absorption. When minimizing this, a detection limit of 5 ng N can be obtained.[47] F can be determined via the GaF molecular band absorption, as shown by the quantification of fluorine containing drug 5-fluorouracil (5-FU) in cancer cells by molecular absorption high-resolution continuum source molecular absorption spectrometry. Here a detection limit of 0.23 ng of 5-FU could be obtained by graphite furnace atomization.[48] For the case of S, where there is a high need to determine the element in petroleum products, it could be shown both in flame and furnace atomization that the CS molecular bands at 258.056 nm allows determinations with a detection limit of 18 mg kg^{-1} in flame and 12 ng in furnace AAS. In the case of the furnace method, a Pd + Mg modifier was used.[49] In the case of the determination of Al in blood, the use of molecular absorption of the AlF band was found to solve a number of difficulties through matrix effects encountered in working with the Al line absorption. With platform atomization, a detection limit of 1.8 μg L^{-1} was realized (see signals in Figure 1).[50]

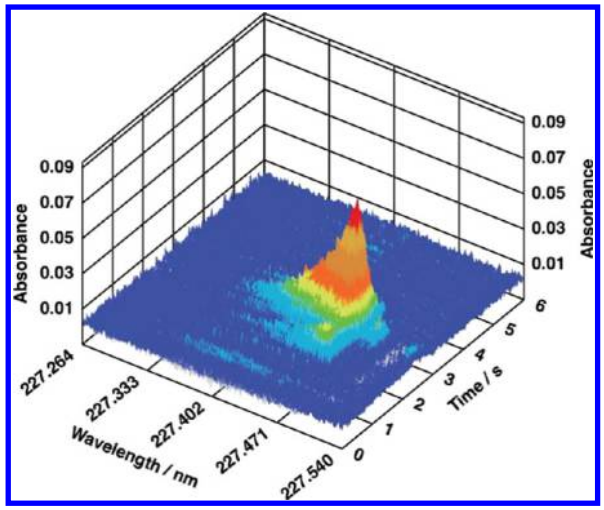

Figure 1. 3D Time and wavelength resolved absorbance spectrum for 10 μL of a 50 ng mL^{-1} Al standard solution + 10 μL of a 5% $NH_4F{\cdot}HF$ fluorinating solution. Reprinted with permission from ref 50. Copyright 2011 The Royal Society of Chemistry.

Because of the good possibilities for background correction, high-resolution continuum source graphite furnace AAS is especially suited for direct solids sampling, where the risks for higher and more structured background absorption through noncomplete atomization of the matrix are higher than in work with solutions. This was shown at the example of the monitoring for Pd in airborne dust particulates of the PM 2.5 fractions of urban aerosols. Here a detection limit of 0.07 pg m^{-3} was obtained.[51] For the case of Hg in airborne particulate matter collected on glass fiber filters with direct solids sampling, a detection limit of 0.12 ng m^{-3} could be obtained for an air volume of 1440 m^3 collected within 24 h.[52]

The possibility of truly simultaneous determination of several elements remains limited with the instrumentation available as the spectral window available during one shot remains limited because of the necessity of working at high resolution. In a number of cases, however, simultaneous determinations are possible. This was shown in the example of the simultaneous determination of Cd and Fe in sewage sludge under the application of slurry sampling. Here the Cd 228.802 nm line and the less sensitive Fe 228.725 nm line could be used as the concentration ratios for the two elements matched with the sensitivity ratios of the lines, where detection limits of 0.03 and 90 μg g^{-1} for Cd and Fe, respectively, were obtained.[53]

■ ATOMIC FLUORESCENCE SPECTROMETRY

For the trace and ultratrace determination of Hg, the cold-vapor technique is the method of choice and the detection with atomic

dx.doi.org/10.1021/ac3031459 | Anal. Chem. 2013, 85, 670−704

fluorescence spectrometry (AFS) because of spectral background interferences often the better choice over atomic absorption measurements. This also applies for elements with high excitation potentials brought in the gaseous phase through vapor generation methods, as it is the case for the volatile hydride forming elements. Because of the ecotoxicity of these elements, a considerable number of publications dealing with methodological innovation is still published.

For the determination of Hg in river water samples, online digestion of humic matter is essential. Through an automated flow injection based system, including irradiation of the sample with a UV lamp, the addition of 1% H_2O_2 and a nanogold collector for preconcentration of dissolved mercury species and AFS measurements subsequent to the release of Hg^0 detection limits of down to 0.14 ng Hg L^{-1} were obtained and the results for real samples could be validated through comparison with the results of a reference method.[54] Cold vapor techniques coupled to AFS now is a standard EPA method for the monitoring of Hg levels in the environment.[55] Improvements of the power of detection were described to be possible by online enrichment steps, such as preconcentration on a microcolumn coupled online with the cold vapor AFS system[56] or preenrichment of the Hg on a Au column followed by a release into the AFS unit. The latter approach could be very successfully applied for the determination of down to subμg L^{-1} concentrations of Hg in biodiesel.[57] It could be shown that in the case of chemical vapor generation AFS under the use of tetrahydroborate, both the inorganic and organic Hg is determined but that by the complexing with cysteine the sum of the monomethylmercury and ethylmercury species can be determined by microflame AFS.[58] Further speciation of Hg is easily possible by coupling separation of the species by HPLC using multi-isocratic elution with 2-mercaptoethanol ammonium acetate mixture and entering the effluent online in a cold-vapor AFS unit. In this way $MeHg^+$, Hg^{2+}, and $EtHg^+$ could be determined with detection limits of 0.03, 0.11, and 0.09 μg L^{-1}.[59] A similar system could be used for the determination of inorganic and organic Hg species in waste waters.[60] Similar determinations of the same Hg species in sewage sludge samples can be performed by HPLC coupled to the cold vapor technique and AFS subsequent to ultrasound assisted extraction.[61]

Apart from Hg, also volatile species forming elements can be determined very successfully with AFS. This is shown for the case of Se(IV) by the determination of Se by microextraction into an organic drop which is back-extracted under ultrasound-assistance.[62] The determination of Sb(V), Sb(III), and TMSb(V) in urine by HPLC coupled to AFS also was described.[63] Electrochemical hydride generation in the alkaline mode coupled to AFS has been described to be useful for the determination of As and Sb in the trivalent state in river water. The complete inorganic As and Sb can be determined after a prereduction step. The alkaline mode was found to be less prone to interferences as compared to working in acid solutions.[64] Continuous flow hydride generation coupled to laser induced atomic fluorescence was found to be useful for the determination of Pb in water and sediment samples. Here the lead hydride is generated in $K_3Fe(CN)_6$-HCl medium using $NaBH_4$ as the reducing agent. Laser excitation of Pb has been performed at 283.306 nm, and fluorescence has been measured at 365 and 405.8 nm.[65]

■ ATOMIC EMISSION SPECTROMETRY

Arcs and Special Sources. Conventional dc arc emission spectrometry for the direct analysis of refractory powders again becomes of interest due to its coupling with modern CCD-based spectrometers, as it has been shown for the simultaneous determination of Al, Ca, Cr, Cu, Fe, Mg, Mn, Na, Ni, Si, Ti, and Zr in boron carbide powders. Here the detection limits ranged from 0.2 (Mg) to 25 (Na) μg g^{-1}, and it was shown that many types of Al_2O_3, BN, SiC, coal fly ash, graphite, and obsidian rock can be analyzed with the same calibration curve. This testifies that the approach is as powerful and even easier than many advance direct solids method developed today.[66] For the oscillating dc arc with a continuous aerosol sample supply, the enhancements of emission line intensities by induced oscillations were studied and the role of the gas-phase atom-oxide bond energy in the entire enhancement effect underlined.[67] Further direct solids sampling in the analysis of animal organs by two-jet plasma atomic emission spectrometry was described.[68]

As a new source for atomic emission spectrometry, the theta-pinch imploding thin film plasma source has been described. The theta-pinch configuration has been used to generate a pulsed, high-energy-density cylindrical plasma at atmospheric pressure with energy from a 20 kV, 6.05 μF capacitive electrical discharge coupled inductively to a thin Al film. Spectra of Sb have been obtained from solid antimony oxide samples.[69] A further plasma studied is the helicon plasma, where a radio frequency driven helical antenna is placed around a dielectric cylinder but with a direct current axial magnetic field applied in the region of the plasma generation allowing the excitation of a helicon wave within the source of the plasma. Here measurements of line intensities emitted by plasma particles should inform on the plasma properties.[70]

Some smaller sources were studied as well. They included the tungsten coil in an Ar/H_2 atmosphere which could be used for the direct atomic emission spectrometric determination of Cr, Eu, and Sr but also for atomic absorption spectrometric determinations of Cu, Cd, and Sn in solutions down to the μg L^{-1} range.[71] Further an alternating current driven atmospheric-pressure liquid discharge for the determination of elements with optical emission spectrometry was described. Here the sample solution serves as one of the electrodes, and for Na and Cd the detection limits were 0.04 and 0.09 mg L^{-1}, respectively.[72]

Inductively Coupled Plasmas. The inductively coupled plasma (ICP) still is the subject of investigations on the plasma processes and their relevance for its spectrochemical properties. Lindner[73] in the group of Bogaerts in Antwerp performed simulation studies on plasma temperatures, flow velocities, and injector diameter effects and could well compare experimental data obtained in the group of Niemax in Germany with the outcome of the calculations, an example of which is shown in Figure 2. Taylor[74] in the group of Farnsworth made radially resolved argon metastable density measurements with the aid of combined diode laser and pulsed dye laser experiments. The increased knowledge on the excitation processes enabled it also to assess semiquantitative ICP-AES assuming simple partial LTE and the use of a single element calibration, as shown by Dettmann and Olesik.[75] Also it has been shown that in ICP-AES plasma-related matrix effects could be considerably lowered by measuring at the so-called crossover points.[76] The usefulness of internal standardization with the aim to improve the precision obtainable as well as to decrease matrix effects remained a further point of study for ICP-AES. Grotti et al.[77] studied the time correlation between emission line intensities using an axially viewed CCD-based ICP-AES system and found from the use of ultrasonic nebulization using desolvation that the sample introduc-

dx.doi.org/10.1021/ac3031459 | Anal. Chem. 2013, 85, 670−704

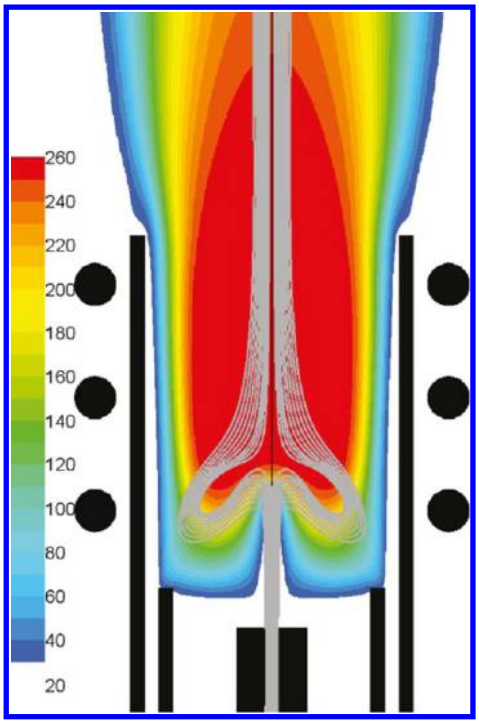

Figure 2. Path lines of the injector gas for a flow rate of 0.20 L min^{-1} displayed together with the viscosity. The viscosity is given in μPa s. Reprinted from ref 73. Copyright 2011 American Chemical Society.

tion system has to be considered so as to obtain flicker-noise limited signals. Reinsberg et al.[78] showed that with pooled regression and also with principal component regression the precision in the main components determination can be improved as well. Also online calibration by online standard addition using a new multinebulizer based on flow blurring technology could be used for the compensation of matrix effects in ICP-AES.[79]

The analytical performance of ICP-AES can be improved by optimizing the way of sample introduction, which since the early years of ICP work was a topic of intensive research.

Slurry nebulization remains an interesting possibility of ICP-AES, when it comes to the rapid analysis of materials in the powder form or in the slurry state without need for dissolution by wet chemical treatment. This is the case for sewage sludge analysis as shown by Baralkiewicz et al.[80] The approach is also useful to determine the concentration and the particle size distribution for powders of nanoparticles. As shown by Garcia et al.,[81] single Au and SiO_2 nano- and microparticles can be characterized by ICP-AES using monodisperse droplets of standard solutions for calibration. Single particle signal evaluation as well as a coupling of plasma spectrometry with field flow fractionation, as shown by Krystek et al.,[82] can be used for the analysis of engineered nanoparticles in suspensions and products. Further the use of ICP-AES with pneumatic nebulization remains an interesting method for determinations in organic media. Here the organic solvent load in the plasma remains a limiting factor and solutions like the use of air-segmented flow injection combined with a heated spray chamber have to be applied. Then, however, it was possible to minimize the matrix influences between alkanes, aromatic compounds, and petroleum products.[83] Also in biodiesel and vegetable oil, trace elements could be determined following alcohol dilution.[84] A special feature of the use of AES is the determination of isotopes like ^{233}U when a high-resolution atomic emission spectrometer is used.[85]

The online coupling of preenrichment with ICP-AES using pneumatic nebulization was applied with several aims and with several techniques. Speciation of Cr(III) and Cr(VI) in the case of solid phase extraction on a column[86] here is mentioned as an example. Another example is the study of the binding of Zn and albumin using capillary electrophoresis and ICP-AES.[87] Field flow fractionation coupled to ICP-AES can be used in the case of soil analysis so as to accomplish matrix removal.[88] Also ultrasonic nebulization remains a further way especially to improve the power of detection. By using flow injection solid phase extraction with carbon nanotubes as substrates and ultrasonic nebulization, Cd could be determined in solid environmental samples.[89] In ultrasonic nebulization, it was shown that the desolvation system with reasonable success could be replaced by a pre-evaporation tube.[90]

The formation of volatile analyte compounds by chemical reactions just as in AAS is applied in ICP-AES. Here the hydride generation through the use of suitable nebulizer concepts can be performed simultaneously with conventional pneumatic nebulization and then both for elements that are known for their formation of volatile hydrides as well as for a number of transition metal improvements of the detection limits could be obtained.[91] Even for Sc, volatile species could be formed and preconcentrated on a column using the sodium tetrahydridoborate reaction.[92] Special techniques like UV-assisted vapor generation could be applied here as in AAS for the case of Fe[93] and for the case of Hg.[94] In the case of Sb(III), a volatilization as bromide could be applied and it was found that the presence of iodide stimulated the reaction.[95] A special way of sample volatilization certainly is the use of a solution glow discharge as it is discussed later-on.[96]

Thermal methods are also very helpful so as to increase the power of detection in ICP-AES. An innovative approach is the use of a microwave cavity combined with desolvation, by which the detection limits versus pneumatic nebulization could be improved by a factor of up to 50.[97] Further, known approaches like tungsten coil vaporization were used for the determination of the total carbon in soft drinks,[98] and Cd was determined in zinc-base metal by an improved double chamber electrothermal vaporization coupled to ICP-AES.[99] Electrothermal vaporization using slurry sampling in ICP-AES could be used for the direct determination of trace metals in boron carbide powders,[100] and in high-purity copper samples trace elements could directly be determined in the solid samples by electrothermal evaporation using halocarbons as volatilization aids.[101]

Spark and laser ablation both in ICP-AES just as in ICPMS are favorite techniques for direct solids sampling in the case of compact solid samples. The influence of laser−particle interaction in the laser plasma on the ablation both in the case of laser induced breakdown spectrometry and in the case of the excitation of the laser produced aerosol in ICP-AES was studied.[102] Ablation with an infrared laser could be successfully applied for accurate direct analyses in copper using synthetic copper standards.[103] An interesting application of laser ablation ICP-AES is the direct determination of Pd, Pt, and Rh in fire assay lead buttons obtained in automotive exhaust catalysts as an example.[104] Another interesting possibility of laser ablation ICP-AES is its use for the determination of Cd, Cr, and Cu in salt samples after their preconcentration by electrodeposition.[105] For direct solids sampling in ICP-AES, the use of powder dispersion in an air flow for geological applications remains a challenge.[106]

dx.doi.org/10.1021/ac3031459 | *Anal. Chem.* 2013, 85, 670−704

Microwave Induced Plasmas. Microwave discharges got a renewed interest as spectrochemical radiation sources, also because a low cost air-based microwave plasma spectrometer now is commercially available. An interesting development also is the use of acoustic, radiofrequency, and microwave rotating fields in producing analytical plasma sources. In the case of He discharges, plasmas which can take up wet aerosols well could be obtained. They have excitation temperatures of 2800−4000 K and rotational temperatures of 1100−3200 K, and also the halogens could be determined down to the trace level.[107] For microwave plasmas, a number of diagnostic studies further were performed. Simon et al.[108] determined temperatures and electron number densities in an atmospheric pressure argon−helium radiofrequency capacitively coupled plasma operated at 5−70 W. Muñoz and Calzada studied the equilibrium deviations in atmospheric pressure argon/helium surface wave discharges,[109] and Palomares et al.[110] used Thomson scattering to determine axial profiles of the electron temperature and electron number density in argon surfatron plasmas operated at pressures of 6−20 mbar and at a power between 32 and 82 W.

A special field of research is the combination of the cheap and easy to operate microwave plasmas with suitable ways of sample introduction so as to be able to make full use of their analytical capabilities. Jiménez et al.[111] described a lateral sample introduction system for gas-phase sample introduction into microwave plasmas. Pohl and Jamroz[112] in a review reported on recent advances of hydride generation and other volatile species generation for transition metals combined to microwave induced plasmas with atomic emission spectrometry (MIP-AES), and Matusiewicz and Ślachciński[113] reported on arsenic speciation by microchip capillary electrophoresis coupled to MIP-AES, where detection limits of 3.9 ng mL^{-1} and 5.4 ng mL^{-1} for As(III) and As(V), respectively, were obtained. The approach of multielement determinations of transition and noble metals (Au, Ag, Pd, Pt, Rh) as volatile species by MIP-AES also was studied in the case of a triple-mode microflow ultrasonic nebulizer and in situ chemical vapor generation.[114] Further, the online preconcentration and separation of inorganic As and Sb by poly(aryl ether ketone) containing pendant carboxyl groups and MIP-AES was studied.[115] The Ar radiofrequency capacitively coupled plasma operated at 275 W also was shown at the example of Zn to be a useful atom reservoir for atomic fluorescence spectrometry and in the case of an electrodeless discharge lamp as primary source detection limits of 8 $\mu g\ L^{-1}$ were obtained.[116] Microwave plasmas also successfully have been used for cavity ring-down spectroscopy with a tunable diode laser for the detection of fluorine at the trace level.[117]

Microplasmas. Microplasmas have become an actual topic of interest for research in spectrochemical analysis, and many groups contributed to this field in the last years. Both applies to the description and diagnostics of new sources as well as to the combination of these sources with suitable ways of sampling so as to come to cheap and powerful systems for analytical purposes.

Dielectric barrier discharges form a group of sources with a small size, low gas temperature, atmospheric operation, and excellent dissociation capability. It was shown that they well can be combined with hydride generation and are useful for the determination of As and Sb by atomic fluorescence, with detection limits of 0.04 and 0.05 $\mu g\ L^{-1}$, respectively.[118] The same principle was applied for the determination of thiomersal in vaccines. The analyte here is degraded to inorganic Hg which is reduced with the aid of tetrahydroborate or tin(II)chloride to generate Hg vapor. Here detection limits of 0.06 $\mu g\ L^{-1}$ thiomersal in solution were reported.[119] When used as a source for AES, one also can determine ultratraces of N_2 in high-purity Ar with a detection limit of 34 ppb.[120] A miniaturized liquid electrode dielectric barrier discharge also can be used for elemental determinations by atomic emission spectrometry in liquid samples, which are fed into the discharge at a flow rate of 20 $\mu L\ min^{-1}$ provided 1 mol L^{-1} of HNO_3 is provided in the sample liquid, which also forms the cathode. Detection limits ranging from 0.02 mg L^{-1} for K to 6.9 mg L^{-1} for Ba were reported.[121] Instead of using a liquid as the electrode, one also can have it run over an electrode. When using a W wire electrode, a Cu counter electrode and the sample solution running over a glass plate between the electrode with an ac-high voltage of 3.7 kV at 30 kHz a plasma can be formed, and detection limits in the liquid in the case of AES range from 7 $\mu g\ L^{-1}$ for Na to 79 $\mu g\ L^{-1}$ for Zn and the method is suitable for work with microsamples.[122] It was shown that a dielectric-barrier-discharge-based "sniffer" also can be used in the molecular emission mode for the differentiation of classes of organic compounds such as alkanes, aromatics, oxygenates, chlorinated, and nitrogen-containing organic compounds.[123]

Among other types of microplasmas described, the use of a plasma pencil, reported by Novosád et al.,[124] is to be mentioned. It is a radiofrequency capacitively coupled plasma jet running under atmospheric pressure in Ar, He, N_2, H_2, SF_6, and other gases, and its operation is possible in the frequency range from dc to HF. At a forward power of 140 W, aqueous solution-based aerosols can be incorporated into the plasma without desolvation and detection limits of 27 (Ca), 49 (Cu), 58 (Mg), 40 (Li), 13 (Na) and 180 (Zn) $\mu g\ L^{-1}$ are obtained. Weagant et al.[125] reported on a battery-operated argon−hydrogen microplasma on hybrid, postage stamp-sized plastic-quartz chips for elemental analysis of liquid microsamples using a portable optical emission spectrometer. Here a miniaturized electrothermal vaporization device (40 W maximum power) is used, and K in water could be accurately determined at the 4 $\mu g\ L^{-1}$ level. With the miniaturized microwave induced plasma inside a quartz plate, as shown in Figure 3, element-specific detection of Cl and Br in the case of a discharge in He could be performed in the effluent of a gas chromatograph and the absolute detection limits for volatile

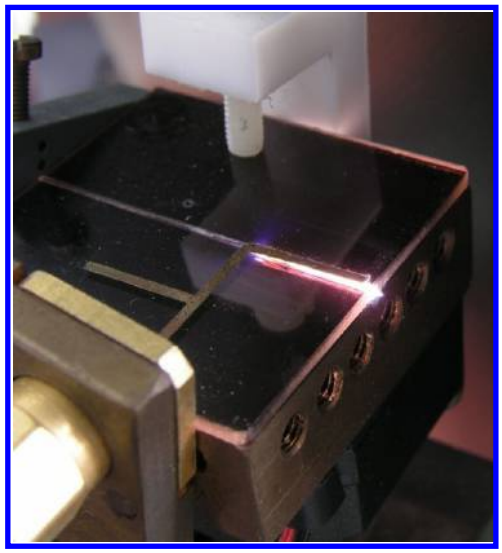

Figure 3. Microplasma used for element-specific detection in gas chromatography, as described in ref 126.

dx.doi.org/10.1021/ac3031459 | *Anal. Chem.* 2013, 85, 670−704

halogenated compounds were found to be in the ng range when using a miniaturized CCD-based emission spectrometer.[126] Further, the use of a low power capacitively coupled plasma microtorch for simultaneous elemental determinations by atomic emission using microspectrometers has been described by Frentiu et al.[127] Here an Ar plasma with a power of 30 W at 13.56 MHz is used, and for liquid samples without desolvation detection limits of 3 ng mL^{-1} (Li) and 1.5 μg mL^{-1} (Mn) were reported. Tung et al.[128] described a sensing technique of Ag nanoparticles as labels for an immunoassay using liquid electrode plasma atomic emission spectrometry without using a plasma gas. Human chorionic gonadotropin was used as a model target protein, and the immunoreaction in which it is sandwiched between two antibodies, one of which is immobilized on the microwell and the second is labeled with Ag nanoparticles, was performed. The protein could be determined down to the pg mL^{-1} level. From the same group, the highly sensitive determination of Cd and Pb by liquid electrode plasma atomic emission spectrometry with a quartz glass chip and sample flow was described and detection limits with the high-voltage (1500 V) pulsed discharge through a microchannel were 0.52 and 19.0 μg L^{-1} for Cd and Pb at optimized conditions.[129] As a related method, work on hole-burning spectroscopy as a probe of nanoenvironments and processes in biomolecules can be mentioned.[130] Here the electrostatic conditions created by macromolecules can be probed from the broadening of bands. The field of microplasmas also leads into new ion sources for mass spectrometry, as it can exemplary be shown at work done on the measurement of He metastable atom densities in a plasma-based ambient ionization source.[131]

LASER INDUCED BREAKDOWN SPECTROMETRY

Laser induced breakdown spectrometry (LIBS) became a very popular method, which is reflected by the many publications in the field. Indeed, for the journals consulted for this review more than 150 of the 550 papers considered for the field of AAS and AES deal with LIBS. Review papers on the field of LIBS were published in two papers of Hahn and Omenetto. In a first paper, the state of the art of the knowledge on basic diagnostics in LIBS and especially the field of plasma−particle interaction is dealt with.[132] It is shown how the properties of the plasma with relation to excitation and ionization can be described by classical equilibrium relations and therefore on the assumption that the plasma is in local thermal equilibrium (LTE). It is also shown, however, that the transient nature of the plasma and its spatial inhomogeneity need to be considered to justify the theoretical assumptions made. In their second paper,[133] the authors treat the instrumental and methodological approaches to material analysis and applications to different fields. Especially new directions, such as double- and multipulse LIBS, calibration-free approaches, hyphenated approaches, where techniques such as Raman and fluorescence are coupled with LIBS, resonantly enhanced LIBS, signal processing and optimization and finally applications are treated. In a perspective paper, Russo et al.[134] treated the wide range of capabilities of laser plasma spectrochemistry. Laser plasmas are shown to offer the ability to perform elemental, isotopic, molecular, quantitative, and qualitative sample analysis with submicrometer spatial resolution, and each feature can be measured at standoff distances.

Fundamental Studies. Fundamental investigations deal with diagnostics of the plasma, mainly. With Thomson scattering electron temperatures from 5 700 to 11 100 K were measured and electron number densities of 4.3×10^{23} to 2.4×10^{22} m^{-3} for the case of a Nd:YAG laser at 532 nm and a 15 mJ beam.[135] The measurements were performed with high time resolution. Kumar et al.[136] reported on the effect of a transversal magnetic field on the laser-blow-off plasma plume emission in the presence of ambient gas. Here the intensities of Li I and Li II lines were measured at 2 mm distance and 1.33 Pa and 6 mm distance and 133.3 Pa, respectively, at variable magnetic fields and the results explained by considering the role of various plasma processes. Ribière and Chéron[137] analyzed relaxing laser-induced plasmas by absorption spectroscopy. Broad-band near UV absorption spectroscopy was used to analyze atmospheric laser-induced plasmas on metallic (Al−Mg and Cu−Ni) and refractory (C/SiC) targets and achieved high spatial resolution in the measurement of absolute number densities in expanding laser plasmas. The technique brought a support to the validation of collisional-radiative models attempting to describe evolutions of laser-induced plasmas. Gornushkin and Panne[138] published a review on the radiative models of laser-induced plasma and pump-mode diagnostics relevant to laser-induced breakdown spectroscopy. Efforts in modeling of laser-induced plasmas and overviews on plasma diagnostics here were given. Special attention is given to collisional-radiative and collisional-dominated plasma models where radiation processes play an important role. Also calibration-free models are considered which may endow with the possibility for standardless spectrometric analysis. In the diagnostic part, methods based on the use of additional diagnostic tools such as auxiliary lasers, optics and probes, and image-based diagnostics including shadowgraphy, schlieren and interferometry, absorption and fluorescence, Langmuir probe, and Thomson scattering were treated. By Diwakar et al.,[139] the analyte dissociation and diffusion in laser-induced plasmas were studied. For this aim, plasma−particle interactions are explored through the introduction of single microdroplets into laser-induced plasmas. Both spectroscopic analysis and direct imaging of the analyte atomic emission were used to provide insight into the various fundamental processes, namely, desolvation, atomization, and atomic diffusion. By doping the 50 μm droplets with Lu, Mg, or Ca, the analyte excitation temperature and the ion-to-neutral emission ratio were explored as a function of the plasma residence time following breakdown. Temporal H and Ca emission data were found to suggest that water vaporizes first. Holá et al.[140] studied the influence of physical properties and chemical composition of the sample on the formation of aerosol particles generated by nanosecond laser ablation at 213 nm. They used three sets of materials with a similar matrix (Co-cemented carbides with a variable content of W and Co, steel samples with minor differences in elemental content and silica glasses with various colors) and measured the concentration of ablated particles in the ranges 10−250 nm and 0.25−17 μm by using an optical aerosol spectrometer. Additionally, the structure of the laser-generated particles was studied after their collection on a filter with the aid of scanning electron microscopy. With respect to the use of laser sources for ablation-only purposes as in laser ablation optical emission spectrometry (OES) and MS, numerical simulation analyses of flow patterns and particle transport in the laser ablation cells used are very useful. As described by Lindner et al.[141] for a high efficiency aerosol dispersion cell, the critical velocity for the onset of particle losses was found to be independent of the ejection angle at the crater spot. Making use of the results of the simulations, it was possible to modify the cell so that extremely short washout times were obtained. The simulations yielded a signal of less than 10 ms,

dx.doi.org/10.1021/ac3031459 | Anal. Chem. 2013, 85, 670−704

which was produced by more than 99% of the introduced sample mass.

Applications. Manifold applications of laser induced breakdown spectrometry now occur in the literature. This is due to its applicability to any type of sample, the absence of any sample preparation, remote sensing capability, and its speed of analysis, with the advantages named in ref 141. Below, only some examples of applications in the most important fields are briefly discussed. For industrial recycling purposes of Al cast and wrought alloys, Werheit et al.[142] described a LIBS spectrometer. It is comprised of a Nd:YAG laser running at 200 Hz delivering a 200 mJ double pulse for plasma generation and a high-performance three-axis galvo-scanner to guide the laser beam onto single pieces moving at 3 m s^{-1} through a measurement volume of 600 × 600 × 100 mm^3 with a precision of ±1.5 mm and a 20 channel Paschen-Runge spectrometer. Sorting of Al postconsumer scrap charges with a correctness of >96% was possible. Another application is the online determination of a magnesium coating thickness on electrolytically galvanized steel in motion.[143] Variable Mg layer thicknesses between 100 and 1200 nm and 2−9 μm Zn layer thicknesses could be monitored at a pilot plant in a steel mill, whereas minimal damage due to craters with diameters less than 150 μm was caused to the surface.

A considerable advantage of LIBS is that the method perfectly performs irrespective of whether the sample is electrically conductive or not. Accordingly, a double-pulse LIBS method for the analysis of molten glass could be realized.[144] Using low-melting glass doped with different amounts of additives as a model system for recycling slags, the optimum number of shots, laser-interpulse, and acquisition delay times could be optimized for solid and liquid glass (1200 °C) and limits of detection of 7 (Mn) to 194 $\mu g\ g^{-1}$ (Zn) are achieved at a distance of 75 cm away from the sample. Also Pb and As in soils could be directly determined by LIBS.[145] Here the laser plume produced was additionally reheated and the analyte emission enhanced by applying a high voltage fast spark discharge across the plasma. By scanning electron microscopy, evidence could be obtained that the plasma reheating by the spark discharge was suggested to be presumably the main mechanism for the observed signal enhancement. LIBS also was used for distinguishing between bacterial pathogen species and strains.[146] Here chemometric analysis of the LIBS data was required so as to differentiate the bacterial pathogens *Escherichia coli*, three clonal methicillin-resistant *Staphylococcus aureus* (MRSA) strains, and one unrelated MRSA strain. This might be of use for applications in medical, water, and food safety. Another field of interest is the analysis of explosive residues in human fingerprints using optical catapulting LIBS.[147] Here particles are ejected from the substrate by means of the acoustic pulse or pressure wave generated when the laser pulse is transmitted along the substrate and the particles are analyzed by LIBS. The identification of the explosives is possible on the detection of C, H, N, and O as well as molecular emissions from CN radicals and C_2 molecules. As a further application, the development of a mobile fast-screening LIBS system for field-based measurements of nanometer sized particles in aqueous solutions is to be mentioned.[148] Here the energy ratio of every laser pulse before and after passing the laser beam through the aqueous sample is used to detect laser-induced plasma events. With a Nd:YAG laser operated at 20−100 Hz in water samples, losses of nanoparticles of up to 75% in 15 mL and 35% in 5 L containers after 3 months could be detected and also the nanoparticle contents of water after different purification steps at a drinking water plant could be monitored. An interesting application may arise from strategy studies for Mars remote LIBS determinations of sulfur in geological samples.[149] Here univariate analysis of sulfur emission lines could be used to differentiate between different minerals, and in addition H and O peaks could be included to better differentiate the samples.

LIBS applications are not limited to solid samples. Douglas et al.[150] described initial experiments with a technique they call laser ablation of a sample in liquid (LASIL). Here the ablation occurs at a solid sample surface submerged in a liquid. The analytical characteristics of LASIL are its ease of quantification and of generating suspended solids in solution from insoluble materials and the control over dissolution and dilution to generate measurable concentrations. The features of the technique were shown at the example of an analysis of the NIST 611 trace elements in glass CRM. Also for the atmospheric carbon dioxide measurement, LIBS has been proposed.[151] Here the strong C(I) emission at 247.85 nm was used which yielded a detection limit of 36 ppm with a laser pulse energy of 145 mJ. Real-time measurements have been performed, and it was found that a single measurement can be made within 40 s with a relative standard deviation of 3.6%.

Outlook. LIBS now is a mature method, where however considerable methodological innovation still can be expected. Especially, instrumentation for single-shot LIBS, which because of its nearly nondestructive nature is interesting for many applications in science and industry as reviewed by Michel,[152] requires the use of suitable spectrometric detection with high absolute sensitivity and sufficient time and wavelength resolution. Also the use of diode pumped solid state lasers (DPSS) for combined LIBS and Raman spectroscopy measurements, as discussed by Hoehse et al.[153] certainly is an interesting possibility. A diode pumped solid state laser operated at repetition rates between 1 Hz and 200 kHz, with a pulse energy of ∼1 mJ and pulse durations of ∼20 ns, was added to a flashlamp pumped Nd:YAG laser (10 Hz, 400 mJ, 6 ns) and herewith for Cu, Cr, and Ni in ultrapure iron samples detection limits of 0.7, 1, and 5 $\mu g\ g^{-1}$, respectively, could be obtained, whereas aside from elemental also molecular composition mapping of a mineral sample could be performed. This strongly implies that DPSS lasers are the promising source for LIBS, Raman, or combined LIBS-Raman spectrometry. Popov et al.[154] showed that a spatial confinement of laser-induced plasma may be useful to enhance the sensitivity of LIBS, as exemplarily described for the analysis of soils. Here for single-pulse LIBS, a small chamber with a 4 mm diameter equipped with polished brass walls and high efficiency collection optics is used. After a thorough optimization of the rinsing procedure and the focusing of the laser radiation on the sample for As, Hg, Pb, Mn, V, and Ba in soils, detection limits of 30, 25, 90, 140, 1, and 50 ppm were obtained, which is certainly 2−5 times lower than obtained with a free-expanding plasma. A promising approach is laser ablation molecular isotopic spectrometry, as described by Russo et al.[155] The technique uses radiative transitions from molecular species either directly vaporized from a sample or formed by associative mechanisms of atoms or ions in a laser ablation plume. The method not only can determine chemical composition but also isotopic ratios of elements in the sample as shown in the examples of the elements H, B, C, or O when making use of isotopic shifts in the molecular spectra. Finally also liquids from aerosols and microdrops also can be analyzed by LIBS, as discussed by Cahoon and Almirall.[156] Herewith for 90 pL droplets, analysis by single-pulse and collinear double-pulse LIBS could be performed when using a 532 nm dual-head laser and detection limits in the liquid samples

dx.doi.org/10.1021/ac3031459 | *Anal. Chem.* 2013, 85, 670−704

in the μg mL^{-1} range for Sr, Mg, and Ca obtained. This corresponds to absolute detection limits of the order of 1 pg and opens possibilities for applications in many fields.

GLOW DISCHARGE OPTICAL EMISSION AND MASS SPECTROMETRY

Both glow discharge optical emission spectrometry (GD-OES) and mass spectrometry (GDMS) are routinely used for bulk and depth profiling analysis of solid materials. Nevertheless, several new developments and analytical improvements, as well as fundamental studies, were reported in the previous 2.5 years, especially in the field of pulsed GD sources. Besides, GD sources and related plasma designs, operating at atmospheric pressure, are further gaining increasing interest for gas and liquid analysis.

Fundamental Studies. Although the general behavior of GD plasmas is already known from extensive modeling and experimental efforts in the past 2 decades, fundamental studies continue to be important to further improve the analytical practice of GD-OES and GDMS.

Wagatsuma and co-workers[157−160] recorded optical emission intensities to elucidate the importance of specific collision processes in the GD. In ref 157, emission spectra of gas species were measured in several binary gas mixtures, i.e., Ar−He, Kr−He, Ar−Kr, and Kr−Ar, in order to elucidate the collisional energy transfer between these gas species. In the Ar−He mixture, a significant amount of redistribution in the population among the excited levels was observed due to Ar−He collisions. This was not the case in the Kr−He plasma and could be explained because the excitation energy and spin multiplicity between collision partners follow both the energy resonance conditions and spin conservation rule in collisions of the second kind in the Ar−He system but not in the Kr−He system. Also in the Ar−Kr and Kr−Ar mixtures, no significant energy exchanges between Ar and Kr species were observed. In ref 158, the spatial distribution of the excitation temperature in a Grimm-type GD was measured by means of a 2D imaging spectrometer. The temperature was estimated to be 4 650−4 950 K in most of the plasma region and did not vary significantly even when changing the voltage and pressure. Finally, so-called Boltzmann plots were recorded for many iron atomic[159] and ionic[160] lines. In both cases, a nonlinear relationship was observed, with an overpopulation of the higher excitation levels. In the atomic case,[159] this was attributed to Penning ionization with metastable Ar or Ne atoms, followed by electron-ion recombination and stepwise de-excitation, populating these higher excited energy levels, lying just below the ionization limit. This process appeared to be more significant in argon, attributed to the higher Ar metastable densities. In the case of the ionic lines,[160] a resonance charge transfer from the ground state Ar^+ ions was stated to be responsible for the overpopulation of the higher levels. From the enhancement factor of the emission intensity, it could be deduced that this charge transfer collision could elevate the number density of the corresponding excited levels by a factor of $\sim 10^4$.[160]

Steers and colleagues[161−164] also studied optical emission intensities to obtain a better insight in the fundamental plasma processes. More specifically, the intensities were recorded by Fourier transform (FT) spectrometry, which allows one to investigate a large number of lines over a wide spectral range. In ref 161, a detailed comparison of iron and titanium spectral line intensities was carried out between plane and hollow cathodes in a Grimm-type GD source. Clear trends in intensity increase and reduction were detected, according to the excitation energies of the emission lines. For instance, all lines with excitation energy below 5 eV showed a higher intensity in the hollow cathode discharge, indicating that the latter could be advantageous for analytical applications. On the other hand, the asymmetric charge transfer excitation process responsible for some ion lines appeared to be suppressed in the hollow cathode discharge. A comparison between hollow (~10−15 mm deep) and shallow (~2 mm deep) cathodes gave additional information on the depth influence of the hollow cathode effect.[161] The effects of oxygen addition (in the range 0.04−0.8% v/v) on spectra, as well as on sputter rates and ion signals, were investigated in refs 162−164 using not only FT-OES but also time-of-flight mass spectrometry (TOF-MS).[163] A sudden drop in the sputter rates, the intensities of argon and analyte atomic lines, and the ion signals was observed at a certain threshold fraction of oxygen, which was more pronounced than previously encountered for Ar/H_2 and Ar/N_2 mixtures. This was attributed to a so-called poisoning effect, i.e., the formation of an oxide layer on the cathode surface.[162,163] Beyond this threshold fraction, a further drop in ion signals was noticed, explained by the quenching of ions and Ar metastable atoms by oxygen in the flowing afterglow.[163] Furthermore, it was reported that at the threshold oxygen fraction, the drop in ion signals was orders of magnitude higher than the decrease in optical emission intensities from analyte and gas ions, which was also attributed to reactions in the flowing afterglow. On the other hand, a significant increase in ion signals in the negative ion mass spectra was observed at a certain critical oxygen content.[163] Finally, in ref 164 the effect of added oxygen or hydrogen on the occurrence of asymmetric charge transfer in an Ar or Ne Grimm-type GD was studied. Asymmetric charge transfer involving oxygen ions was observed in the spectra, whereas other analyte lines, typically excited by charge transfer with Ar ions, were found to become weaker, due to the quenching of Ar ions by oxygen addition.[164]

To further elucidate the importance of asymmetric charge transfer in a GD, Korolov et al.[165,166] developed a method to determine the rate coefficient for this process, by means of a combination of plasma diagnostics and a kinetic model for the afterglow plasma. A schematic diagram of the reaction cell and the optical setup is illustrated in Figure 4.[166] The discharge cell has two plane and two hollow cathodes, made of the material for which the charge transfer rate coefficient will be determined. The reason that two different cathode shapes are chosen is to cover a wide range of possible values for the charge transfer rate

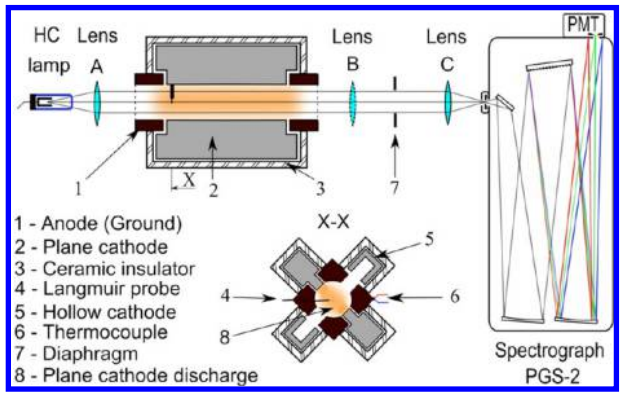

Figure 4. Scheme of the experimental setup, including reaction cell and optical setup, used in refs 165 and 166 to determine the values of charge transfer rate coefficients. The X-X section is perpendicular to the optical axis. Reprinted with permission from ref 166. Copyright 2011 Elsevier.

dx.doi.org/10.1021/ac3031459 | Anal. Chem. 2013, 85, 670−704

coefficient to be determined, as the value is not known in advance. By monitoring the temporal evolution of the densities of different species in a stationary afterglow experiment, i.e., by means of atomic absorption spectrometry for the metal vapor density and by OES for the charge transfer-excited Ar^+ ion lines, the rate coefficient for this reaction could be obtained. This method was applied for the reaction between Ar^+ ions and Fe atoms in ref 165 and between Ar^+ ions and Ni atoms in ref 166. In our opinion, these studies are very important. Indeed, in contrast to the other papers mentioned above, which mainly yield qualitative information about the occurrence of certain reactions in the plasma, the work by Korolov et al. gives quantitative data, which can be used for modeling and in this way it really contributes to a better understanding of the GD plasma.

Indeed, a good knowledge about such rate coefficients is of primordial importance for modeling of the GD plasma, as was demonstrated already in several papers, many years ago. Although in the last 2.5 years, not so many new modeling studies were reported, still some papers described modeling approaches focusing on specific aspects of a GD plasma. For instance, Simon and Bogaerts[167] calculated the vibrational level population of nitrogen impurities, present in an Ar GD with concentrations between 0.1 and 1%, as it is known from plasma physics literature that these vibrational levels can play a very important role in gas discharges, depending on the conditions. The main mechanisms responsible for the population and depopulation of the vibrational levels and for the overall shape of the vibrational distribution function were pointed out. It was found that vibration−vibration collisions play only a minor role, and therefore the population of the vibrational levels was found to be basically determined by the electron temperature.[167] Another modeling study was presented by Derzsi and Donko[168] based on a two-dimensional hybrid plasma model for describing the behavior of electrons, atoms, and ions of both the discharge gas and the sputtered cathode material, in a Grimm-type GD, complemented with a set of equations for the external circuit, in order to investigate the effect of the external electrical circuit on the ignition of the GD. This made it possible to simultaneously determine (i) the temporal and spatial evolution of the plasma and (ii) the time-dependence of the discharge voltage and of the different current components flowing in the circuit. The authors reported that in the future, this model will be applied to discharges operating at higher voltages and currents during short pulse operation.[168]

It is indeed clear that pulsed GDs are continuously attracting a lot of interest, not only from the application point of view (see below), but also for fundamental studies. Voronov, Hofmann, and colleagues investigated the processes of sample ion transport in a microsecond (μs) pulsed fast-flow Grimm-type GD by experiments and modeling.[169] They demonstrated that the formation of the analytical signal of the sample is temporally and spatially separated from the pulsed discharge area and called this a native property of the fast flow source concept, owing to the intensive transportation of the sample material from the discharge area by the gas flow.[169] The same authors, in a collaborative effort with the Hieftje group, presented an interesting study on so-called pressure waves in argon and helium dc pulsed GDs, by means of an inserted microphone.[170] First and second harmonics of pressure vibrations were detected, in good agreement with the resonant frequency (2.7 kHz) of the discharge cell. The pressure changes were found to have a significant effect on the plasma characteristics, such as electrical current and optical emission. Some possible mechanisms for the generation of pressure waves were discussed, related to gas heating and expansion phenomena. It was pointed out that these pressure changes should be taken into account in plasma simulations and diagnostics and for discharge optimization. In a follow-up paper,[171] the same authors developed a Monte Carlo simulation for describing the behavior (i.e., flow and heating) of Ar gas atoms in a microsecond pulsed dc GD and combined this model with their existing microsecond pulsed GD model. The simulation results revealed that the gas heating, and the resulting concentration reduction, takes place near the cathode, and the Ar concentration might be reduced by a factor of 2−3 compared to the initial concentration. Furthermore, the gas heating, followed by expansion, was stated to be responsible for the electrical prepeak and pressure waves generated by the leading edge of the microsecond-pulse.[171]

It is indeed generally known that thermal effects can influence the performance of GD devices, but nevertheless, gas and sample temperature are not often measured. As the gas temperature does not only depend on the power absorbed but also on the temperature of the walls (i.e., sample and anode cell walls), Efimova et al. investigated the influence of the anode material of a Grimm-type GD on the voltage-current characteristics, crater shapes, and GD spectra.[172] Anode materials with a wide range of thermal conductivities were used. The temperature of the sample was measured from the back side. It was found that cooling of the sample, and anode materials with good thermal conductivities, resulted in a higher electrical current. Furthermore, the choice of the anode material had no significant influence on the crater shape but resulted in slightly different sputtering and strong differences in the GD spectra.[172]

Günther and co-workers also performed some fundamental studies of a pulsed GD.[173,174] In ref 173, the spatial, temporal, and current dependence of Ar metastable species in a pulsed dc GD was recorded by means of optical measurements through an iCCD camera. The authors reported that the Ar metastables exhibited a maximum density near the cathode (∼1 mm) during the pulse, whereas this maximum was shifted to a region far from the cathode (∼6−8 mm) in the afterglow. This maximum was reached within the first 100 μs after pulse termination, and it decayed within 200−250 μs.[173] In ref 174, the plasma chemistry of single plasma pulses of a pulsed GD was investigated, during the introduction of organic solvents with gas chromatography. It was found that a small amount of solvent (e.g., a few hundred nanoliters) already leads to a significant quenching of the after-peak ion signals. From the recovery of the plasma after the quenching, information could be obtained on the plasma chemistry involved in the quenching. For instance, the introduction of hydrogen with the organic solvent resulted in a changed ionization yield of copper and an increase of hydrides.[174] It is clear that these findings have to be carefully considered, using transient sample introduction systems with a pulsed GD.

Yan et al.[175] studied the emission characteristics of the afterglow of a microsecond-pulsed GD to obtain insight in the excitation and recombination processes of analyte and fill gases. All emission lines exhibited an intense peak in the beginning of the discharge pulse, and some lines also showed an intense postpulse signal, with a broader profile and a maximum at 25−35 μs after plasma termination. In general it was found that lines originating from low energy levels have smaller afterpeaks than lines arising from high energy levels. The authors suggested that in a microsecond pulsed GD, highly excited argon and copper atoms are probably generated through electron-ion three-body recombination, in contrast to millisecond-pulsed

dx.doi.org/10.1021/ac3031459 | Anal. Chem. 2013, 85, 670−704

GDs, where dissociative recombination was reported as the important mechanism.

The Oviedo group[176] also performed time-resolved measurements of the emission profiles for a wide range of Cu lines, in a pulsed rf GD, but focusing mainly on the prepeak. The effects of pulse frequency, duty cycle, pulse width, and power-off time were investigated as well as the effect of pressure and power. It was shown that the intensity of the prepeak can be 10 times as large as the plateau value for resonant Cu lines and up to 5 times for transitions to the metastable levels. The authors suggested that the presence of the prepeak was probably due to the lack of self-absorption during the first 50 μs and not to the ignition of the plasma. It was therefore concluded that the prepeak emission can be used as analytical signals to increase the linearity of the calibration curves for resonant lines subject to self-absorption at high analyte concentrations.[176] In ref 177, the same group performed side-on measurements of the emitted radiation of a pulsed rf GD and investigated again the effect of pulse frequency. It appeared that the excitation of Ar atoms, Ar ions, and Cu atoms was favored at different frequencies, and for the Cu atoms also a strong dependence on the upper energy level was observed. Moreover, the spatial distribution of Ar and Cu emission seemed to differ from each other: the Ar atom emission extends longer in the plasma than the Cu atom emission, and the ions have their maximum emission close to the anode. The latter suggests that it is possible to detect ionic emission at distances far away from the negative glow, in regions where usually the sampler cone is placed in GDMS.[177]

Efimova et al. also investigated the effect of pulse duration and duty cycle on the electrical characteristics of a microsecond-pulsed GD, and the optimum parameters were reported.[178] A comparison between dc and rf modes was also made, and strong similarities between both modes were observed when using the effective voltage in the rf mode as an equivalent to the dc voltage. In both cases, a drop in the current, caused by heating of the discharge gas at higher power, was found. Finally, DeJesus et al.[179] measured ion intensity profiles for both discharge gas and sputtered species in a millisecond-pulsed dc GD, using time-gated detection with a time-of-flight-mass spectrometer (TOF-MS), for a wide range of parameters, including sampling distance, pulse power, gas pressure, pulse width, and duty cycle. It was again demonstrated that through the careful selection of the plasma parameters, the sputtered ion signals could be maximized, while suppressing the ion signals from the discharge gas.[179]

Methodological Studies and Applications of GD-OES and GDMS. As several commercial GDMS and GD-OES instruments are on the market, instrumental developments in this field were limited in the past 2.5 years. Hieftje and co-workers[180] coupled a dc GD source with a Mattauch-Herzog mass spectrometer and a third-generation Faraday-strip array detector. This combination offers simultaneous determination of multiple elements and provides superior resolving power and therefore improved limits of detection. It was stated that the resolving power was only limited by the mass spectrometer and not by this third-generation array detector.[180] Churchill et al. developed a new microsecond-pulsed dc GD assembly on a fast flow high power source for time-resolved analysis with a high-resolution MS.[181] This new assembly allowed submicrometer layer analysis for depth profiling of thin layered structures, such as photovoltaic films. For GD-OES, Wagatsuma and Urushibata reported on a fast Fourier transform (FFT) analyzer to estimate the emission intensity from an rf GD.[182] As this analyzer can disperse the components by frequency from an overall signal, it works as a selective detector in modulation spectroscopy. A dc bias current was introduced and could be pulsated to modulate the emission intensities, and subsequently the modulated component was selectively detected with the FFT analyzer. In this way, the data precision was greatly improved.[182]

Some efforts were presented on quantification and calibration procedures for both GDMS and GD-OES. Gusarova et al. reported on the calibration of two different GDMS instruments, i.e., the VG9000 and the Element GD.[183,184] In ref 183, different calibration strategies for the analysis of zinc samples were compared. The calibration with doped pellets was found to be the best quantification technique. In addition, relative sensitivity factors for several different matrixes were reported. In ref 184, pin-shaped synthetic standards pressed from solution doped copper and zinc matrixes were adopted. The impact of the sample pin cross section (circular or square) was investigated. RSFs for 50 elements in copper and zinc matrixes were presented. It was concluded that the field of applicability of GDMS may be considerably extended by the analysis of pin geometry samples, based on their ease of preparation.[184] Di Sabatino et al. used the Element GD for the quantitative analysis of impurities in silicon for photovoltaic applications.[185] For this purpose, RSFs first needed to be determined for silicon matrixes, using independent analytical methods. The authors reported that the tuning parameters of the Element GD, mainly the discharge gas flow rate, influence the RSF values. Moreover, the RSF values were found to be matrix specific.[185]

In the framework of GD-OES quantification improvements, Weyler and Bengtson investigated the so-called "hydrogen effect" (i.e., the enhancing or suppressing effect of traces of hydrogen on spectral line intensities as a function of discharge parameters, in order to develop effective correction methods for quantitative depth profiling analysis.[186] A simple but effective experimental method was employed, i.e., the decrease or increase in intensity of several emission lines was correlated with the intensity of the hydrogen emission line. Systematic investigations for a range of currents and voltages provided a good matrix of data, to find a model describing these variations. The information extracted from these studies will be important for routine depth profiling analysis, as the hydrogen correction is a relevant tool in software quantification algorithms.[186]

Certainly a new development of the past few years is the improvement of surface elemental imaging by GD-OES.[187−190] Hieftje and co-workers[187] presented a method for correcting instrumentally introduced image distortion in a monochromatic imaging spectrometer (MIS). Correction of the distorted images was performed computationally by means of bilinear interpolation. It was demonstrated that significant differences between vertical and horizontal emission profiles from distorted emission maps could be successfully corrected. Gamez et al.[188] showed that lateral information from the sputtered sample could be obtained with GD-OES, when operating in pulsed mode. A new approach for the collection of the GD-OES signal with lateral, spectral, and temporal resolution was presented, using a push-broom geometry hyperspectral imager for the GD-OES elemental mapping. The higher light throughput of the push-broom geometry allowed faster image acquisition times, compared to other spectral imaging systems, and thus the depth resolution was maintained below 10 nm. Voronov et al.[189] developed a novel acousto-optical imaging spectrometer, with spatial resolution of 125 μm, spectral resolution in the range of 0.05−0.3 nm, and time resolution of 5 ns. These characteristics were found to be sufficient for application in GD imaging

dx.doi.org/10.1021/ac3031459 | Anal. Chem. 2013, 85, 670−704

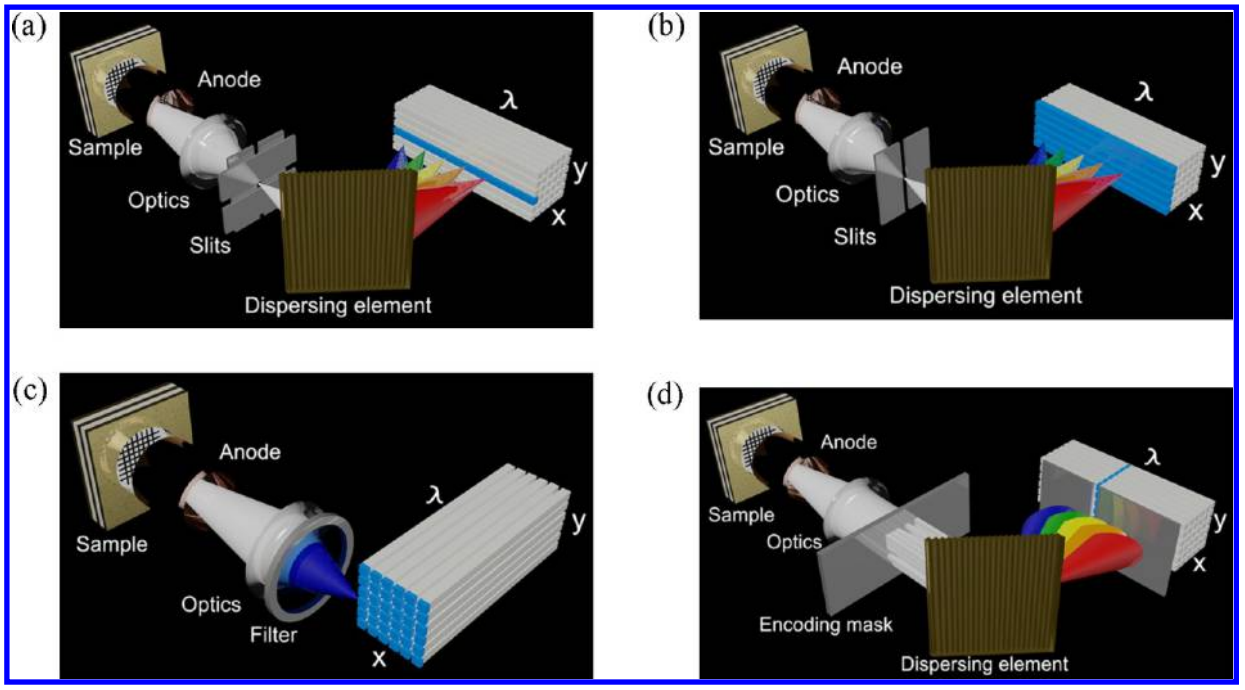

Figure 5. Schematic diagram of (a) whisker-broom, (b) push-broom, (c) staring spectral imaging systems, and (d) Hadamard transform spatial imaging system for GD-OES elemental mapping of a sample. More details can be found in ref 190. Reprinted with permission from ref 190. Copyright 2012 Elsevier.

spectroscopy. It was reported that fast switching between different spectral lines within 200 μs could be used, e.g., to investigate the evolution of different spectral lines quasi-simultaneously. Finally, the authors of the latter three papers wrote together an interesting review paper on various spectral imaging techniques used for GD-OES elemental mapping, including whisker-broom, push-broom, and staring spectral imaging as well as Hadamard transform spatial imaging.[190] These four imaging techniques are schematically illustrated in Figure 5. Also the fundamental limits were explained, in relation to the pulsed mode, gas pressure and gas flow, and detector limits. Furthermore, the use of a GD array was discussed. The authors concluded that GD-OES elemental mapping offers high-throughput determination of the 3D surface elemental composition of large areas of samples. Possible applications range from the characterization of the homogeneity of reference materials to quantification and identification of proteins in mixtures separated by 2D gel electrophoresis.[190]

The Oviedo group was particularly active in the last 2.5 years, especially in their research on pulsed rf GDs, either coupled to TOF-MS[191−205] or OES.[206−209] A number of review papers from this group was published in recent years.[191−193] In ref 191 they gave an overview on inorganic mass spectrometry techniques used for the characterization at the nanoscale. Two main groups of techniques were reviewed, i.e., on the one hand the techniques used for the analysis of liquids and on the other hand those allowing direct solid analysis with spatial resolution capabilities, i.e., lateral (imaging) and/or in-depth, including GDMS. A comparison was made between the capabilities of GDMS, laser ablation-inductively coupled plasma mass spectrometry (LA-ICPMS), secondary ion mass spectrometry (SIMS), and sputtered neutrals mass spectrometry (SNMS). In ref 192, a review on GD analysis of nanostructured materials and nanolayers, both by MS and OES, was published. The latest advances and presently available GD-OES and GDMS instrumentation (either commercial, prototype, or laboratory equipment) were described, and analytical strategies for the analysis of surface and depth profiling of (ultra) thin layers were discussed. Also, selected examples of GD-OES and GDMS for the nanometer range analysis (including nanolayers, 2D nanostructured materials, and depth profiling of polymer-based coatings) were discussed, demonstrating the increased interest of GD-OES and GDMS for nanotechnological applications. Finally, in ref 193, Pereiro et al. presented a nice review paper on GD-TOF-MS, focusing on instrument developments and recent applications, both for the elemental and molecular direct solid analyses of materials and for analytes in the gaseous phase (including a detector for gas chromatography). Pulsed versus continuous GD-TOF-MS for elemental analysis was evaluated. Applications for elemental analysis of thin films and for molecular analysis (including polymers and solid-state metal speciation) were illustrated. Quantifaction by GD-TOF-MS was discussed, as well as alternatives to conventional GD-TOF-MS, including magnetically boosted GD sources, alternative discharge gases, and combined laser ablation (LA) GD-TOF-MS.[193]

In ref 194, a modified in-house built GD ion source was presented, with a reduced internal volume and no flow tube, allowing the use of lower gas flow rates, as well as improved ion transmission efficiencies, because the source can be placed closer to the sampling cone of the mass spectrometer. Therefore, the limits of detection were found to be more than an order of magnitude better with this modified GD source and can be further improved by using pulsed rf GD-TOF-MS. The analytical potential of this source was demonstrated for the analysis of small gas volumes and bubbles in glass. In ref 195, a so-called purged argon prechamber was investigated for rf GD-TOF-MS, to minimize the risk of microleaks in the seal between the sample and the GD source. This surrounding chamber with a continuous isolating argon flow around the solid sample indeed reduced the microleaks, as the recorded mass spectra contained a much lower

dx.doi.org/10.1021/ac3031459 | *Anal. Chem.* 2013, 85, 670−704

level of polyatomic ions, yielding less polyatomic interferences. Also the depth profiling capabilities seemed to improve. The benefits were most apparent for the rf nonpulsed mode.

Several papers discussed the capabilities of pulsed rf GD-TOF-MS for the depth profiling analysis and thickness quantification of ultrathin (∼nanometer sized) multilayers.[196−200] In ref 197, the quantitative depth profiling of boron and arsenic ultralow energy implants on silicon was investigated, demonstrating nanometer depth resolution. The obtained results were found to be in good agreement with results from complementary techniques, including SIMS and grazing incidence X-ray fluorescence. In ref 198, the depth profiling analysis of ultrathin $Nb/Al_{1-x}Co_x$ bilayers and their interfaces was presented, in order to evaluate segregation/diffusion processes at the interfaces. The results were compared with TOF-SIMS results, and the analytical performance of both techniques was found to be comparable, although with a poorer depth resolution for GD-TOF-MS. On the other hand, the analysis time was much shorter, the cost was reduced, and the restrictions imposed by the need of ultrahigh vacuum conditions of SIMS could be avoided. Therefore, the authors concluded that pulsed rf GD-TOF-MS could be a valid alternative to SIMS, in those cases when lateral resolution was not required. In ref 199, the capabilities for fast and reliable depth profiling analysis, as well as for the detection of contaminants introduced during the synthesis process, were illustrated for self-assembled metallic nanostructures. Finally, in ref 200, the depth profiling analysis of ultrathin (∼nanometer-size) Si−Co bilayers was studied, using the analyte prepeak region, i.e., the pulse region where the analyte ions peak after the initial sputtering process, with the aim to obtain improved depth resolution with minimum polyatomic spectral interferences. The obtained results compared well with those obtained by TOF-SIMS.

The optimization of (pulsed and continuous) rf GD-TOF-MS for the identification of organic polymers, and for molecular depth profiling, was presented in ref 201. It was demonstrated that especially the pulsed mode offered a great analytical potential to characterize such organic coatings. Moreover, some formed polyatomic ions appeared to be useful to identify the different polymer layers, so that layers with similar elemental composition but different polymer structure could also be identified. In ref 202, the same technique was applied for the screening of polymer-based coatings containing brominated flame retardants. The analytical performance of microsecond and millisecond pulsed regimes was compared, and better detection limits were obtained for the millisecond pulsed regime. The authors concluded that this method can be successfully applied to the identification and discrimination among different polymers.

Pulsed rf GD-TOF-MS also proved to yield interesting results as a gas-chromatographic detector for compounds of environmental concern, for the simultaneous collection of elemental and molecular information.[203] A compound-independent calibration was carried out, and the intensity ratios (analyte to internal standard) were linear with the corresponding ratio of the concentrations. Moreover, the detection limits were improved by 1 order of magnitude compared to using external calibration. The applicability of this approach was demonstrated for the determination of chloroform in drinking and river waters. Likewise, in a collaboration between Vanhaecke and co-workers and the Oviedo group, the capabilities and limitations of pulsed rf GD-TOF-MS were explored for the precious metal determination in lead fire assay buttons.[204] As the matrix of these materials consists almost entirely of lead, the occurrence of doubly charged (Pb^{2+}) ions can hinder accurate determination of Rh, but this problem was overcome by the time-resolved formation of different ion types during the pulse, which allowed discrimination against the Pb^{2+} ions. Finally, the influence of hydrogen contained in amorphous hydrogenated Si (a-Si:H) thin films on pulsed rf GD-TOF-MS was investigated in ref 205, and the results were compared with the addition of hydrogen to the discharge gas. It was demonstrated that pulsed rf GD-TOF-MS is capable of performing depth profiling analysis of coated materials, such as used in thin film solar cells, but the hydrogen concentration on these a-Si:H films is typically around 10%, which represents a challenge for quantitative depth profiling, due to the so-called "hydrogen effect" (see above). Therefore, a comparison was carried out by pulsed rf GD-TOF-MS between hydrogen introduced in molecular gaseous form (so-called exogenous hydrogen) and hydrogen sputtered as a sample constituent (so-called endogenous hydrogen). It was found that exogenous hydrogen had a large influence on the pulse profiles of the analytes, whereas the effect of hydrogen sputtered from the samples was of much lower importance.[205]

Besides pulsed rf GD-TOF-MS, the potential of pulsed rf GD-OES was also investigated by the same group, for the bulk and quantitative depth profiling analysis of various conductive and nonconductive coatings.[206−209] In ref 206, thin film solar cells based on a-Si:H thin films were characterized. Quantitative depth profiles obtained by either pulsed or continuous mode were compared, and the effects of different pulse conditions, such as pulse frequency, duty cycle, and power, as well as the optimum conditions for both continuous and pulsed rf GD-OES, were reported. It was concluded that rf GD-OES is a power tool for this application, allowing one to discriminate the different parts of the photovoltaic devices, and to study the diffusion processes between the coating layers, which has an important influence on the final efficiency of the photovoltaic devices. Furthermore, the endogenous and exogenous hydrogen influence for the analysis of a-Si:H films by pulsed rf GD-OES was analyzed.[207] Enhanced emission intensities were measured for most elements in the presence of hydrogen, despite the observed reduced sputtering rate. It was again reported that hydrogen originating from the discharge gas has a more pronounced effect than intrinsic hydrogen present in the sample itself. These investigations might be useful for a further improvement of the quantification algorithms, developed to correct for the hydrogen effect, for routine GD-OES analysis (see also above). In ref 208, a simple multimatrix calibration procedure for pulsed rf GD-OES was described and validated by analyzing conductive layers of thicknesses varying from a few tens of nanometers up to 20 μm and a range of different compositions. In ref 209, pulsed rf GD-OES was applied for the bulk and depth profiling analysis of conductors and insulators, and a critical comparison of the practical analytical performance characteristics of rf GD-OES in continuous and pulsed modes was made. More specifically, crater shapes, sputtering rates, and emission yields were investigated, demonstrating that enhanced emission yields could be obtained in the pulsed mode, when using small pulse widths. Also, an improvement of the depth resolution was clearly observed when applying the pulsed mode. Finally, the observed advantages of pulsed rf GD-OES were successfully tested by analyzing real-life samples, including commercial tin plates and multilayered glass.

The Oviedo group also reported on the analytical capabilities of continuous rf GD-OES,[210−212] which was found to be a promising tool for the depth profiling analysis of challenging materials, such as self-aligned nanotubes and arrays of nanowires.[210] In ref 211, a method for improved analytical

dx.doi.org/10.1021/ac3031459 | Anal. Chem. 2013, 85, 670−704

performance of rf GD-OES for nonconductive samples was presented. More specifically, a thin conductive layer was deposited on both sides of the sample, to increase the voltage transfer coefficient, which is defined as the ratio between the peak voltage at the front and at the back of the sample. The influence of the thickness and diameter of the thin conductive layer on the optical and electrical signals was investigated. In addition, a magnetic field was applied to obtain higher sputter rates and better ionization and excitation efficiencies, yielding higher emission intensities. Finally, in ref 212, a new experimental setup was presented to perform spatially resolved measurements of the optical emission intensities in an rf GD. The emitted radiation was not only detected through an end-on window but also by axially resolved side-on measurements. The spatial distribution of various excited species was analyzed for varying argon flow rate and pressure. Above a certain pressure, enhanced analyte emission, more confined within the proximity of the anode, was observed. These side-on measurements are important for the interpretation of GDMS results, because the ions detected with GDMS typically originate from the vicinity of the sampler orifice.

A number of other groups also reported on the use of pulsed rf GD-TOF-MS.[213,214] Canulescu et al. presented a new method for elemental and molecular analysis of halogen-containing samples by GD-TOF-MS, by means of the detection of negative ions from a pulsed rf GD in Ar.[213] The analyte signals were mainly extracted from the afterglow region. Furthermore, the negative ion formation from sputtering of metals and metal oxides was compared with the positive ion formation, and it was shown that the negative ion signals of F^-, for instance, were enhanced compared to positive ion signals and can be used for studying the distribution of a tantalum fluoride layer. Comparison was also made with GD-OES measurements, where elemental fluorine could only be detected in a Ne plasma. Finally, the ionization mechanisms for negative ion formation in a GD-TOF-MS were briefly discussed. King and co-workers used a millisecond-pulsed rf GD-TOF-MS system for the direct speciation of various iron oxides.[214] It was stated that appropriate adjustment of sampling distance, temporal regime, gas pressure, pulse frequency, and duty cycle is necessary to enable such speciation. The discrimination between FeO, Fe_2O_3, and Fe_3O_4 was possible by means of recording variations in $Fe^+/FeOH^+$ ratios.

Finally, some papers were also published using dc GD-OES for various applications.[215−218] Galindo et al. reviewed the state-of-the-art of GD-OES, in comparison with three other depth profiling characterization techniques, i.e., Rutherford backscattering spectroscopy (RBS), SIMS, and X-ray photoelectron spectroscopy (XPS), focusing mainly on nanometric resolution in multilayer depth profiling.[215] It was concluded that the application of mathematical tools, such as deconvolution algorithms and a depth-profiling model, pulsed sources, and surface plasma cleaning procedures will greatly improve the GD-OES depth resolution. Schmitt et al. performed chemical and optical characterization of Al-doped ZnO films for photovoltaics by GD-OES.[216] A measurement procedure was established, to determine simultaneously the thickness, mean chemical composition and refractive index of homogeneous films by using GD-OES and profilometry. The authors concluded that GD-OES is a suitable analysis technique in the development of photovoltaic thin films. Hoffmann et al. reported on the analysis of gaseous reaction products of wet chemical silicon etching, more specifically the formed H atoms, by dc GD-OES. The results gave information on the etching mechanism of silicon.[217] Finally, Chen et al. reported on the measurement of carbon solubility in magnesium alloys using GD-OES.[218] The authors showed that the quality of the internal atmosphere in a GD has crucial effects on the carbon measurements. Therefore, recipes were developed to reliably measure the carbon content in trace amounts, including atmosphere quality checking, atmosphere purification by burning dummy samples, prolonged preburning time, and frequent drift corrections.

New GD Sources for Novel Applications and Combined GD-LA Systems. Continuing on the trends of previous years, GD sources are gaining more and more interest for liquid and gas analysis, besides the more classical solid analysis, as described above. Several different types of GD source designs have been constructed, typically operating at atmospheric pressure. A few fundamental studies on atmospheric pressure GDs (APGDs) have been carried out,[108,131,219,220] which is very important, in our opinion, in order to improve the applications of these new source designs.

Simon et al. investigated the physical and analytical characteristics of an atmospheric pressure Ar−He rf capacitively coupled plasma, including the excitation temperature of Ar, He, and H, the rotational temperature of the OH band, the electron temperature and the electron number density, as well as the evolution of several atomic emission lines or molecular bands.[108] The optimum atomic emission analysis parameters were established using pneumatically nebulized liquid solutions. It was found that the presence of helium enhanced the emission intensities and detection limits. Broekaert and co-workers developed a new dc APGD operating in He, and presented a spectroscopic characterization.[219] More specifically, the rotational, excitation and ionization temperature, and the electron number density were determined as well as the current−voltage characteristics. The rotational and excitation temperature were found in the order of 900−1200 K and 4500−5500 K, respectively, indicating that the discharge is not in LTE, despite the atmospheric pressure. At optimized conditions, the discharge operates in the normal regime of the current−voltage characteristics. Spatially resolved temperature measurements were also performed, both in axial and radial direction, and showed relatively flat profiles. Finally, axially resolved emission intensity profiles for several species were determined. Franzke and co-workers also presented spatially resolved spectroscopic measurements of an atmospheric pressure DBD plasma jet both in argon and helium, which was developed for liquid chromatography (LC)−MS and as an ionization source for ion mobility spectrometry.[220] The DBD plasma jet could be regarded as a soft ionization technique, characterized by only minor fragmentation. The obtained mapping of the plasma jet showed very different number density distributions of relevant excited species in argon and helium. Indeed, much stronger N_2^+ and N_2 lines were observed in helium, and the position of the maxima in these intensities indicated the regions where the highest efficiency of the water ionization and the protonation process was expected. The difference with argon was attributed to the fact that Penning ionization of nitrogen molecules was orders of magnitude less probable in argon than in helium, so that no efficient protonation could take place in an Ar plasma. Finally, Heywood, Taylor and Farnsworth studied the He metastable densities in a DBD, used as an ambient ionization source by means of collisionally assisted laser-induced fluorescence.[131] The fluorescence images did not correlate well with emission maps from highly excited He atoms. It was also seen that the He metastable state was severely quenched by adding hydrogen to the helium gas, but nevertheless, when the

dx.doi.org/10.1021/ac3031459 | Anal. Chem. 2013, 85, 670−704

source was used to analyze a dye, an improvement of nearly a factor 2 was found for the sensitivity of the signal.

Mezei et al. studied a low pressure GD with a Cr metal cathode, operated in various gas atmospheres, including helium, ambient air, and water vapor.[221] This study was intended to better understand the behavior of the electrolyte cathode atmospheric glow discharge (ELCAD), one of the first GD sources for liquid analysis, developed by the authors in 1993. It was found that in the helium and ambient air atmospheres, the Cr line intensities all peaked near the cathode, but when operated in water vapor, the Cr−I resonant line disappeared, whereas the intensity of a Cr−I nonresonant line was enhanced. This was attributed to resonant energy transfer collisions between vibrationally excited OH radicals and excited Cr atoms. Similar energy transfer processes are expected to take place in the ELCAD, explaining the zero intensity of the Cr resonant lines in this type of discharge. Moreover, the results in this paper showed that the investigated Cr nonresonant line can be used for analytical purposes in the ELCAD.[221]

Several other authors applied the ELCAD or developed different types of source designs for liquid analysis.[72,121,122,129,222−228] Shekhar et al. applied the ELCAD in combination with OES as a simple, rapid, and sensitive method for the determination of mercury in hepatitis-B vaccine.[222] The accuracy of the results was within 2−9%, the analytical precision was 2−5%, and the detection limits were found to be 25 ng mL^{-1}. Huang et al. presented an alternating-current (ac) driven atmospheric pressure liquid discharge, where the electrolyte solution was also used as one cathode, like in the ELCAD.[72] The pressure system could be operated at low flow rates in the range of 0.1−0.8 mL min^{-1}, which is considered as a clear advantage. The effects of the discharge electrolyte anion, the pH, and solution flow rate on the emission signals were investigated. Kitano et al. presented a highly sensitive liquid-electrode plasma OES system by combination of a quartz glass chip and a sample flow system.[129] The sample solution was put into a microfluidic channel, made narrower in the center. When applying high voltage pulses at both ends of the channel, the sample evaporates at the narrow part and generates plasma. The limits of detection were investigated for various conditions of accumulation time, material of the chip, and sample flow. Jamroz et al. reported on a dc APGD operating in open air and generated in contact with a flowing small size liquid cathode at a flow rate of 0.6 mL/min. The analytical performance of this device was tested for samples of tea and its infusions and mineral water.[223] Another type of liquid-film DBD OES source was developed by He et al.,[122] for the elemental determination of microsamples. The source consists of a Cu electrode, a W wire electrode, and a piece of glass slide between them, serving as the dielectric barrier as well as the sample plate. The sample solution is deposited on the surface of the glass slide, forming a thin liquid film. An ac voltage is applied, generating a plasma between the tip of the W wire electrode and the liquid film surface. The analytical characteristics of this source were determined. The authors pointed out several advantages compared to other liquid discharge systems, including the small sample volume, high-throughput analysis, and avoiding a sample flow system.

Franzke and co-workers also developed a miniaturized atmospheric pressure DBD, or dielectric capillary barrier discharge, for the detection of metals dissolved in liquids, by means of OES.[121,224] Extremely low sample volumes were required, because of the very low flow rates of ∼1 μL/min.[224] The plasma was formed inside a fused silica capillary between a flowing liquid surface and a tungsten electrode. The discharge appeared to be quite stable and could be sustained in the range of 1 h and more. This achieved stability, in combination with the low flow rate, opens perspectives as a monitoring device in flow systems or coupling with microseparation devices.[121]

Finally, Marcus and co-workers published some interesting work on liquid analysis.[225−228] In ref 225, a commercially available gas chromatography mass spectrometer (GC/MS) was converted into a liquid chromatography particle beam (LC-PB) GDMS system. The nebulization characteristics as well as the GD source temperature and plasma conditions were optimized relative to caffeine (test compound) responses, and the optimized conditions were comparable to similar work performed earlier by the authors. Detection limits were found in the ng mL^{-1} range. In ref 226, caffeic acid derivatives in echinacea extracts were analyzed by the authors with their LC−PB/MS system, employing both electron impact and GD ionization sources. The mass spectra obtained provided clear and simple molecular fragmentation patterns for each of the target analytes, and absolute detection limits were determined to be at subnanogram levels. In ref 227, a new liquid sampling (LS)-APGD ionization source was presented, for the elemental MS analysis of aqueous solutions, operating at low power (<5 W). The surface of the liquid emanating from a glass capillary, with a typical flow rate of 100 μL/min, acts as the cathode of the dc GD. This new source was connected to a commercial Orbitrap MS, i.e., mounted in place of an electrospray ionization source, without any other modifications. It was suggested by the authors that this new LS-APGD source can be a practical alternative to the existing high power (>1 kW) plasma sources typically employed for this application, especially when cost, simplicity, or integrated elemental/molecular analysis are important.[227] A parametric evaluation of the role of discharge current, solution flow rate, Ar sheath gas flow rate, and ion sampling distance for this LS-APGD ionization source was performed in ref 228, and preliminary limits of detection were established. It was reported that the overhead costs of this source operation, i.e., ∼10 W dc power, <50 μL/min solution flow rate, and <10 mL/min gas flow rate, are very attractive, making this source indeed a practical alternative to ICP sources.

Hence, it is clear that several different source designs are presented by the various authors. However, it is not always clear to us how much (some of) these new source designs really differ from each other. The authors often claim that their design allows smaller solution flow rates than previous designs, but this seems now the case for most of these new source designs. In our opinion, it would be more beneficial if the various groups active in this field, instead of developing new source designs, agree on a kind of standard design (e.g., an improved ELCAD design or LS-APGD), on which they collaborate to improve the analytical capabilities, among others by performing more fundamental studies, as was also done a few decades ago for rf gas discharges used in microelectronics applications (the so-called GEC reference cell).

For gas analysis, several new source designs were developed as well,[229−231] and the same comment applies also here. Li et al. presented a DBD molecular emission spectrometer, which showed promising applications as a multichannel GC detector for halohydrocarbons.[229] The performance of this method was evaluated by the separation and detection of a model mixture of chlorinated, brominated, and iodinated hydrocarbons, and a completely resolved identification was achieved by taking advantage of both chromatographic and spectral resolution.

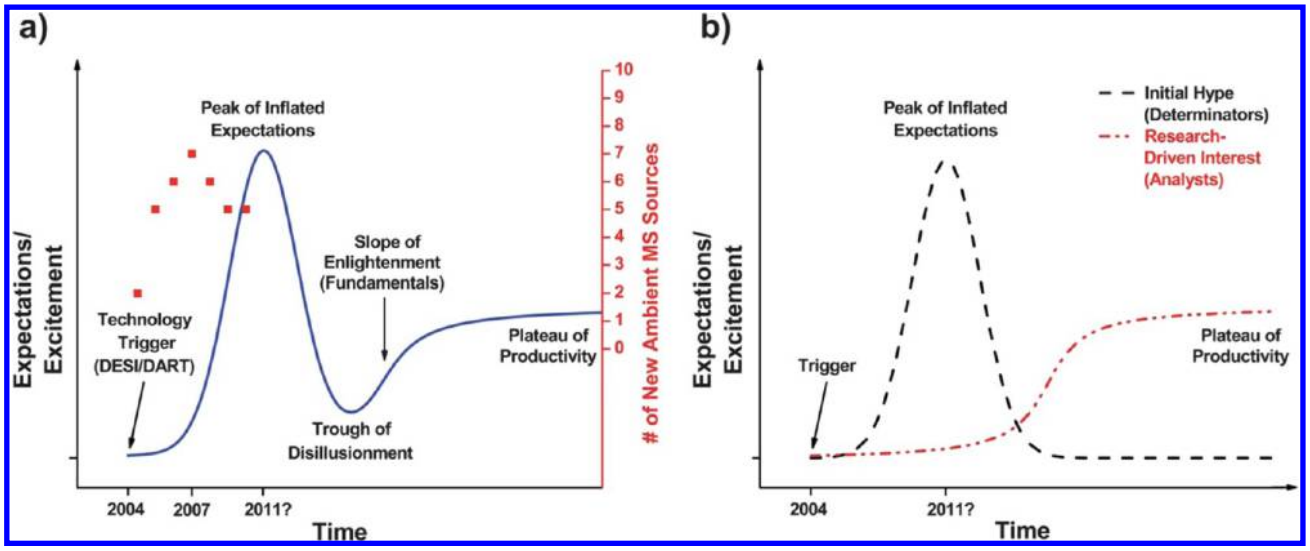

Figure 6. (a) Gartner "hype cycle" model (blue curve), indicating the five phases of a new technology, and formatted by Shelley and Hieftje[232] for the case of ADI-MS. The technology trigger was the introduction of desorption electrospray ionization (DESI) and direct analysis in real time (DART) in 2004. The red symbols show the number of new ADI-MS sources introduced each year. (b) Two factors that are responsible for this hype cycle. The initial hype (black curve) is caused by immediate human reaction to a new technology, without knowledge of the fundamental limitations. Research-driven interest (red curve) occurs independently of the initial hype and is guided by fundamental research. There should be overlap between both curves to avoid complete abandonment of the technology. Reprinted with permission from ref 232. Copyright 2011 Royal Society of Chemistry, and from "Mastering the Hype Cycle: How to Choose the Right Innovation at the Right Time" by Jackie Fenn and Mark Raskino. Harvard Business Press, 2008. Copyright 2008; all rights reserved.

Franzke and co-workers presented a low-cost microhollow cathode discharge (MHCD) for gaseous atomic emission spectrometry, for application as an analytical microplasma gas detector.[230,231] The setup combines the advantages of a hollow cathode geometry in a miniaturized system, offering atmospheric pressure operation. The plasma was driven by a rf generator, reducing the electrode sputtering by a factor of 6.5 compared to common dc operation, leading to an extension of the lifetime of the microplasma chip. The analytical results indicated that this microplasma chip might be suitable for lab-on-a-chip application.[230] In ref 231, a further improvement was proposed, where the plasma was formed inside a microfabricated multilayer structure with a dielectric barrier (DB). The insulation of the electrodes by the dielectric layer prevents deterioration of the electrodes and furthermore eliminates contamination of the gaseous analyte with electrode material. This enables long-term operation of the DB-MHCD over several days. The analytical performance was demonstrated with halogenated hydrocarbons, showing excellent detection limits.[231]

An emerging field for the analysis of either gaseous but also solid compounds is so-called ambient desorption/ionization mass spectrometry (ADI-MS). Sample pretreatment and separation steps are eliminated here by directly desorbing and ionizing analytes from a sample surface, for analysis by mass spectrometry. Shelley and Hieftje published a very interesting perspective article about ADI-MS.[232] They reported that the field had gained significant interest since its introduction in 2004. However, the response seems to follow a so-called "hype cycle" model and is currently at its peak, to be followed by a drop in interest (the so-called "trough of disillusionment"), which could destroy the field. To avoid this, the authors stated that much effort must be put into a more fundamental understanding of the underlying processes,[232] which is very true in our opinion. Figure 6 illustrates this "hype cycle" model, indicating the different phases as well as two factors that are responsible for the formation of this hype cycle.[232]

One of the problems ADI-MS is facing is that it suffers from matrix effects. Therefore, Shelley and Hieftje investigated ionization-related matrix effects in three plasma-based ADI-MS sources, i.e., the flowing atmospheric pressure afterglow (FAPA), direct analysis in real time (DART) and the low temperature plasma (LTP) probe, which is based on a DBD design.[233] The FAPA was found to be the least susceptible to ionization matrix effects in every case, but when the proton affinity of the matrix species was lower than that of the analyte, no matrix effects were observed at all for DART, whereas an effect persisted for both FAPA and LTP. The paper demonstrated the importance of matrix effects for both qualitative and quantitative analyses with ADI-MS. Furthermore, because only ionization processes were considered in this study, the matrix effects in ADI-MS will probably be even more severe, and this will be studied in future work by the authors. Kratzer, Mester, and Sturgeon also compared three plasma-based ambient pressure sources, i.e., a laboratory built DBD, an rf-driven APGD, as well as a commercial DART source, for ADI-MS of acetaminophen.[234] It appeared that the desorption and ionization mechanisms were identical for this analyte, for the three plasma sources. Furthermore, helium was reported to be the best plasma gas, providing 100−1000-fold higher analyte response than with argon or nitrogen. The analyte signal in the MS correlated with the ion density in the plasma and with emission intensity from the excited species, supporting an ionization process by proton transfer from protonated water clusters to analyte molecules. In ref 235, Hieftje and co-workers carried out a fundamental characterization of the LTP probe. Maps of the reactive species, created in both the plasma and the afterglow, were recorded. This allowed one to deduce the origin of impurities important in mass spectrometric analysis, such as N_2, O_2, and H_2O. The dominant mechanism of excitation for both N_2 and N_2^+ was found not to be through electron impact, but the excited N_2 molecules are most probably formed by electron-N_2^+ recombination. Electron number densities and rotational temperature were also determined. The effect of

dx.doi.org/10.1021/ac3031459 | Anal. Chem. 2013, 85, 670−704

plasma parameters on emission spectra was correlated with mass spectra results previously reported for the same ionization source. Finally, completely different gas-phase chemistry was observed when argon was used as the plasma gas, instead of helium. It was concluded that the excited state chemistry of helium is crucial for the creation of reactive nitrogen species.[235]

Some combinations of GDs, operating either at atmospheric or reduced pressure, with laser ablation (LA) or ICPMS were reported as well.[145,236−239] Xing et al. combined a LTP probe with ICPMS for depth profiling analysis of nanometer coatings.[236] The sample material was ablated by the LTP, with a diameter of several tens of micrometers, and converted into an aerosol, and subsequently transported to the ICPMS. A lateral resolution of 200 μm was achieved, and depth profiling of a 100 nm single layer sample and a multiple layer sample (with layer thicknesses in the 50−250 nm range) has been successfully performed. It was concluded that this method offers unique advantages in terms of high spatial resolution, fast analysis, and ease of implementation, and it may be considered as an alternative to existing depth profiling methods, such as GDMS/GD-OES and SIMS. Carado et al. described the use of a compact LS-APGD ionization source to ionize metal particles within an LA aerosol.[237] The LS-APGD source generated a low-power plasma between the surface of an electrolyte solution flowing through a fused silica capillary and a counter electrode consisting of a stainless steel capillary, which was used to deliver the LA particles to the plasma. The LA particles of ∼100 nm were generated with a femtosecond laser. An orbitrap mass analyzer, capable of producing mass resolution exceeding $m/\Delta m$ 160 000, was employed. Results from a LA depth profiling experiment revealed retention of the relative locations of the ∼10 μm layers.

Finally, LA has also been combined with low pressure GDs, operating in the pulsed regime.[145,238,239] Kexue et al. combined LA with a fast pulse discharge plasma.[145] The discharge was used to reheat the laser plasma and to enhance the plasma emission. The precision of the measurements and the signal-to-noise ratio were also improved. Günther and co-workers[238,239] combined LA with a millisecond-pulsed GD-TOF-MS, for quasi-simultaneous elemental and molecular analysis of organic materials and polymers. The laser ablated material was introduced into two different temporal regimes of the pulsed GD, i.e., the plateau and afterglow region. In this way, complementary elemental, structural, and molecular information was obtained within one single discharge pulse. Indeed, the elemental ions and fragments were recorded during the plateau region, whereas the protonated molecular ions were detected in the afterglow, allowing chemical speciation of the analyte. To demonstrate the analytical potential of LA-GD-TOF-MS, analysis of commercially available pharmaceutical tablets was carried out.[238] In ref 239, the authors compared the LA-GD-TOF-MS results with matrix-assisted laser desorption ionization (MALDI) spectra. The sensitivity of this prototype LA-GD-TOF-MS was still lower than the commercially available MALDI-TOF-MS system, and therefore, some technical details to increase the sensitivity were discussed. Nevertheless, the authors concluded that the LA-GD offered tunable ionization and provided reduced matrix dependence.[239]

INDUCTIVELY COUPLED PLASMA MASS SPECTROMETRY

The increasing demand for high sample throughput in routine analysis and the need for highest possible sensitivity and precision combined with fast and preferably simultaneous multielemental detection capabilities are still the driving forces for developments in the field of elemental mass spectrometry. Remaining ionization source- and spectrometer-related shortcomings are the major subjects of modern research. As a result, different mass spectrometric techniques in combination with various sample introduction techniques, as well as instrumental developments concerning multicollector, sector field, time-of-flight, and alternative mass analyzers were predominant focal points of the research conducted within the period covered by this review article, although most of the published material mainly deals with applications of inductively coupled plasma mass spectrometry (ICPMS). Different approaches for the introduction of liquids, through sample nebulization or in combination with chromatographic and electrophoretic separation techniques were investigated. Most notably, the acceptance of laser ablation (LA) coupled to ICPMS as a technique for direct analysis of solid samples has continued to increase substantially during the last 2 years. Also, high-resolution multiple collector sector field ICPMS has significantly expanded in the field of isotope analysis. In contrast, a further decreasing number of novel or fundamental studies using collision and/or reaction cells for the specific removal or reduction of polyatomic ions was recognized, although many applications are still being published especially in the field of the analysis of biological material and environmental samples. This indicates that ICPMS has matured and has without a doubt by now become a routine method for elemental analysis, which is also the case for hyphenated techniques for speciation and bioanalysis, e.g., structure determination of organometallic species.

This section deals with new developments in ICPMS in the field of fundamental studies, instrumental developments, and applications that have been reported since the last update.[5] It should be mentioned, that the selection of papers was once again quite difficult, due to the increasing number of ICPMS publications, and it represents a somehow subjective choice of manuscripts dealing with only new applications employing new methodologies, since papers, exclusively focusing on the application of ICPMS are thoroughly treated in alternative review articles.[240] In addition to the journals mentioned in the first section of this article, the following periodicals were considered for the selection of the papers: *International Journal of Mass Spectrometry*, *TRAC, Trends in Analytical Chemistry*, *Rapid Communication in Mass Spectrometry*, *Journal of the American Society for Mass Spectrometry*, *Mass Spectrometry Reviews*, *Proteomics* and *Metallomics*.

Engelhard[241] reviewed some recent trends and developments in ICPMS, with special focus on instrumental development and emerging applications. Some trends were highlighted, including a recently developed novel mass spectrometer for elemental and speciation analysis in Mattauch-Herzog geometry with a focal-plane-camera array detector for the simultaneous recording of the full elemental mass range. Monitoring fast transient signals in chromatography or laser ablation was found to be now possible and, e.g., for isotope ratio analysis. Additionally, instrumental developments were reported that allow the direct analysis of microparticles and single cells. In a series of two critical review papers on ICP and GD sector field mass spectrometry, Jakubowski et al. focused on both the fundamentals and instrumental developments[242] as well as on applications.[243] Also possible future trends and developments were identified by the authors. In an article by Beauchemin,[244] numerous ways in which ICPMS has been used for the analysis of environmental samples since it was commercially introduced in 1983 were reviewed. Diverse sample preparation techniques, calibration strategies, matrix effects, and possible (non-) spectroscopic interferences were addressed and

dx.doi.org/10.1021/ac3031459 | *Anal. Chem.* 2013, 85, 670−704

the characteristics and analytical figures of merit of various methodologies employing different mass analyzers were outlined. In a focal point review article, Pröfrock and Prange provided an overview of recent developments and capabilities of ICPMS coupled with different separation techniques for applications in the fields of quantitative environmental and bioanalysis.[245] Technical improvements were highlighted, and the benefits and possibilities of using state-of-the-art hyphenated ICPMS approaches for quantitative analysis were discussed. Fundamental research on nonspectroscopic (matrix) interferences in ICPMS using nebulization as a sample introduction technique was critically examined in a review by Agatemor and Beauchemin.[246] Fundamental processes were discussed that may be a source of matrix effects during sample introduction, ion generation in the ICP, ion extraction through the interface, and ion transport through the ion optics to the detector. Various methods for attenuating matrix effects were also reviewed and illustrated with some examples. Instead of exhaustively reviewing the literature, the authors decided to rather use representative references to comprehensively describe the main issues, several of which are also common to ICP-OES.

As a result of rapid instrumental development, the application field of isotopic analysis by means of ICPMS is also continuously growing, especially in the field of provenance determination. A comprehensive paper by Vanhaecke and co-workers[247] reviewed such developments in and the recent applications of isotopic analysis in the above-mentioned research field. In the authors' opinion, multicollector (MC) ICPMS can nowadays be seen as a very strong competitor of thermal ionization mass spectrometry (TIMS), while it even provides information on the small isotopic variations shown by, e.g., elements with a high ionization energy that are not or hardly accessible by means of TIMS.

A review on the hyphenation of chromatography-based techniques to MC-ICPMS for isotopic studies that were published until the end of 2010 was presented by Rodriguez-Gonzalez et al.[248] A brief historical retrospective of the measurement of isotope ratios from transient signals by ICPMS with different sample introduction techniques was also outlined and the most important experimental parameters and data reduction strategies affecting the accurate and precise measurement of compound-specific isotope ratios by either HPLC or GC coupled to MC-ICPMS were discussed. The presented applications were critically reviewed in terms of analytical characteristics, performances, optimization, advantages and disadvantages, and future applicability to the environmental, geochemical, or bioinorganic studies. Easter et al.[249] have given an overview on recent developments and novel applications in ICPMS hyphenated to gas chromatography (GC) with special emphasis on solid phase microextraction. New explorations in the analysis of the traditional metal species, as well as novel applications of species of non-traditional elements, were also presented.

Haider et al. have critically reviewed the applications based on the online hyphenation of gel electrophoresis (GE) with ICPMS and have outlined the advantages and limitations of the technique for various applications and its potential in proteomics, genomics, and metallomics.[250] It was concluded that GE-ICPMS is a powerful tool for simultaneous separation, detection, and quantification of biomolecules, which has so far been applied to the determination of P in DNA, phosphoproteins, and phosphopeptides, Au in nanoparticles, Fe in metalloproteins, I in aerosols, and cisplatin−oligonucleotide interactions. In a review article by Bettmer,[251] recent developments and applications in the field of quantitative protein analysis were highlighted and critically assessed. The author concluded that both the detection of heteroatom-containing proteins and the artificial introduction of metal-containing labels have attracted much attention in current research, in which ICPMS-based isotope dilution techniques have developed into a useful quantification tool in proteomics.

Fundamental Studies. In two very interesting fundamental studies, Houk and co-workers have focused on the measurement of gas kinetic temperatures (T_{kin}) for polyatomic ions[252] and on the determination of the dissociation temperature for ArO^+ in ICPMS.[253] The authors examined various mathematical refinements to the calculated partition functions for their effect on the determined temperatures. In the case of T_{kin}, it was found that excited electronic states should be included for ArO^+, neutral NO, and O_2 and, interestingly, that a 10% error in solvent load, sample gas flow rate, vibrational constant, rotational constant, or measured ion ratio results only in a 1−3% error in T_{kin}. On the other hand, a 10% error in dissociation energy produces an error of approximately 10%. Surprisingly, high temperature corrections to the partition functions were found to produce a minimal change and can in the authors' opinion generally be neglected. The group also applied the method of comparing experimental and calculated ion ratios to determine T_{kin} characteristic of the origin of a polyatomic ion in ICPMS to ArO^+. The same group has carried out measurements of the abundance of metal argide (MAr^+) ions during the ablation of pure samples of transition metals in LA-ICPMS.[254] The abundance of such ions relative to M^+ ions for various elements was found to increases as the dissociation energy of the ion increases. T_{kin} were determined from the calculated MAr^+/M^+ ratios and were then used to indicate the origins of MAr^+ ions. The calculated T_{kin}-values are in the range of 8 000 K to ≥20 000 K, which indicate that MAr^+ ions are much less abundant in the mass spectrum than expected based upon plasma conditions, which might be due to collision-induced dissociation during the ion extraction process. Furthermore, the same group suggested that a better understanding of the origin of polyatomic ions in LA-ICPMS and their behavior in mixed gas plasmas might help to minimize polyatomic interferences in the ICPMS.[255] Thus, differences in the origins of polyatomic ions in wet plasma conditions versus dry plasma conditions were investigated and oxide ratios were measured while additional gases were introduced into the carrier gas. It was found that N_2 decreases the MO^+/M^+ signal ratio by maximizing atomic sensitivity at lower total gas loads, while the addition of He reduces polyatomic ions throughout the plasma.

In a study by Taylor and Farnsworth,[256] an experimental characterization of the effect of skimmer cone design on shock formation and ion transmission efficiency in the vacuum interface of an ICPMS was carried out. Laser-induced fluorescence has been used to evaluate five commercially available skimmer cone designs. The efficiency was measured as the ratio of analyte density downstream from the skimmer tip to analyte density upstream from the tip. The strongest shock was recorded for a skimmer with a cylindrical throat, and the weakest shock was produced by the skimmer with the largest diameter and a conical throat. Transmission efficiency increased with increasing orifice diameter. Coulombic effects, revealed in a comparison between the behaviors of neutral barium atoms and barium ions, were found to be small. A comprehensive computational study on the effect of an MS interface on the characteristics on the ICP as ion source was performed by Aghaei et al.[257] Typical plasma characteristics, such as gas flow velocity, plasma temperature, and electron density, were calculated in two dimensions and were compared with and without an MS sampling interface. The

dx.doi.org/10.1021/ac3031459 | Anal. Chem. 2013, 85, 670−704

results from the proposed model were found to be in good agreement with experimental data reported in the literature. As expected, a dramatic increase in the plasma velocity was reported in the region close to the interface and a cooled metal interface was found to lower the plasma temperature and electron density on the axial channel close to the sampling cone, while increased corresponding values were assigned to the off axial regions. It was concluded that the effect of the interface strongly depends on the measurement position and even a small shift from the actual position of the sampler leads to a considerable change of the investigated values.

Agatemor and Beauchemin suggested the use of argon−nitrogen mixed-gas plasma for the reduction of matrix effects in ICPMS.[258] Furthermore, improved detection limits were observed for Al, Co, Pd, and V with the optimized mixed-gas plasma compared to an argon plasma at maximum sensitivity. The robustness of this mixed-gas plasma was further demonstrated through the accurate determination of U and Mo in a seawater certified reference material using a simple external calibration, without matrix-matching or internal standardization. The use of spatial profiling results in a better energy transfer between the toroidal zone, and the central channel in the mixed-gas plasma was suggested. Gackle and Merten[259] have studied the plasma parameters influencing fractionation in LA-ICPMS and reported on the development of methods permitting to test the influence of the matrix as well as of its local and temporal distribution on the plasma conditions. For this purpose, the MS interface was used as a plasma probe allowing one to investigate the average plasma condition within the ICP zone observed in terms of temporal and spatial distribution of the matrix. It was found that inserted matrix particles can cause considerable changes in both electron density and plasma temperature, thus influencing the ionization equilibrium of the individual analytes. It was shown that the deviation of the intensity ratio from the concentration ratio increases with a larger difference between the ionization potentials of the analytes, decreasing plasma temperature, and higher matrix concentration.

In two very interesting papers, an investigation was given of the influence of the design and the operating parameters of pneumatic nebulizers on the aerosol characteristics and ICPMS performance. Geertsen et al.[260] described the development of a very simple microflow pneumatic nebulizer based on a commercial glass concentric slurry nebulizer and a fused-silica capillary. The "liquid-capillary-tip to gas-exit stick-out " parameter was found to be of crucial importance both for the primary spray homogeneity in terms of droplet velocity distribution and for tertiary signal intensity and stability; however, no influence on the oxide ratio or on the droplet size distribution was found. The beneficial use of a flat-end-capillary instead of a commonly used tapered end was outlined, and the existence of an optimum nozzle configuration in terms of sensitivity and stability, which is dependent on the capillary inner diameter, was presented. Todoli and coworkers[261] comprehensively compared 26 nebulizers regarding their characteristics and their achievable ICPMS sensitivities. In total, 17, 6, and 3 different nebulizers of A-, C- and K-type were included in this study. For a given nebulizer design, the gas exit cross-sectional area has been shown to critically influence the aerosol characteristics. The aerosol generation mechanism has been explored, and it has been concluded that for A-type nebulizers the nebulization is more efficient than for C and K-type ones. It has been observed that sample capillary was not perfectly centered with regard to the gas exit bore for several nebulizers. The authors suggest that spray chambers equipped with impact beads may be used to minimize the problems associated with this bad alignment but to the detriment of the sensitivity.

In LA, the characteristics of the gas flow through the ablation cell is of outstanding importance for an efficient and rapid aerosol wash out. Therefore, Asogan et al.[262] have performed numerical simulations of gas flows through an open, noncontact cell. The investigated cell consists of dual, annular, concentric microjet gas arrays to entrain ablated material (the carrier flow) and exclude atmosphere (the curtain flow). It was shown that the design of the cell affords a very high degree of exclusion of atmospheric gases, using a relatively low curtain flow of 2.5 L min^{-1} with a carrier flow of 1.2 L min^{-1} He. The efficacy of the microjet arrays in providing an axially symmetric exclusion zone was demonstrated with minimum particle transit times through the cell of the order of 50−100 ms. Frick and Günther[263] have performed an interesting fundamental study on the ablation behavior of carbon in LA-ICPMS with respect to the suitability as an internal standard, driven by the need to develop suitable calibration standards for biological and medical applications. The authors state that although the applicability of carbon as an internal standard has already been in dispute over years, its behavior during LA is still not sufficiently understood. Thus, 12 common carbon matrixes were investigated, using a gas exchange device to study the formation of C-containing gaseous species (CCGS) during LA. A matrix-dependent partitioning of carbon into CCGS and carbon containing particles was observed while trace element analytes are exclusively transported as the particulate phase. The production of CCGS was also found to critically depend on the presence or absence of oxygen and the affinity of matrix constituents toward oxygen.

The emerging field of nanomaterial analysis was addressed by Olesik and Gray[264] through the discussion of unique considerations to determine the number of particles per liter and analyte mass distributions from single particle ICPMS measurements with quadrupole or sequential sector field ICPMS. As expected, the short, transient nature of signals from single particles was found to affect the optimum selection of dwell times and pulse counting versus analog detection. The signal peak width due to a cloud of ions produced from a single particle also limits the maximum number of single particles that can be accurately measured in a given total measurement time and the dynamic range of the particle number concentration. The authors also concluded that the range of analyte mass measurements is limited by the rates of vaporization and diffusion. Approaches to calibrate the number of particles detected as a function of the number of particles per mL and to calibrate the signal from a single particle as a function of analyte mass were discussed. Flamingi et al.[265] reported on the visualization, velocimetry, and mass spectrometric analysis of engineered and laser-produced particles passing through the load coil region of ICP sources. Modifications of the ICP operating conditions such as plasma power, gas flow rate, and torch injector diameter were found to significantly influence the gas velocity if helium is admixed in excess of >50% of the total gas flow passing through the injector. The analyses of laser-produced aerosols carried out at constant volumetric flow rates but reduced injector diameters resulted in decreased signal intensities of elements such as Y, Ce, or U by up to 2 orders of magnitude suggesting incomplete particle evaporation as well as notably different aerosol penetration depths. Sensitivities measured in this case turned out to correlate with boiling points of the respective oxides rather than the element-specific ionization potentials commonly observed. The mechanisms controlling

dx.doi.org/10.1021/ac3031459 | Anal. Chem. 2013, 85, 670−704

gas velocity and sensitivity variations were discussed, and consequences on LA-ICPMS analyses were presented.

Instrumental Developments and Applications. The novel instrumental concept of a mass spectrometer in combination with solid-state charge-detection array, the focal-plane camera (FPC), was presented by Hieftje and co-workers. The so-called distance-of-flight mass spectrometer (DOFMS) is a velocity-based mass-separation technique in which ions are separated in space along the plane of a spatially selective detector. The mass-to-charge ratio of ions is thus determined by the distance each ion travels during a fixed time period. This necessitates the use of a position-sensitive detector to simultaneously record the mass spectrum.[266] The use of such an FPC detector resulted in improvements in analytical performance, usability, and versatility over a previous generation instrument that employed a microchannel-plate/phosphor detector. The achievable mass resolution was also improved by at least a factor of 2.[267] The merits of solid-state detection for DOFMS were evaluated, and methods to extend the DOFMS mass range were considered.

Sensitive and preferably interference-free quantification is a major need in the field of ICPMS analysis. Fernandez et al.[268] presented the first study using a novel triple quad ICPMS (ICPQQQ) as a tool for polyatomic interference removal applied to absolute quantitative proteomics and phosphoproteomics. The novel system is based on the concept of tandem mass spectrometry (QQQ) typically used in molecular MS. The authors operated the first quadrupole as a 1 amu window bandpass mass filter to select target analyte ions allowing only selected ions to enter the cell and to react with O_2, reducing the interferences produced by matrix ions as well as background noise. After optimization of the cell conditions, product ions were detected allowing lowest detection limits ever published for the HPLC−ICPMS analysis of S- and P-containing species (11 and 6.6 fmol, respectively).

Rappel and Schaumlöffel[269] described a novel nanonebulizer (nDS-200e) with extended liquid flow rate range for ICPMS sample introduction from 50 to 4000 nL min^{-1}. It was found to be more robust and less prone to clogging compared to the formerly presented prototype design, and the stability of the sample introduction was demonstrated by low relative standard deviations between 2 and 4% at flow rates above 200 nL min^{-1}. The nanonebulizer combined with a single-pass spray chamber was used as a multifunctional interface for sheathless and sheath flow nanoHPLC−ICPMS coupling, including the postcolumn addition of an internal standard. A novel system based on the thermal inkjet principle and the use of modified thermal inkjet cartridges for the introduction of liquid samples into analytical plasmas was presented by Bings and co-workers for the first time.[7] The proposed "drop-on-demand" (DOD) aerosol generator employs a lab-built microcontroller, which allows accessing all parameters important for driving the dosing cartridge for the generation of picoliter-droplets from sample volumes in the microliter range. The droplet generation frequency, thus the resulting liquid flow rate of the device, is variable over a wide range from the generation of isolated droplets up to a flow rate of several μL min^{-1} mostly limited by the thermal resilience of the heating filament of the dosing device. Figure 7 shows a cascade of droplets ejected during a single dosing event as a result of the breakup of the liquid jet into individual droplets of a highly reproducible volume. In the presented study, the flow rate was investigated in the range from 20 nL min^{-1} to 6.3 μL min^{-1}, and a calibration strategy based on the droplet generation frequency instead of on the use of standard solutions of different

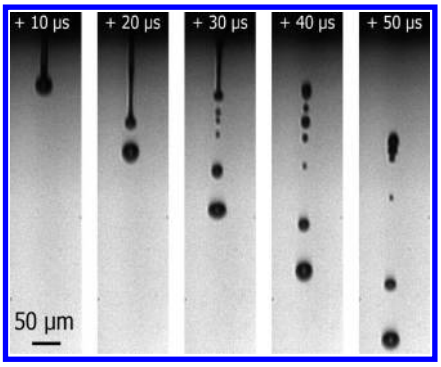

Figure 7. Photographic images (10 μs time shift) of a cascade of droplets ejected from the thermal inkjet-based "drop-on-demand" aerosol generator during a single dosing event, as described in ref 7.

concentrations was presented. The new system is characterized, and the achievable analytical figures of merit of such a DOD aerosol generator coupled to a quadrupole ICPMS are outlined and compared to a commercially available pneumatic low-flow MicroMist nebulizer. Superior sensitivity by a factor of 8−18, improved limits of detection, and better background equivalent concentrations for the investigated elements were found for the new system. The achievable precision in multielemental DOD-ICPMS analysis was comparable to the data gained with the corresponding commercial system. In a subsequent study, the independent operation of two sampling nozzles was investigated, which expands the system capabilities to independent dosing of two liquids simultaneously into the carrier gas stream of an ICPMS.[270] The applicability of the proposed dual-DOD (dDOD) ICPMS method to the analysis of real urine samples was outlined. Its susceptibility to matrix effects was studied through 2-D ion distributions within the ICP for different matrixes. A calibration strategy for ICPMS based on the dosing frequencies of the dDOD (dosing frequency-based calibration, DFC) and its application to trace metal analysis in microvolumes of real samples with high matrix content were presented. Using this method, Li, Sr, Mo, Sb, and Cs were accurately determined in the concentration range of 8−122 μg L^{-1} in urine reference material. The advantages of the DFC, e.g., minimum sample and analysis time consumption, were outlined and the quality of the achievable results with respect to accuracy and precision was critically discussed. All analytical data were again compared to those obtained with a conventional MicroMist nebulization system in combination with ICPMS using classic calibration procedures.

An approach for ICPMS sample introduction using diode laser thermal vaporization (DLTV) was evaluated by Foltynova et al.[271] Laser power was sufficient to induce pyrolysis of a suitable substrate with the deposited sample leading to aerosol generation, and it was concluded that the method allows quantitative determination of metals in submicroliter volumes of liquid samples. Unlike existing sample introduction systems based on laser ablation, the presented system uses a NIR diode laser rather than an expensive high-energy pulsed laser. The limits of detection for Co, Ni, Zn, Mo, Cd, Sn, and Pb deposited on the preprinted paper were found to be in the range of 0.4−30 pg. The method was characterized, optimized, and applied to the determination of Co in a drug preparation, Pb in whole blood, and Sn in food samples without any sample pretreatment.

Elemental Speciation, Analysis of Biological Samples and Nanomaterials. The number of applications of elemental

dx.doi.org/10.1021/ac3031459 | *Anal. Chem.* 2013, 85, 670−704

speciation analysis using ICPMS has again increased significantly during the recent years, which is due to the analytical characteristics of the ICPMS, such as, e.g., extremely low detection limits for almost all elements, the possibility for multielemental analysis, and the possibility to apply isotope dilution mass spectrometry. It was reported by Popp et al.[272] that two methodological approaches, i.e., HPLC− and GC−ICPMS, dominate the field. Not just the investigation of metals and metalloids and their species (e.g., Sn, Hg, As) representing "classic" elements in environmental science, but recently other elements (e.g., P, S, Br, I) amenable to ICPMS determination were addressed. In addition, the introduction of isotope dilution analysis and the development of isotopically labeled species-specific standards have contributed to the success of ICPMS in the field. These developments were reviewed, and current trends in the application of ICPMS coupled to GC and HPLC for environmental analysis were outlined.[272] Recent strategies of sample preparation were described and discussed by Mesko et al.[273] for biomolecules separation/extraction for further metal(oid) or metal(oid)-containing compounds determination by ICPMS. Various examples for the determination of metals and metaloids in animal and plant tissues, fluids, and related samples reported in the last 15 years were described. The authors included a review of nonconventional sources of energy for sample preparation, especially those related to ultrasound and microwaves but also focused on extraction and solubilization procedures, derivatization, preconcentration, cleanup, and also digestion for total metal analysis.

Complementary molecular spectrometric tools are often required for a complete identification of macromolecules in the field of speciation studies. Thus, an increased research effort can be observed focusing on the development of integrated instruments to carry out the complete chemical speciation within a sample using a single instrument. Sanz-Medel and co-workers[274] have reviewed the use of complementary techniques operating in parallel after splitting to a single chromatographic separation providing simultaneous elemental and molecular information. Also, instrumental developments involving the use of stationary plasma sources operated in nontraditional modes were also discussed, and the capabilities of tunable plasma-based ionization sources as a relatively simple and cheap approach were revised. In a recent review by Dressler et al.,[275] the progress achieved during the last 10 years in the area of As, Hg, I, Sb, Se, and Sn speciation in biological tissues and body fluids was outlined. Applications of other hyphenated techniques than LC−, GC−, and CE−ICPMS were also included but to a lesser extent. Relevant applications of methodologies used for species specific determination of the aforementioned elements in biological tissues and body fluids were highlighted.

In an interesting study, Horner and Beauchemin[276] investigated online continuous leaching and ion exchange chromatography coupled to ICPMS for the speciation analysis of bioaccessible As in rice. The presented method was found to offer several advantages over commonly used batch methods including quicker and easier sample preparation, reduced risk of contamination, and access to real time leaching data. Results from a certified reference material as well as cooked and uncooked white rice showed that the majority of As was leached by saliva. Results obtained using the continuous online leaching method were comparable to those obtained using a batch method. Speciation analysis of the saliva leachate was performed using ion exchange chromatography coupled to ICPMS allowing one to separate the four most toxic forms of As (As(III), monomethylarsonic acid, dimethylarsinic acid, and As(V)) within 5 min in a single chromatographic run. Ito et al.[277] developed and validated a LC−ICPMS method for routine monitoring of arsenobetaine in whole blood and urine in addition to the four aforementioned As species. The analysis was completed within 12 min in the case of whole blood and within 11 min in urine. The reported methodological detection limit is <0.3 $\mu g\ L^{-1}$ for each arsenic species. For the determination of the bioavailability in vitro of As species from edible seaweed, Garcia-Sartal et al.[278] suggested for the first time to use combined ICPMS with electrospray ionization tandem mass spectrometry with two-dimensional HPLC, namely, size exclusion followed by anion exchange. Collection of specific fractions from the size-exclusion column to be analyzed using anion-exchange HPLC−ESI-MS/MS enabled improved chromatographic selectivity, particularly for the less retained arsenosugar (glycerol sugar), facilitating confirmation of the presence of arsenosugars in seaweed extracts and dialyzates. Through this approach, the authors succeeded to confirm the presence of arsenobetaine in sea lettuce samples.

Xing and Beauchemin[279] reported for the first time on the application of a speciation analysis method involving ion exchange chromatography coupled to ICPMS to perform a kinetic study of Cr(VI) reduction in a certified reference material consisting of acidified riverine water. This water sample was spiked with Cr(VI), with or without Cr(III), and evolution of each Cr species as a function of time was monitored by speciation analysis, which showed that the reduction of Cr(VI) was a pseudo first order reaction. The reduction rate was found to increase with decreasing pH and increasing temperature.

In a study by Karst and co-workers,[280] methods were developed for the analysis of Auranofin and its adducts with endogenously available thiols. Auranofin is a Au(I)-based pharmaceutical for the treatment of rheumatoid arthritis which undergoes ligand exchange reactions in vivo to generate reactive metabolites. The species was characterized by LC−ESI-MS and LC−ICPMS, respectively, and the reactions of Auranofin with the thiols were quantitatively traced over several days by ICPMS. On the basis of the obtained data, the authors proposed a potential reaction pathway of Auranofin with the two investigated thiols.

Raju et al.[281] presented a sensitive method for the determination of different Gd-based MRI contrast agents in environmental water samples using hydrophilic interaction chromatography (HILIC) coupled with ICPMS. A study of various parameters responsible for the efficient separation was performed. The limit of quantification for all contrast agents were found to be less than 100 $ng\ L^{-1}$, which allows the developed method to be applied to the separation and determination of contrast agents in surface and wastewater treatment plant samples.

Jia et al.[282] performed the species specific determination of Hg in liquid cosmetic samples by ionic liquid based dispersive liquid−liquid microextraction combined with HPLC−ICPMS. The developed method was thoroughly optimized, and afterward a spike test was performed to verify the accuracy of the achieved results. Inorganic Hg(II) was found to be the main species in the investigated cosmetic samples.

For the first time, cellular uptake studies of cisplatin were addressed by Koellensperger and co-workers[283] through elemental speciation analysis at biological relevant concentration levels, i.e., drug exposure concentration ranging at 5 μM. The quantification of intact, free cisplatin in cell models was investigated by two complementary LC−ICPMS methods, using chromatographic separations based on pentafluorophenylpropyl siloxane bonded stationary phases and on porous

dx.doi.org/10.1021/ac3031459 | Anal. Chem. 2013, 85, 670−704

graphitized carbon. Limits of detection for cisplatin were 0.013 and 0.11 $\mu g\ L^{-1}$, respectively. Efficient protein removal was found to be a prerequisite for accurate quantification in complex biological matrix such as cell lysate and according to the presented study centrifugal filtration was the method of choice. Exposure of two different cell models to 5 μM cisplatin for 24 h resulted in cisplatin concentration levels ranging between 0.2 and 1.5 $\mu g\ g^{-1}$ protein. Despite the poor recovery of the columns regarding total Pt in filtrated samples, the accuracy of cisplatin quantification was given, which was shown via species specific isotope dilution MS and standard addition.

The coupling of size exclusion chromatography (SEC) and normal phase (NP) HPLC using entirely organic mobile phases with ICPMS were developed and investigated by Caumette et al.[284] for the molecular distribution of Ni and V in crude oils. The resolution achieved allowed the discrimination of at least three classes of Ni and V species with varying proportions of the metals as a function of the origin of crude oil, crude oil fraction, and dilution factor. The metal species in the SEC fractions were found to be sufficiently stable to be collected and preconcentrated to allow the development of a 2D chromatography SEC-NP-HPLC−ICPMS for the probing of the metal distribution in crude oils in terms of molecular weight and polarity.

Another emerging field in elemental speciation employing ICPMS is the species specific determination of brominated compounds as they are being increasingly used as, e.g., flame retardants. The separation and detection of 10 polybrominated diphenyl ethers was performed by Szpunar and co-workers[285] through the coupling of fast ultrahigh-pressure liquid chromatography with ICP mass spectrometer fitted with an octopole collision cell. The compounds were eluted within 12 min and directly introduced into the ICPMS. The LOD (as bromine) was found to be 17 ± 1 ng mL^{-1} and was independent of the mobile phase composition. The method offered, as a main advantage over molecular MS, the virtual independence of the signal intensity of the molecular structure of the compound and thus the possibility to detect unknown metabolites. Meermann et al.[286] presented the speciation analysis of metabolites in feces samples collected within a clinical study during which a bromine-containing antituberculosis drug was administered to patients with multidrug resistant tuberculosis infection. Owing to slow elimination of the drug, no ^{14}C label was used within this study. Quantification of the bromine species was accomplished using HPLC−ICPMS in combination with online isotope dilution (ID), while structural elucidation of the species was performed using HPLC coupled to ESI-MS. On the basis of the reported figures of merit, the HPLC−ICPMS approach can be applied to a human in vivo metabolism study, such that exposure of the human volunteers to the ^{14}C radiolabel can be avoided. The same group used reverse online isotope dilution in combination with HPLC−ICPMS in drug metabolism studies.[287] For quantification of the metabolites, the respective drug is traditionally synthesized with a radiolabel (^{14}C or ^{3}H) and the metabolites present in different matrixes (blood, urine, feces) upon drug administration are determined by means of high-performance liquid chromatography (HPLC) coupled to radiodetection. In some cases, the use of a radiolabeled compound in human in vivo studies is not advisible, e.g., for drug compounds or their metabolites showing a long plasma or tissue half-life. Then HPLC−ICPMS becomes a promising alternative approach. The authors presented an HPLC−ICPMS-based method combined with reverse online ID which was evaluated by the analysis of feces samples from rats dosed with a ^{81}B-labeled drug compound. The method allows for both valid quantification of the drug metabolites and distinction among endogenous, exogenous, and mixed species, based on their isotopic fingerprint. A good repeatability and limit of detection of the same order of magnitude as those observed for normal online ID HPLC−ICPMS and HPLC followed by radiodetection were achieved.

Kundel et al.[288] reported on the application of mass spectrometric techniques for trace analysis of short-lived iodine-containing volatiles emitted by seaweed since knowledge of the composition and emission rates of such volatiles from major widespread seaweed species is important for modeling the impact of halogens on gas-phase atmospheric chemistry, new particle formation, and climate. The authors presented the application of MS techniques for the quantification of short-lived iodine-containing volatiles emitted by eight different seaweeds. An online time-of-flight aerosol mass spectrometric method was used to determine I_2 emission rates and to investigate temporally resolved emission profiles. Simultaneously, iodocarbons were preconcentrated on solid adsorbent tubes and quantified offline using thermodesorption-gas chromatography/mass spectrometry. The total iodine content of the seaweeds was determined using microwave-assisted tetramethylammonium hydroxide extraction followed by ICPMS analysis. The investigated algae differed significantly regarding the total iodine content and I_2 emission. The total iodocarbon emission rates were about 1−2 orders of magnitude lower than those of molecular iodine, demonstrating that I_2 is the major iodine containing volatile released by the investigated seaweed species.

Alonso and co-workers[289] have evaluated different analytical strategies for the quantification of S-containing biomolecules by HPLC−ICPMS. Compound independent calibration (CIC), postcolumn ID, and postcolumn isotope pattern deconvolution (IPD) were investigated. Furthermore, two quadrupole based instruments, with and without a collision cell, respectively, one single collector double focusing and one multicollector double focusing Neptune instrument were included in the comparative study. It was observed that postcolumn IDA using ^{33}S was suitable for the absolute quantification of sulfate, cysteine, glutathione, and methionine by HPLC−ICPMS when gradient elution was performed. However, traditional equations used for postcolumn IDA can no longer be applied when two different S enriched isotopes are employed. For the characterization of ^{34}S-labeled yeast, the authors have developed a postcolumn IPD procedure that allows one to discriminate between natural abundance and ^{34}S-enriched sulfur species in the ^{34}S-labeled yeast.

Gammelgaard et al.[290] have studied the urinary excretion of Se after ingestion of isotope labeled selenite and selenate in seven healthy volunteers. An aqueous solution containing 330 μL of ^{82}Se-selenate was given orally, and urine samples were subsequently collected during the following 24 h. The scheme was repeated 4 weeks later with a 280 μL ^{82}Se-selenite solution. The amount of total Se in the urine samples was determined by ICPMS. LC−ICPMS analysis of the urine samples showed that the majority of the Se excreted after selenate ingestion was unchanged selenate for six of the individuals while one individual had metabolized a fraction of approximately 20% of the selenate to selenosugar. Ingestion of 10 times larger doses of selenite in two individuals resulted in 13−23% excretion, primarily excreted as selenosugar. These results suggest that the human metabolic pathways of selenite and selenate are different and once again indicate that not all selenate, although well absorbed, may be available for the beneficial health effects.

dx.doi.org/10.1021/ac3031459 | Anal. Chem. 2013, 85, 670−704

In the postgenomics era, proteomics has become a central branch in life sciences.[291] It became clear that understanding of biological functions does not only rely on protein identification but also on protein quantification in a living organism. While Linscheid and co-workers outlined a very promising ICPMS-based approach for the absolute quantification of labeled proteins and peptides through the use of metal-coded affinity tags,[292] a number of different review articles presented by, e.g., Wang et al.,[291] Sanz-Medel,[293] and Tholey and Schaumlöffel[294] selectively discussed the recent advances of ICPMS-based techniques, which can be expected to become one of the key methods in quantitative proteomics.

In environmental and biological studies, the qualitative and quantitative characterization of target proteins of organisms can be of potential use for monitoring processes. Serum transferrin (Tf) has turned out to be a key protein related to iron transport and its metabolism. Grebe et al.[295] presented a study on the development and comparison of different approaches for the accurate, absolute quantification of Tf isolated from blood samples of North Sea harbor seals with the aim to use possible changes in Tf glycoform patterns as an additional parameter in extended studies, focusing on the assessment of their immune status. For this purpose, different HPLC−ICPMS approaches have been developed, which allow the highly resolved separation and detection of up to nine different Tf glycoforms in seal blood samples in less than 30 min, as well as their sensitive and specific absolute quantification on the basis of their characteristic iron content.

Hann et al.[296] have developed comprehensive, fully automated fast column switching 2D-chromatography in combination with ICPMS detection for intact protein separation. The reported LODs obtained for proteins considering the heteroelemental tag sulfur, which was detected as SO^+ employing the dynamic reaction cell technique, are in the picomole-range. The method was implemented for screening the interaction of metallodrugs with proteins in biological samples, which are known to play a key role in in the field of drug development. In a feasibility study, cisplatin was studied in serum samples demonstrating the potential of the method in preclinical studies on candidate drugs.

Elemental labeling followed by ICPMS detection was also employed for the identification of proteinaceous-binding media in art works by Barbante and co-workers,[297] who presented the first studies in this field of application. This application is of interest, "because in the history of art, artists have used many different organic compounds to dissolve pigments and apply them onto a support to obtain a paint layer".[297] Proteins were commonly used with animal parts or milk and eggs as traditional protein sources. Some of these materials are still commonly used as an adhesive. Laboratory models prepared in-house were used for HPLC−ICPMS method development, resulting in the correct identification of the different classes of proteinaceous binders typically used. In addition, some unknown paint layer samples have been analyzed demonstrating that the method is applicable to small sample amounts normally available for this kind of analysis. In the authors' opinion, the achieved results demonstrate the effectiveness of the method, suggesting the potential future use as novel diagnostic tool in the scientific study of artworks.

Recent studies and applications of ICPMS to the analysis of natural and engineered nanoparticles in the environment were reviewed by Jimenez et al.[298] Several methods like gel electrophoresis (GE),[299] field-flow fractionation (FFF),[300−303] and size exclusion and hydrodynamic chromatography (SEC and HDC)[304,305] hyphenated with ICPMS were considered as important separation methods prior to the mass spectrometric measurements, which help to investigate the bioavailability, mobility, and toxicity of elements in life and environmental sciences. The capabilities of the ICPMS to detect single particles for the selective identification, characterization, and determination of engineered nanoparticles were also critically discussed in recent articles.[306,307]

Günther and co-workers[308] presented a study on the ICPMS analysis of single particles in the nanometer size range, embedded in liquid droplets. Various modifications of particle delivery and data acquisition systems commonly used were carried out and described to install an adequate setup for supplying 30−40 μm (diameter) droplets generated by a commercial microdroplet generator with nearly 100% efficiency and high uniformity to the ICP. Analyses were performed using both standard solutions of dissolved metals and highly diluted suspensions of Au and Ag nanoparticles with sizes below 110 nm. Detection efficiencies of 10−6 counts per atom were reported, while size-related limits of quantification were found to be 21 and 33 nm for Au and Ag, respectively. Furthermore, the advantages of utilizing microdroplet generators vs conventional nebulizers for nanoparticle analyses by ICPMS were critically discussed.

Engelhard and co-workers[309] have evaluated the analytical performance of three sample introduction systems, a PFA micronebulizer with a Peltier-cooled cyclonic spray chamber (PC3), a PFA micronebulizer with a heated cyclonic spray chamber and three-stage Peltier-cooled desolvation system (APEX Q), and a monodisperse droplet generator (Microdrop) in combination with an in-house built spray chamber for the characterization of Ag nanoparticles with different sizes (20−100 nm) using single particle ICPMS. With continuous polydisperse and pulsed monodisperse droplet sample introduction, single 30 and 20 nm particles (APEX Q, Microdrop), respectively, were detected. Detection efficiencies (20−100 nm particles) were in the range of 10^{-5} to 10^{-4} counts per atom, and the presented size measurements single particle ICPMS were validated by transmission electron microscopy measurements. Additionally, simultaneous detection of Ag nanoparticles and Ag(I) ions was studied with droplet sample introduction. The combined use of nanoelectrospray ion mobility spectrometry (IMS) with off-line ICPMS for determining engineered nanoparticles in aqueous solution was demonstrated by Kapellios and Pergantis.[310] The presented analytical technique has the potential for determining the size and metal content of nanoparticles and was found to be useful for the determination of the particles' concentration. The resolving power exhibited by IMS along with the high sensitivity offered by single particle mode ICPMS were outlined as the main features that make this combination attractive for the analysis of nanoparticles.

Laser Ablation for Direct Solid Sampling. The number of reports on novel instrumental developments in the field of nanosecond- and femtosecond-laser ablation (LA) and corresponding applications in combination with ICPMS detection for the direct determination of major, minor, and trace elements as well as isotope-ratio measurements in a broad variety of sample types and research fields in which direct multielemental or isotopic analysis is required has once again substantially increased during the last 2.5 years. The driving force for this rapid development of LA is most likely the substantially increasing need to characterize complex materials, both in industry and in various fields of research. Koch and Günther[311] have reviewed the basic principles and recent developments of

dx.doi.org/10.1021/ac3031459 | *Anal. Chem.* 2013, 85, 670−704

LA-ICPMS for the element- and isotope-selective trace analysis of solid materials. Important topics were highlighted, such as aerosol formation/transportation processes, quantification issues, as well as technical aspects concerning the system configuration and ICP operating conditions are outlined. Also the performance of femtosecond (fs) LA-based analyses as one of the most important advancements made over the past years was thoroughly discussed. The benefits offered by fs-LA in comparison to ns-LA were demonstrated on the basis of oxide layer and silicate glass analyses with different applied calibration strategies. Resano et al.[312] have provided a systematic review of publications that reported the use of LA-ICPMS in an archeological context. The authors outlined main capabilities and limitations of the technique and discussed the most relevant parameters that influence the performance of LA-ICPMS.

Wiltsche and Günther[313] have presented a study on the quantification of 23 metallurgical relevant elements in unalloyed, alloyed and highly alloyed steels, and super alloys using fs-LA-ICPMS. It was shown that by using scanning mode ablation with large ablation spot diameters (250 μm), stable and representative sampling can be achieved for the majority of elements, except for Bi and Pb. For the latter elements up to 46%, temporal relative standard deviation was encountered, whereas for most other elements these values were below 10%. Calibration with matrix-matched and nonmatrix-matched standards provided similar agreement within the uncertainty of the certified values. However, the nonmatrix-matched standard-based quantification was more influenced by interferences rather than ablation- or excitation-related matrix effects. The authors concluded that the total matrix internal standardization is applicable, which requires no knowledge about the steel samples prior to analysis.

It is known that fs-LA is preferable over ns-LA for metallic samples because of the shorter time interval during which energy is delivered to the sample material. In a comprehensive study, Vanhaecke et al.[314] have investigated the influence of various laser parameters, such as beam diameter, repetition rate, and laser fluence, on the ablation of Pb as a heavy metallic matrix using an infrared (795 nm) fs-LA system (150 fs pulse duration). The merits of Ar and He as carrier gases were compared, and He did not provide a substantial improvement in the limits of detection, while deposition of sample material on the window of the ablation chamber was more pronounced. The effect on the ICP caused by the introduction of various amounts of sample aerosol was studied by monitoring the signal intensity for $^{38}Ar^{+}$. It was shown that maximizing the amount of sample ablated and thus, the amount of sample aerosol introduced into the ICP, did not result in maximum sensitivity, which was rather obtained under "compromised" conditions. Günther and co-workers[315] have also performed a study on the quantification of Li-doped and pure magnesium diboride crystals by ns- and fs-LA-ICPMS. In both cases, nonmatrix matched calibration using a silicate glass was performed. The application of ns-LA-ICPMS resulted in a stoichiometry of MgB, while data obtained by fs-LA-ICPMS suggested MgB_2, which was supported by supplementary measurements on the basis of X-ray diffraction. Concentration discrepancies of main constituents that suggest a wrong stoichiometry have not yet been reported but can in the author's opinion be considered an example of extreme laser-induced elemental fractionation. In a fundamental study, the same group has used shadowgraphy and light scattering to monitor the shockwave propagation and aerosol formation in ambient air during fs-LA of dielectric materials, such as $Li_2B_4O_7$ and $Y:ZrO_2$.[316] Three independent shockwave fronts were observed originating from the instantaneous compression of ambient gas during the initial stage of fs-LA, a secondary compression caused by material ejection, and an air breakdown well above the target surface. In addition, particle size distributions were found to be multimodal implying the coexistence of condensational growth and supplementary particle production pathways such as phase explosion or critical point phase separation. As a consequence, fs-LA of $Li_2B_4O_7$ resulted in the formation of primary aggregates reaching diameters of >10 μm. In contrast, aggregates formed during fs-LA of $Y:ZrO_2$ covered a size range <1 μm. The authors conclude the existence of a breakdown channel in the ambient atmosphere being capable to carry plasmatic, i.e., noncondensed matter beyond the primary shockwave barrier which may occasionally causes a spatial separation of material released.

Fliegel et al.[317] have studied the influence of the addition of carbon using methane or methanol/water to an ICP via the carrier gas flow on the sensitivity in LA-ICPMS. During the ablation of SRM NIST 610 with simultaneous addition of 0.6−1.4 mL min^{-1} CH_4, a sensitivity enhancement of more than 1 order of magnitude for selected analytes was observed, while all other investigated elements showed a sensitivity enhancement by a factor of 2 (minimum). Potential explanations include charge transfer reactions, a change in the ICP shape, and a temperature increase in the plasma. Furthermore, the aspiration of a methanol−water mixture into a cooled spray chamber and the simultaneous addition to the laser ablated aerosol was investigated, which was found to lead to a sensitivity enhancement up to a factor of 20. To prevent clogging of the sampler cone and skimmer cone by carbon deposition, a fast cleaning procedure for the interface was tested during running of the ICP.

In a comprehensive study performed by Glaus et al.,[318] the aerosol particle morphology and elemental composition generated by two state-of-the-art laser systems (ArF excimer ns-UV laser and Ti:sapphire fs-IR laser) were investigated by electron microscopic techniques. Electrostatic sampling of the aerosols directly onto appropriate targets allowed studying the morphology and elemental composition of the aerosols using transmission electron microscopy and energy dispersive X-ray spectroscopy, respectively. The results of the electron microscopic studies were compared to the LA-ICPMS signals of the main matrix components. The investigations were carried out for nonconducting materials (glass and zircon), metallic samples (steel and brass), and semiconductors (sulfides). The studies confirmed that ns-LA-generated aerosols dominantly consist of nanoparticle agglomerates while conducting samples additionally contain larger spherical particles. In contrast to ns-laser ablation, fs-LA-generated aerosols were found to consist of a mixture of spherical particles and nanoparticle agglomerates for all investigated samples. The differences in elemental composition between nanoparticle agglomerates and spherical particles produced with fs-LA were much more pronounced than in the case of ns-LA, especially for zircon (Si/Zr fractionation) and brass (Cu/Zn fractionation). These observations indicate different ablation and particle formation mechanisms for ns- and fs-LA. The authors proposed gas-to-particle conversion followed by agglomeration and additional hydrodynamic sputtering for conducting samples as the particle growth mechanism for ns-LA. A phase explosion was assumed to be responsible for the mixture of large spherical particles and nanoparticle agglomerates as found for fs-LA-generated aerosols. An interesting approach to achieve separation of isobaric interferences and minimization of matrix related interferences for LA-ICPMS electrothermal heating of laser generated aerosols

was investigated by Günther and co-workers[319] through the analysis of a range of solid samples. It was shown that individual elements can be removed from the laser-generated aerosol at characteristic temperatures for different solid materials. Signal reduction as high as 3 orders of magnitude were achieved for volatile elements, such as Ag and Cd when heating laser-generated aerosol of NIST SRM 610 silicate glass. A signal reduction of more than 99% was obtained for Rb while Sr remained practically unaffected. A temperature- and matrix-dependent change of particle size distribution after aerosol heating was observed by means of laser light scattering and scanning electron microscopy. Also, element unspecific signal suppression was observed, which could be related to a change of the particle size distributions.

The application of LA-ICPMS is still hampered by the lack of available reference materials for calibration. Therefore, different approaches for the preparation of matrix-matching standard materials or the development of alternative calibration strategies are steadily under investigation. Stark and Wennrich[320] investigated a method for the preparation of thin layers of spiked agarose gels as references samples for calibration in LA-ICPMS. Aqueous solutions of agarose spiked with defined amounts of the analytes were cast on a carrier and then dried. The analysis of cell cultures was performed by direct LA-ICPMS using the proposed calibration strategy. The presented results were in accordance with values previously achieved by ICPMS analysis after sample digestion.

Panne and co-workers[321] have investigated different calibration strategies for the determination of trace elements in pure Cu metal by ns-LA-ICPMS. In addition to CRMs, pellets of doped copper powder were used for calibration. The micro homogeneity of the CRMs as well as the solution-doped pellets was found to be sufficient to use them as calibration standards in combination with a laser spot size of 200 mm. In contrast, pellets doped with analytes in solid form showed a significant heterogeneity. For most of the investigated analytes and copper CRMs, the measured mass fractions were within ±20% of their certified values when other copper CRMs were used as calibration samples. When solution-doped powder pellets were used as calibration samples, a systematic trend toward mass fractions below the certified values was observed for nearly all elements determined in the analyzed CRMs. Again, the extend of thermal fractionation during the ablation of the solution-doped pellets was found to depend on the laser irradiance, whereas fractionation was reduced at higher irradiance. Compernolle et al.[322] have reported on the application of isotope dilution and single standard addition/internal standardization in the analysis of Pb buttons obtained by fire assay using LA-ICPMS as an attempt to improve and evaluate the ultimate accuracy and precision of the analytical method. Also external calibration versus matrix-matched lead standards was performed to determine the precious metal concentrations in the same samples, thus allowing comparison of the figures of merit with those of the combined isotope dilution and standard addition/internal standardization approach. Isotope dilution was shown to provide results for the determination of Pt, Pd, and Ag in lead buttons that are more accurate than those obtained by external calibration. For the monoisotopic elements Au and Rh, determined via single standard addition and internal standardization, no significant difference was observed between the results provided by the three methods investigated. Pugh et al.[323] have presented a novel calibration scheme for elemental quantification and imaging of biological thin sections by LA-ICPMS. The proposed procedure is based on spiking whole blood or blood serum with elemental standards (Sr, Gd, Pt), freezing and sectioning the spiked aliquots. The approach was found to be robust, convenient to implement and to afford matrix matching of standards to samples. Linear calibration and good method reproducibility were achieved with limits of detection at the ng g^{-1} level. Application to quantitative analysis and imaging of metallodrugs (Sr, Pt, and MRI contrast agent (Gd was demonstrated)).

An interesting approach for calibration in LA-ICPMS, and also for X-ray fluorescence or secondary ion MS, is the use of dried residues of droplets of liquid samples, as formerly reported, e.g., by Fittschen et al.[324] Do et al.[325] have adopted this strategy for the analysis of real liquid samples through LA-ICPMS. The proposed method was found to provide accurate and precise results when placing 1 μL of a liquid standard solution or a real sample onto the filter surface and then converting the solution into a very small, thin dry spot. The feasibility of the approach was demonstrated by a comparative LA-ICPMS- and conventional ICPMS-based determination of 13 elements in 5 water samples. In comparison with the established sample introduction by nebulization, the avoidance of time-consuming sample preparation steps and possible sample contamination was found to be advantageous. Similarly, Kumtabtim et al.[326] applied this strategy to the analysis of urine samples from Fabry disease patients and controls. The aims of the study were to develop a new and rapid analytical procedure for the determination of trace metal concentrations in single droplets of urine and to establish preliminary results for trace metal concentrations in Fabry disease patient urine samples and controls.

A number of papers have been published on the exploration of new sampling strategies in LA-ICPMS. Kovacs et al.[327] have described an atmospheric sampling approach of various materials in ambient air without using a closed or any ablation cell. The laser generated aerosol containing air was directly sucked into a transport tube connected to the ICPMS via a diaphragm pump. In front of the ICP, air was exchanged to Ar by means of a gas exchange device. After exchanging air to Ar, oxide formation, count rates of the gas blank, and potential spectral interferences caused by polyatomic ions on most m/z ratios were found to be similar or lower in comparison to He exchanged by Ar, which indicates a complete exchange of air by Ar. LA-ICPMS analysis of various metallic samples under atmospheric conditions provided results with similar accuracy as commonly achieved with closed transport systems. This type of sampling opens new applications, especially for objects difficult to place inside an ablation cell, such as archeological samples. Asogan et al.[328] have performed numerical simulations of gas flows through an open, noncontact cell for laser ablation. The described cell consists of dual, annular, concentric microjet gas arrays to entrain ablated material (the carrier flow) and exclude atmosphere (the curtain flow). The authors pointed out that the design of the cell affords a very high degree of exclusion of atmospheric gases, using a relatively low curtain flow of 2.5 L min^{-1} with a carrier flow of 1.2 L min^{-1} He. High efficiency of the microjet arrays in providing an axially symmetric exclusion zone was also demonstrated. The calculated minimum particle transit times through the cell were of the order of 50−100 ms. Similar open ablation cells of different intrinsic volume were used by Wagner and Jedral[329] for the multielement analysis of historic glass and ceramic objects. Comparative investigations with different closed ablation cells were also carried out. The achievable spatial resolution was improved by using open cells for which the rinse out time of the aerosol was shortened by a factor of 3 compared to the standard cell.

dx.doi.org/10.1021/ac3031459 | Anal. Chem. 2013, 85, 670−704

The advantages of such open LA-cells for the analysis of large objects in, e.g., archaeometry and conservation science was recognized. Fricker et al.[330] have developed an ablation cell for large or several small samples offering fast washout and thus high spatial resolution. A 70% faster aerosol washout was recognized compared to the standard ablation cell. In this case the cell's gas flow patterns were also modeled by computational fluid dynamics and were then validated by measurements on two reference materials. The potential of the LA-cell was demonstrated through the ablation of derivatized ovalbumin from polyacrylamide gels after electrophoretic separation.

The Günther group[331] has also developed a portable laser ablation sampling device using a diode pumped solid state laser and fiber-optics in order to extend the field of application to objects outside which cannot be transferred to the laboratory. The system is designed for collecting the sampled material on a membrane filter, which is subsequently analyzed by LA-ICPMS. The analytical performance of this approach was in this study investigated for glass and gold reference materials. Accuracies of better than 20% were reached for most elements, and typical limits of detection were found to be in the range of 0.01−1 $\mu g\ g^{-1}$.

Resano et al.[332] have explored the suitability of a new commercially available ICPMS instrument with Mattauch-Herzog geometry equipped with an array detector for the determination of Au, Ir, Pd, Pt, Rh, and Ru in NiS buttons obtained by fire assay of platiniferous ores. The method evaluated is comprised of the NiS fire assay of a representative amount of the ore sample (40−75 g), grinding of the NiS buttons subsequently obtained, pelleting of the resulting powders using polyethylene wax as a binder, and LA-ICPMS analysis of the sample using in-house matrix-matched standards for calibration. The use of this new ICPMS device proved beneficial, offering a level of precision (2−3% RSD for Pt, Pd, Rh, and Ru and 6−11% RSD for Au and Ir) owing to its simultaneous capabilities and its extended linear range, which enabled an improved performance of the internal standard (^{61}Ni). Moreover, the low level of argide-based interferences and the detection power of the instrument provided low limits of detection (10 ng g^{-1} level) even for Pd, Rh, and Ru, which could be potentially affected by $ArNi^+$ and $ArCu^+$ overlap in this particular matrix. The resulting method can be thus considered very attractive as a faster and greener strategy for the control of these types of samples in the platinum group metal industry, circumventing the need for the cumbersome and environmentally unfriendly digestion procedures currently employed.

The quantification capabilities for nitrogen with LA-ICPMS were studied by Bohme et al.[333] The investigations were carried out on binary calcium nitrides prepared either with ^{14}N or ^{15}N. Whereas the detection of ^{14}N is completely hampered by interference with nitrogen originating from air, a distinct signal of ^{15}N is detectable. On the basis of this knowledge, the ablation parameters were optimized with respect to the signal intensity of ^{15}N. Subsequently, ^{15}N was determined by use of three different quantification strategies which were presented in detail. Precision and accuracy were found to be about ±5%. While the LOD for ^{15}N was determined as 5 mg g^{-1}. Martinez et al.[334] have presented a novel method for the preparation of crude oil samples based on a xerogel matrix for LA-ICP-SFMS analysis. The samples and aqueous solution were successfully encapsulated using zirconium *n*-propoxide. The use of xerogel results in stable and homogeneous pellets avoids splashing of the sample and allows the use of aqueous inorganic standards for calibration. S, Ni, and V were selected as test elements, and In was used as the internal standard. Abrego et al.[335] have published details on a developed method for the detection and identification of gunshot residue (GSR) particles from firearms discharges based on scanning LA-ICPMS. Tape lifts were used to collect inorganic residues from skin surfaces. The laser ablation and ICPMS conditions were optimized for the detection of ^{121}Sb, ^{137}Ba, and ^{208}Pb present in GSR. In experiments with real samples, different firearms, calibers, and ammunitions were used. The performed method evaluation confirms that the developed methodology can be used as an alternative to the standard scanning electron microscopy technique, with the significant advantage of drastically reducing the analysis time.

Kumtabtim et al.[336] presented the application of LA-ICPMS as a microanalytical strategy for biomonitoring of As and toxic and essential metals in single hair strands. Two different calibration strategies in LA-ICPMS were developed using either certified hair standard reference material or prepared matrix-matched laboratory hair standards doped with analytes of interest. Powdered hair standards and human hair strands mounted on a sticky tape in the LA chamber were analyzed under the same experimental conditions. The achieved LOD was 0.6 $\mu g\ g^{-1}$ for As and ranged from 0.3 to 7.8 $\mu g\ g^{-1}$ for the other analytes. Distinct elemental exposition time profiles were observed in hair samples from five volunteers.

A large number of manuscripts were published on the application of LA-ICPMS for the imaging of metals and nonmetals with spatial resolution at the micrometer scale in thin biological tissue sections, especially for the determination of concentrations at the trace and ultratrace level. Therefore, comprehensive review articles outlining the progress in LA-ICPMS imaging as a stand-alone technique but also in combination with molecular MS were prepared by Becker[337,338] and Hare et al.[339] Sanz-Medel and co-workers[340] have also summarized the state-of-the-art of quantitative imaging of elements in biological tissues with special emphasis on the analysis of heteroatom-tagged proteins after their separation and purification by gel electrophoresis and the analysis of proteins that do not naturally contain ICPMS-detectable elements, thus necessitating the use of labeling strategies.

Urgast et al.[341] have performed microanalytical isotope ratio measurements and elemental mapping using LA-ICPMS for tissue thin sections with the aim of Zn tracer studies in rats. The determined isotope ratios were evaluated by additional measurements of tissue digests. Accumulated tracers which made up more than 0.1% of total Zn were identified in the tissues of the treated rats. It was established that at least 50 measurements from the microsampling were necessary to distinguish between controls and a tracer treated rat resulting in reduced resolution of the bioimage. With the parameters used, features in the tissue thin sections of at least 250 μm^2 in size were found to be necessary to detect the incorporation of a tracer. Using the bioimages and pool measurements from one physiological feature, it was possible to show that the aorta cell walls incorporate the Zn tracers given to rats at different time points. Becker et al.[342] have adapted LA-ICPMS for the analysis of native mouse spinal cord cryosections of 3.1 mm × 1.7 mm. Element images of the spinal cord were presented and the spatial distribution of Rb was mapped for the first time in biological tissue. Metal concentrations were quantified using matrix-matched laboratory standards and normalization of the respective ion intensities to the average ^{13}C ion intensity of standards and samples as a surrogate of slice thickness. The authors stated that the presented

dx.doi.org/10.1021/ac3031459 | *Anal. Chem.* 2013, 85, 670−704

mass spectrometry imaging approach for the analysis of healthy wild type spinal cords demonstrates the suitability of the technique for investigating diseased or transgenic states in future imaging studies.

The same group[343] has reported the achievement of improved spatial resolution of LA-ICPMS for elemental imaging of biological tissue samples by employing a modified laser microdissection system (LMD) for laser ablation. Using this LMD-ICPMS arrangement, a spatial resolution of about 3 μm was obtained allowing mass spectrometric measurements of metal distributions and simultaneous inspection of the tissue section via the microscope of the LMD.

Conventional LA-ICPMS has been used by Pugh et al.[344] to map the spatial distribution of Gd-based magnetic resonance imaging (MRI) contrast agents in histological sections in order to explore synergies with in vivo MRI. Images from respective techniques were presented for two separate studies. The LA technique was found to be a powerful compliment to MRI not only in offering improved sensitivity, spatial resolution and signal quantitation but also in giving added value regarding the fate of administered Gd and Pt agents. Giesen et al.[345] have presented a LA-ICPMS method for single cell and cell nucleus imaging. Iodine was used as an elemental dye for fibroblast cells and for thin tissue sections. At an incubation time of 60 s, iodine is located mainly within the cell nuclei, which was illustrated in fibroblast cells. The surrounding cytoplasm was iodinated as well but to a lesser extent. The spatial resolution attained was sufficient to detect even smaller cell nuclei within a liver biopsy tissue. Furthermore, iodine was successfully employed for biomolecule labeling. The same group[346] has presented results of the optimization of multiplexed immunohistochemistry (IHC) on breast cancer tissue. Lanthanides were used for labeling of primary antibodies, which are applied in IHC, and LA-ICPMS was elaborated as a detection tool for multiplexed IHC of tissue sections. The results were found to prove the high selectivity of applied antibodies, which was sustained after labeling. Up to three tumor markers were detected simultaneously in a single multiplex analysis of a 5 μm thin breast cancer tissue at a laser spot size of 200 μm.

Vanhaecke and co-workers[347] have compared the capabilities of the two widely used microanalytical techniques for elemental mapping, namely, LA-ICPMS and scanning micro-X-ray fluorescence spectrometry (micro-XRF) for imaging the distribution of selected elements in the model organism *Daphnia magna* in terms of detection power and spatial resolution. Both techniques offer similar limits of detection for the elements Ca and P and thus allow a cross-validation of the imaging results. LA-ICPMS was particularly sensitive for determining Zn in *Daphnia magna*, while the detection power of micro-XRF was insufficient in this context. However, LA-ICPMS was inadequate for the measurement of the distributions of S, which could be better visualized with micro-XRF. Both techniques are thus complementary in providing an exhaustive chemical profiling of tissue samples.

Collision and Reaction Cells. Dynamic collision/reaction cells (DRC) for the reduction or even elimination of specific polyatomic spectral overlaps due to induced ion−molecule reactions are nowadays routinely used in ICPMS-based trace elemental analysis. However, as stated in the introductory part of this section, a further decreasing number of novel or fundamental studies rather than applications was recognized during the time period covered by this review.

Reactions of charge exchange, atom transfer, adduct formation, condensation, and analyte association/condensation with the reaction gas are the main mechanisms taking place in the DRC. Selecting the most appropriate reaction gas in DRC-ICPMS is the very critical point for the determination of strongly interfered elements. In an article by D'llio et al.,[348] a review was provided on the analytical challenges for a reliable assay of As, Cr, Se, and V by DRC-ICPMS and illustrates different approaches and mechanisms involved in the analysis of polymers, rock, soil, particulate matter, and biological fluids, such as serum, urine, and whole blood.

In a study by Nobrega and co-workers,[349] a new strategy based on minimizing the interfering ion signal variation was used to improve accuracy in K, As, P, and Si determinations in ICPMS, rather than employing a DRC. Different from traditional internal standard methods, Ar species naturally present in the plasma were used as probes to correct fluctuations in the interfering ion rather than in the analyte signal. Accuracy was significantly improved with no instrumental modification or postplasma reactions. Recoveries ranging from 86 to 107% were obtained for all elements evaluated in different certified reference materials and spiking studies. Remarkably, results were comparable and for some elements even better than recoveries obtained with a DRC-interface. Adequate precision, accuracy and sensitivity were obtained while using the $^{38}Ar^+$ probe even for isotopes prone to severe isobaric interferences such as ^{28}Si. Ardini et al.[350] have investigated the behavior of rare earth elements (REEs) ions within a DRC pressurized with oxygen, in order to explore their determination at m/z + 16 by ICPMS. The conversion of REEs to molecular monoxide ions was nearly quantitative (>96%), with the exception of Tm (78%), Eu (11%), and Yb (6%). Moreover, the formation of dioxide ions was generally lower than 1%. According to these results, a new method for the determination of REEs in digests from geological samples was proposed. The accurate determination of Y, La, Ce, Pr, Nd, Sm, Tb, Dy, Ho, Er, and Tm was achieved, as demonstrated by the analysis of both certified reference materials and Antarctic marine sediment samples, using ICP-SFMS for comparison. Eu, Gd, Yb, and Lu could not be measured, thus their separate determination in the standard mode using mathematical correction was found to be still necessary to obtain the complete REE pattern.

Targets of highly enriched actinides or fission products were irradiated in a nuclear reactor and analyzed before and after irradiation for their elemental and isotopic composition, as reported by Chartier and co-workers.[351] The determination of ^{153}Eu was a major analytical challenge because of isobaric interferences of Sm and Gd isotopes after irradiation. An analytical method was developed by using a multicollector ICPMS equipped with a collision/reaction cell in order to circumvent these interferences. It was shown that direct Eu isotope ratio measurements are possible in the presence of O_2 used as a reactant gas in the cell due to the different behavior of Eu and Sm/Gd. SmO^+ and GdO^+ oxide ions are formed, whereas Eu remains present as Eu^+. The separation efficiency of the Isoprobe's collision reaction-cell was studied on both natural Eu and certified ^{153}Eu enriched solutions. Accuracy of the measurement was found to be within the reference value uncertainty. Reproducibility of the $^{151}Eu/^{153}Eu$ isotopic ratio measurement were found to be lower than 0.3 parts per thousand (ppt), in the case of natural solution, and lower than 4 ppt with the ^{153}Eu enriched solution, respectively. In a similar study, the same group proposed the use of CO_2 as a reactive gas to suppress the isobaric interference of ^{238}U on ^{238}Pu.[352] In two studies on the determination

dx.doi.org/10.1021/ac3031459 | *Anal. Chem.* 2013, 85, 670−704

of P and Pt in liposome samples, Gammelgaard and co-workers have used Xe[353] and Ar[354] as a collision gas. Under the optimum conditions with respect to signal-to-noise ratio, the interferences were suppressed and the detection limits of P and Pt were 0.3 and 0.05 ng mL^{-1}, respectively. For the investigation of liposome stability and metallo-drug release from liposomes, a hyphenated method based on size exclusion chromatography was developed for separation of free and encapsulated Pt in a model liposome formulation of oxaliplatin. In the second study, a CE−ICPMS method was developed for the separation of the free oxaliplatin drug substance from liposome-entrapped oxaliplatin. In this case, a detection limit of 29 ng mL^{-1} of Pt and a precision of 2.9% (for 10 μg mL^{-1} of oxaliplatin standard) were reported.

Time-of-Flight Instruments. In the past years, extensive research in the field of time-of-flight MS (TOFMS) in combination with an ICP has been performed, and interesting instrumental developments and applications were reported since the commercial availability of such systems in the late 1990s, but the number of manuscripts published on ICP-TOFMS continued to significantly decrease during the last 2.5 years. However, the advantages of TOFMS are still remarkable and thus Hieftje and co-workers have developed a new time-of-flight mass spectrometer that uses an ESI source and an ICP to extract molecular, structural, atomic, and isotopic information simultaneously from a single sample. In two papers, the authors have focused on the characterization of the ESI channel[355] and the ICP source.[356] In the first manuscript, long-term and short-term spray stability were reported and sensitivities for a number of molecular species were discussed. Skimmer-nozzle collisionally induced dissociation was also explored for adduct removal and analyte fragmentation on the ESI channel. In the follow-up paper, the simultaneous operation of the two sources was demonstrated. Preliminary sensitivities and limits of detection for Cr, Co, Ga, As, Ag, Cs, Ho, Hg, Tl, and Bi on the ICP channel were reported and stability as well as drift of the ICP channel were outlined. In a third manuscript, the same authors have determined Cr(III) and Cr(VI) species with the same dual-source instrument.[357] Indicative ESI species were identified for chromium(III) acetate, chromium chloride, chromium picolinate, and potassium dichromate in methanol and ethanol matrixes. Furthermore, an online dilution apparatus was described for use with ESI for the determination of analytes that react with the solvent.

Arnquist et al.[358] used the combination of an inline electrothermal vaporization (ETV) and nebulization source for ICP-TOFMS. The application of a wet plasma with ETV introduction avoided the need to change power settings and torch positions that normally accompany a change from wet to dry plasma operating conditions. Using the inline-ETV source, improved limits of detection (LOD) were obtained for elements typically suppressed by polyatomic interferences using a nebulizer. LODs were improved by factors of 65 and 22 for ^{51}V and ^{53}Cr, respectively, using the inline-ETV source compared to a conventional concentric glass nebulizer. For elements without polyatomic interferences, LODs from the inline-ETV were comparable to conventional dry plasma ETV-ICP-TOFMS results. The authors pointed out that time-resolved ETV-ICPMS signals could be used to distinguish between an analyte ion and polyatomic isobars. Furthermore the development of ICP-TOFMS-based methods were reported for rapid, simultaneous, and reliable determination of more than 50 elements at ultratrace levels in urine[359] and of rare earth elements, noble metals, U, and Th in biota samples from five different sampling locations at the river Elbe.[360]

High Resolution and Multicollector Instruments. During the last 2.5 years, the number of applications of high-resolution ICPMS (HR-ICPMS) to environmental studies and high precision isotope ratio analysis has again increased significantly, which is due to the techniques extremely low achievable detection limits, high sensitivity and precision, and high mass resolution to overcome spectral interferences for the reliable determination of many trace elements.

High-resolution multicollector (MC-ICPMS) instruments were thus used in a number of different studies for the precise determination of (natural) isotopic composition of, e.g., C,[361] Si,[362] Ge,[363] Se,[364] Sb, and In.[365] A review by Malinovsky and Vanhaecke[366] outlined recent developments in the use of MC-ICPMS in studies of mass-independent isotope chemistry of heavy elements. Origins of mass-independent isotope effects and their relevance to isotope ratio measurements by MC-ICPMS were described, and the extent to which these effects can affect instrumental mass bias was critically discussed. Additionally, key findings reported in studies of mass-independent isotope fractionation in the field of environmental sciences are reviewed because it can provide a new and effective means of studying the biogeochemistry of the respective elements, as the authors stated in this article.

Newman reported the results of a fundamental study on the investigation of relative elemental sensitivities for a number of sample and skimmer cone combinations, with standard and enhanced pumping of the interface region, for a MC-ICPMS.[367] An approximate 2-fold sensitivity enhancement was observed for Sr, Nd, Hf, Pb, and U using the "Jet sample cone" and an enhanced pumping configuration, compared to the standard arrangement. The determined nonlinear contribution to the instrumental mass fractionation with respect to Nd was found to be not specific to a particular MC-ICPMS instrument but rather associated with an increase in the NdO^+/Nd^+ ratio, due to either a change in the plasma operating conditions (e.g., an increase in the sample gas flow, absence of a secondary discharge at the interface, change in plasma gas composition) or modification of the cone geometry. The role of secondary discharge formation and the physical and chemical processes occurring in the supersonic expansion with respect to NdO^+ formation were discussed.

A systematic study by Barling and Weis[368] dealt with the measurement of Pb and Tl isotope intensities and ratios in radial and axial plasma profiles using MC-ICPMS. Signal profiles for ^{204}Pb, ^{206}Pb, ^{207}Pb, and ^{208}Pb were found to display mass dependent radial and axial distributions in the plasma. In radial profiles, lighter isotopes exhibit greater dispersal from the plasma axis than heavier isotopes, in agreement with ICPMS elemental observations. However, signal maxima (I_{max}) for heavier Pb isotopes occur closer to the load coil than I_{max} for lighter Pb isotopes, the reverse of the ICPMS elemental observations. These mass dependent distributions predict that the radial dispersion and axial I_{max} locations for ^{203}Tl and ^{205}Tl isotopes should occur interspersed with the values for simultaneously measured Pb isotopes. Instead however, their values are appropriate for masses greater than ^{208}Pb, indicating that the observed profiles are not the product of a single stage mass dependent process and that other element properties also effect the distributions.

Mason and Henderson[369] have presented a method for the calibration of in-house Th isotope standards for use in U−Th chronology and investigated the instrumental biases on the "Nu Plasma" MC-ICPMS. U and Th mass fractionation were found to

dx.doi.org/10.1021/ac3031459 | *Anal. Chem.* 2013, 85, 670−704

be very strongly coupled, with no evidence of differences in mass bias behavior. Potential biases introduced by intensity-dependent and ion-beam-path dependent variations in ion-counter response were also studied. It was concluded that at count rates similar to 350 000 cps, intensity-dependent gain variation can be accounted for entirely by dead-time, while beam-path differences can cause gain variation of up to similar to 0.8% for different Th isotopes. Pointurier et al.[370] have presented an evaluation of the extent and impact of interferences due to polyatomic species containing heavy elements on the background at masses of plutonium isotopes ^{239}Pu and ^{240}Pu, based on measurement of environmental samples using an ICP-SFMS. It was demonstrated that molecular interferences such as PbO_2^+, $ArHg^+$, and IrO_3^+ must be considered as additional background, which might lead to false detection of femtogram amounts of Pu or overestimation of results. The extents of the formation of the main polyatomic species were found to be highly variable from one analysis to the other, over 1 or 2 orders of magnitude, depending on the selected instrumental settings.

A fast and easy sample preparation and analysis method for the bulk U and Pu analysis of swipe samples was developed by Stefanka and co-workers.[371] For sample preparation, low power microwave-assisted digestion followed by extraction chromatography was applied, while the quantification of the analytes of interest and their isotopic composition were determined by ICP-SFMS. The analytical performance of the method was found to be in good agreement with the requirements in terms of accuracy, precision, and repeatability of the International Atomic Energy Agency-Network for Analytical Laboratories and can thus be applied for routine determination of the isotope ratios and isotope concentrations of U and Pu (^{234}U, ^{235}U, ^{236}U, ^{238}U and ^{239}Pu, ^{240}Pu, ^{241}Pu) present in ultratrace concentration levels in swipe samples. The selection, optimization, and validation of a sample preparation method for ultratrace determination of ^{240}Pu and ^{239}Pu in marine samples by MC-ICPMS was presented by Lindahl et al.[372] Various separation strategies were evaluated, and method validation was performed using certified marine reference materials. The authors concluded that the proposed method allows the determination of Pu at femtogram levels, in small size marine samples (0.6−2.0 g of coral or 15−20 L of seawater). An application of the new method to the determination of historical records of the Pu signature in coral samples from the tropical Northwest Pacific was also shown.

Fontaine et al.[373] have published an interesting report on authenticity and provenance studies of copper-bearing andesines. Therefore, the main and trace element composition of andesines from different origins was determined by using ns-LA-ICPMS. Mexican, Oregon, and Asian samples were clearly distinguishable by their main element content (CaO, SiO_2 Na_2O, and K_2O), whereas the composition of Mongolian, Tibetan, and DR Congo material was within the same range. Since the Li concentration was shown to be correlated with the Cu concentration, the formerly proposed differentiation by the Ba/Sr vs Ba/Li ratio does not distinguish between samples from Tibet and Mongolia but only between red and colorless material. However, when employing fs-LA-MC-ICPMS in high-resolution mode, laboratory diffused samples showed variations for ^{65}Cu/^{63}Cu within one mineral due to the diffusion process. Ar isotope ratio measurements proved that heat treatment will reduce the amount of radiogenic ^{40}Ar in the samples significantly. Only low levels of radiogenic Ar were found in samples collected on-site in both mine locations in Tibet. Together with a high intrasample variability of the Cu isotope ratio, andesine samples labeled as coming from Tibet are most probably Cu-diffused, using initially colorless Mongolian andesines as starting material.

The conception and fabrication of a microsystem for lanthanides separation and its coupling with MC-ICPMS for isotope ratio measurements was shown by Vio et al.[374] The miniaturized isotachophoresis system has been adapted to fit with the authors' laboratory glovebox limitations in view of future spent nuclear fuels analysis. The microdevice was tested by using a mixture of standard solutions of natural elements, and the separation of 13 lanthanides was successfully performed. The isotopes of Nd and Sm were acquired online in multicollection mode after separation of the two elements with an injection amount of 5 ng. Results obtained on the Nd and Sm isotope ratio measurements on transient signals were presented.

AUTHOR INFORMATION

Corresponding Author

*E-mail: bings@uni-mainz.de.

Notes

The authors declare no competing financial interest.

Biographies

Nicolas H. Bings studied chemistry at the University of Dortmund (Germany), where he received his Diploma and Ph.D. degrees in 1993 and 1996, respectively. He worked for 1 year each as a postdoctoral researcher in the Department of Chemistry at the University of Alberta, Edmonton (Canada), and at the Laboratory for Spectrochemistry, Bloomington, Indiana (U.S.). From 1999 to 2005 he was a scientific assistant at the Universities of Leipzig and Hamburg (Germany). After finishing his Habilitation in 2005, he became an Assistant Professor at the University of Hamburg and Visiting Professor at the University of Leipzig. Since 2008 he has been a Professor of Analytical Chemistry at the Johannes Gutenberg-University Mainz (Germany). His current research activities include the development and application of new analytical techniques in plasma source mass and emission spectrometry with special focus on sample introduction, laser ablation, and miniaturized analysis systems for trace elemental determination.

Annemie Bogaerts received her M.Sc. and Ph.D. degrees in chemistry, in 1993 and 1996, respectively, from the University of Antwerp in Belgium. She became a Professor of Physical Chemistry in 2003 at the University of Antwerp. Her current research activities include the numerical modeling of glow discharges and related plasmas (used for analytical chemistry, materials science, environmental and medical applications) as well as the modeling of laser−solid interaction (for laser ablation and laser plasma spectroscopy) and plasma−solid interaction (for surface modifications, thin film deposition, plasma catalysis, and plasma medical applications)

José A. C. Broekaert studied chemistry at the University of Gent, Belgium, and received his Ph.D. in 1976. After an Alexander-von-Humboldt scholarship he joined the ISAS-Institute for Analytical Sciences, Dortmund, Germany, in 1978 and earned the degree of "Geaggregeerde voor het hoger onderwijs" in 1985 at the University of Antwerp, Belgium, where he has lectured since 1983. In 1991, he became an associate professor for inorganic/analytical chemistry at the University of Dortmund, in 1998, full professor of analytical chemistry at the University of Leipzig, Germany, and from 2002 onwards at the University of Hamburg. In 2004 he became an adjunct professor of chemistry at Indiana University, Bloomington, U.S. His research interests are problem-oriented analytical chemistry with special

reference to the determination of the elements and their species mainly by plasma atomic spectrochemical methods.

REFERENCES

(1) Bings, N. H.; Bogaerts, A.; Broekaert, J. A. C. *Anal. Chem.* **2002**, *74*, 2691−2711.
(2) Bings, N. H.; Bogaerts, A.; Broekaert, J. A. C. *Anal. Chem.* **2004**, *76*, 3313−3336.
(3) Bings, N. H.; Bogaerts, A.; Broekaert, J. A. C. *Anal. Chem.* **2006**, *78*, 3917−3945.
(4) Bings, N. H.; Bogaerts, A.; Broekaert, J. A. C. *Anal. Chem.* **2008**, *80*, 4317−4347.
(5) Bings, N. H.; Bogaerts, A.; Broekaert, J. A. C. *Anal. Chem.* **2010**, *82*, 4653−4681.
(6) Protopopov, V. *Appl. Spectrosc.* **2012**, *66*, 496−509.
(7) Orlandini, v.; Niessen, J. O.; Schaper, J. N.; Petersen, J. H.; Bings, N. H. *J. Anal. At. Spectrom.* **2011**, *26*, 1781−1789.
(8) Mermet, J. M. *Spectrochim. Acta, Part B* **2010**, *65*, 509−523.
(9) Porento, M.; Sutinen, V.; Julku, T.; Oikari, R. *Appl. Spectrosc.* **2011**, *65*, 678−683.
(10) Pena-Pereira, F.; Lavilla, I.; Bendicho, C. *Anal. Chim. Acta* **2010**, *669*, 1−16.
(11) Yañez, J.; Campos, A.; Mercado, A.; Soto, C.; Mansilla, H. D.; Neira, J. *J. Anal. At. Spectrom.* **2011**, *26*, 320−324.
(12) Anthemidis, A. N.; Giakisikli, G.; Mitani, C. *Int. J. Environ. Anal. Chem.* **2012**, *92*, 1312−1324.
(13) Miranda, K.; Dionisio, A. G. G.; Pessoa Neto, O. D.; Gomes, M. S.; Pereira-Filho, E. R. *Microchem. J.* **2012**, *100*, 27−30.
(14) Yildiz, Z.; Arslan, G.; Tor, A. *Microchim. Acta* **2011**, *174*, 399−405.
(15) Ĺvov, B. *Spectrochim. Acta, Part B* **2011**, *66*, 557−564.
(16) Katskov, D. A.; Darangwa, N. *J. Anal. At. Spectrom.* **2010**, *25*, 1079−1090.
(17) Katskov, D.; Darangwa, N.; Heitmann, U. *J. Anal. At. Spectrom.* **2010**, *25*, 1091−1101.
(18) Donati, G. L.; Jones, B. T. *J. Anal. At. Spectrom.* **2011**, *26*, 838−844.
(19) Castro, M. A.; Aller, A. J.; Faulds, K.; Littlejohn, D. *J. Anal. At. Spectrom.* **2011**, *26*, 1722−1732.
(20) López-Garcia, I.; Rivas, R. E.; Hernández-Córdoba, M. *Anal. Bioanal. Chem.* **2010**, *396*, 3097−3102.
(21) Alizadeh, K.; Zohrevand, S.; Ghiasvand, A. R.; Hashemi, P.; Shamsipur, M.; Shargi, H.; Khalifez, R. *Microchim. Acta* **2010**, *168*, 115−121.
(22) Cacho, F.; Lauko, L.; Manova, A.; Beinrohr, E. *J. Anal. At. Spectrom.* **2012**, *27*, 695−699.
(23) Teixeira Tarli, C. R.; Andrade, F. N.; de Oliveira, F. M.; Zanetti Corazza, M.; Mendez de Azevedo, L. F.; Gava Segatelli, M. *Anal. Chim. Acta* **2011**, *703*, 145−151.
(24) Morimoto, S.; Ashino, T.; Wagatsuma, K. *Anal. Sci.* **2010**, *26*, 809−813.
(25) Heinrich, H. J.; Kipphardt, H. *Spectrochim. Acta, Part B* **2012**, *70*, 68−73.
(26) Gunduz, S.; Akman, S.; Baysal, A.; Culha, M. *Microchim. Acta* **2011**, *172*, 403−407.
(27) Zeng, C.; Wen, X.; Tan, Z.; Cai, P.; Hou, X. *Microchim. J.* **2010**, *96*, 238−242.
(28) Inui, T.; Fujita, K.; Kitano, M.; Nakamura, T. *Anal. Sci.* **2010**, *26*, 1093−1098.
(29) Paz de Matos, J. C.; Rodrigues, L. F.; de Moraes Flores, E. M.; Krivan, V. *Spectrochim. Acta, Part B* **2011**, *66*, 637−643.
(30) Souza, A. L.; Oliveira, P. V. *J. Anal. At. Spectrom.* **2010**, *25*, 675−680.
(31) Dobrowolski, R.; Otto, M.; Adamczyk, A. *Microchim. Acta* **2010**, *168*, 355−362.
(32) Bai, J.; Nakatani, T.; Sasaki, Y.; Minami, H.; Inoue, S.; Takahashi, N. *Int. J. Environ. Anal. Chem.* **2011**, *91*, 856−865.
(33) Cervenka, R.; Zelinkova, H.; Konecná, M.; Komárek, J. *Anal. Sci.* **2010**, *26*, 989−993.
(34) Pagliano, E.; Onor, M.; Meija, J.; Mester, Z.; Sturgeon, R. E.; ĎUlivo, A. *Spectrochim. Acta, Part B* **2011**, *66*, 740−747.
(35) Kratzer, J.; Dočekal, B.; Heitmann, U.; Dědina, J. *J. Anal. At. Spectrom.* **2011**, *26*, 2230−2237.
(36) Nóbrega, J. A.; Sturgeon, R. E.; Grinberg, P.; Gardner, C. J.; Brophy, C. S.; Garcia, E. E. *J. Anal. At. Spectrom.* **2011**, *26*, 2519−2523.
(37) Arslan, Y.; Matoušek, T.; Kratzer, J.; Musil, S.; Benada, O.; Vobecký, M.; Ataman, O. Y.; Dědina, J. *J. Anal. At. Spectrom.* **2011**, *26*, 828−837.
(38) Musil, S.; Kratzer, J.; Vobecký, M.; Benada, O.; Matoušek, T. *J. Anal. At. Spectrom.* **2010**, *25*, 1618−1626.
(39) Zheng, C.; Sturgeon, R. E.; Hou, X. *J. Anal. At. Spectrom.* **2010**, *25*, 1159−1165.
(40) Deng, H.; Zheng, C.; Liu, L.; Wu, L.; Hou, X.; Lv, Y. *Microchem. J.* **2010**, *96*, 277−282.
(41) Kozak, L.; Niedzielski, P. *Int. J. Environ. Anal. Chem.* **2012**, *92*, 1093−1105.
(42) Xi, M.; Liu, R.; Wu, P.; Xu, K.; Hou, X.; Lv, Y. *Microchem. J.* **2010**, *95*, 320−325.
(43) Tian, Y.; Chen, M. L.; Chen, X. W.; Wang, J. H.; Hirano, Y.; Sakamoto, H.; Shirasaki, T. *J. Anal. At. Spectrom.* **2011**, *26*, 133−140.
(44) Quadros, D. P. C.; Rau, M.; Idrees, M.; Chaves, E. S.; Curtius, A. J.; Borges, D. L. G. *Spectrochim. Acta, Part B* **2011**, *66*, 373−377.
(45) Huang, M. D.; Becker-Ross, H.; Okruss, M.; Geisler, S.; Florek, S. *J. Anal. At. Spectrom.* **2012**, *27*, 982−988.
(46) Lepri, F. G.; Welz, B.; Dessuy, M. B.; Vale, M. G. R.; Bohrer, D.; de Loos-Vollebregt, M. T. C.; Huang, M. D.; Becker-Ross, H. *Spectrochim. Acta, Part B* **2010**, *65*, 24−32.
(47) Huang, M. D.; Becker-Ross, H.; Florek, S.; Heitmann, U.; Okruss, M.; Welz, B.; Ferreira, H. S. *J. Anal. At. Spectrom.* **2010**, *25*, 163−168.
(48) Krüger, M.; Huang, M. D.; Becker-Roß, H.; Florek, S.; Ott, I.; Gust, R. *Spectrochim. Acta, Part B* **2012**, *69*, 50−55.
(49) Kowalewska, Z. *Spectrochim. Acta, Part B* **2011**, *66*, 546−556.
(50) Aramandia, M.; Flórez, M. R.; Piette, M.; Vanhaecke, F.; Resano, M. *J. Anal. At. Spectrom.* **2011**, *26*, 1964−1973.
(51) Atilgan, S.; Akman, S.; Baysal, A.; Bakircioglu, Y.; Szigeti, T.; Óvári, M.; Záray, G. *Spectrochim. Acta, Part B* **2012**, *70*, 33−38.
(52) Araujo, R. G. O.; Vignola, F.; Castilho, I. N. B.; Borges, D. L. G.; Welz, B.; Vale, M. G. R.; Smichowski, P.; Ferreira, S. L. C.; Becker-Ross, H. *Spectrochim. Acta, Part B* **2011**, *66*, 378−382.
(53) Vignola, F.; Borges, D. L. G.; Curtius, A. J.; Welz, B.; Becker-Ross, H. *Microchem. J.* **2010**, *95*, 333−336.
(54) Leopold, K.; Zierhut, A.; Huber, J. *Anal. Bioanal. Chem.* **2012**, *403*, 2419−2428.
(55) Gillenwater, P. S.; Urgun-Demirtas, M.; Negri, M. C.; Alvarado, J. *J. Environ. Monit.* **2012**, *14*, 27−29.
(56) Anthemidis, A.; Cerdà, V.; Miró, M. *J. Anal. At. Spectrom.* **2010**, *25*, 1717−1723.
(57) Torres, D. P.; Dittert, I. M.; Höhn, H.; Frescura, V. L. A.; Curtius, A. J. *Microchem. J.* **2010**, *96*, 32−36.
(58) Angeli, V.; Biagi, S.; Ghimenti, S.; Onor, M.; ĎUlivo, A.; Bramanti, E. *Spectrochim. Acta, Part B* **2011**, *66*, 799−804.
(59) Guzmán-Mar, J. L.; Hinojosa-Reyes, L.; Serra, A. M.; Hernández-Ramirez, A.; Cerdà, V. *Anal. Chim. Acta* **2011**, *708*, 11−18.
(60) Ibáñez-Palomino, C.; López-Sánchez, J. F.; Sahoquillo, À. *Int. J. Environ. Anal. Chem.* **2012**, *92*, 909−921.
(61) Gao, E.; Liu, J. *Anal. Sci.* **2011**, *27*, 637−642.
(62) Wang, Y.; Luo, X.; Tang, J.; Hu, X. *Microchim. Acta* **2011**, *173*, 267−273.
(63) Quiroz, W.; Arias, H.; Bravo, M.; Pinto, M.; Lobos, M. G.; Cortés, M. *Microchem. J.* **2011**, *97*, 78−84.
(64) Zhang, W.; Yang, X.; Dong, Y.; Chu, X. *Spectrochim. Acta, Part B* **2010**, *65*, 571−578.
(65) Ezer, M. *Int. J. Environ. Anal. Chem.* **2010**, *90*, 697−707.
(66) Amberger, M. A.; Barth, P.; Förster, O.; Broekaert, J. A. C. *Microchim. Acta* **2011**, *172*, 261−267.

(67) Stoiljković, M. M.; Pašti, I. A.; Momčilović, M. D.; Savović, J. J.; Pavlović, M. S. *Spectrochim. Acta, Part B* **2010**, *65*, 927−934.
(68) Zaksas, N. P.; Nevinsky, G. A. *Spectrochim. Acta, Part B* **2011**, *66*, 861−865.
(69) Navarre, E. C.; Goldberg, J. M. *Appl. Spectrosc.* **2011**, *65*, 26−35.
(70) Celijk, M. *Spectrochim. Acta, Part B* **2011**, *66*, 149−155.
(71) Donati, G. L.; Wildman, R. B.; Jones, B. T. *Anal. Chim. Acta* **2011**, *688*, 36−42.
(72) Huang, R.; Zhu, Z.; Zheng, H.; Liu, Z.; Zhang, S.; Hu, S. *J. Anal. At. Spectrom.* **2011**, *26*, 1178−1182.
(73) Lindner, H.; Murtazin, A.; Groh, S.; Niemax, K.; Bogaerts, A. *Anal. Chem.* **2011**, *83*, 9260−9266.
(74) Taylor, N.; Spencer, R. L.; Farnsworth, P. B. *J. Anal. At. Spectrom.* **2012**, *27*, 857−867.
(75) Dettman, J. R.; Olesik, J. W. *J. Anal. At. Spectrom.* **2012**, *27*, 581−594.
(76) Chan, G. C.; Hieftje, G. M. *J. Anal. At. Spectrom.* **2010**, *25*, 282−294.
(77) Grotti, M.; Todoli, J. L.; Mermet, J. M. *Spectrochim. Acta, Part B* **2010**, *65*, 137−146.
(78) Reinsberg, K. G.; Schumacher, C.; Nielsch, K.; Broekaert, J. A. C. *J. Anal. At. Spectrom.* **2011**, *26*, 2477−2482.
(79) Aguirre, M. A.; Kovachev, N.; Almagro, B.; Hidalgo, M.; Canals, A. *J. Anal. At. Spectrom.* **2010**, *25*, 1724−1732.
(80) Barałkiewicz, D.; Hanć, A.; Gramowska, H. *Int. J. Environ. Anal. Chem.* **2010**, *90*, 14−15.
(81) Garcia, C. C.; Murtazin., A.; Groh, S.; Horvatic, V.; Niemax, K. *J. Anal. At. Spectrom.* **2010**, *25*, 645−653.
(82) Krystek, P.; Ulrich, A.; Garcia, C. C.; Manohar, S.; Ritsema, R. *J. Anal. At. Spectrom.* **2011**, *26*, 1701−1721.
(83) Sánchez, R.; Todoli, J. L.; Lienemann, C. P.; Mermet, J. M. *J. Anal. At. Spectrom.* **2010**, *25*, 1888−1894.
(84) Chaves, E. S.; de Loos-Vollebregt, M. T. C.; Curtius, A. J.; Vanhaecke, F. *Spectrochim. Acta, Part B* **2011**, *66*, 733−739.
(85) Krachler, M.; Wegen, D. H. *J. Anal. At. Spectrom.* **2012**, *27*, 335−339.
(86) Zachariadis, G. A.; Trikas, E. *Int. J. Environ. Anal. Chem.* **2012**, *92*, 375−381.
(87) Deng, B.; Wang, Y.; Zhu, P.; Xu, X.; Ning, X. *Anal. Chim. Acta* **2010**, *683*, 58−62.
(88) Sansawong, S.; Waiyawat, W.; Shiowatana, J.; Siripinyanond, A. *Spectrochim. Acta, Part B* **2011**, *66*, 476−482.
(89) Parodi, B.; Savio, M.; Martinez, L. D.; Gil, R. A.; Smichowski, P. *Microchem. J.* **2011**, *98*, 225−230.
(90) Asfaw, A.; Beauchemin, D. *Spectrochim. Acta, Part B* **2010**, *65*, 376−384.
(91) Pohl, P.; Broekaert, J. A. C. *Anal. Bioanal. Chem.* **2010**, *398*, 537−545.
(92) Ceretti, S.; Escudero, A.; Gasquez, J. A.; Olsina, R. A.; Martinez, L. D. *J. Anal. At. Spectrom.* **2011**, *26*, 2428−2433.
(93) Zheng, C.; Sturgeon, R. E.; Brophy, C. S.; He, S.; Hou, X. *Anal. Chem.* **2010**, *82*, 2996−3001.
(94) dos Santos, E. J.; Herrmann, A. B.; dos Santos, A. B.; Baika, L. M.; Sato, C. S.; Tormen, L.; Sturgeon, R. E.; Curtius, A. J. *J. Anal. At. Spectrom.* **2010**, *25*, 1627−1632.
(95) Lopez-Molinero, A.; Sipiera, D.; Castillo, J. R. *J. Anal. At. Spectrom.* **2011**, *26*, 1841−1848.
(96) Zhu, Z.; He, Q.; Shuai, Q.; Zheng, H.; Hu, S. *J. Anal. At. Spectrom.* **2010**, *25*, 1390−1394.
(97) Grindlay, G.; Gras, L.; Montiel, J.; Hernandis, V.; Mora, J. *J. Anal. At. Spectrom.* **2010**, *25*, 519−525.
(98) Young, C. G.; Jones, B. T. *Microchem. J.* **2011**, *98*, 323−327.
(99) Matsumoto, A.; Osaki, S.; Kobata, T.; Hashimoto, B.; Ichihara, H.; Nakahara, T. *Microchem. J.* **2010**, *95*, 85−89.
(100) Amberger, M. A.; Broekaert, J. A. C. *J. Anal. At. Spectrom.* **2010**, *25*, 1308−1315.
(101) Hassler, J.; Barth, P.; Richter, S.; Matschat, R. *J. Anal. At. Spectrom.* **2011**, *26*, 2404−2418.
(102) Lindner, H.; Loper, K. H.; Hahn, D. W.; Niemax, K. *Spectrochim. Acta, Part B* **2011**, *66*, 179−185.
(103) Wienold, J.; Traub, H.; Bresch, H.; Seeger, S.; Recknagel, S.; Kipphardt, H. *Spectrochim. Acta, Part B* **2011**, *66*, 432−438.
(104) Compernolle, S.; Wambeke, D.; De Raedt, I.; Kimpe, K.; Vanhaecke, F. *J. Anal. At. Spectrom.* **2011**, *26*, 1679−1684.
(105) Knápek, J.; Komárek, J.; Novotný, K. *Microchim. Acta* **2010**, *171*, 145−150.
(106) Shao, Y. *Spectrochim. Acta, Part B* **2010**, *65*, 967−972.
(107) Jankowski, K.; Ramsza, A. P.; Reszke, E. *Spectrochim. Acta, Part B* **2011**, *66*, 500−507.
(108) Simon, A.; Anghel, S. D.; Papiu, M.; Dinu, O. *Spectrochim. Acta, Part B* **2010**, *65*, 272−278.
(109) Muñoz, J.; Calzada, M. D. *Spectrochim. Acta, Part B* **2010**, *65*, 1014−1021.
(110) Palomares, J. M.; Iordanova, E.; van Veldhuizen, E. M.; Baede, L.; Gamero, A.; Sola, A.; van der Mullen, J. J. A. M. *Spectrochim. Acta, Part B* **2010**, *65*, 225−233.
(111) Jiménez, M.; Muñoz, J.; Calzada, M. D. *J. Anal. At. Spectrom.* **2011**, *26*, 1863−1867.
(112) Pohl, P.; Jamroz, P. *J. Anal. At. Spectrom.* **2011**, *26*, 1317−1337.
(113) Matusiewicz, H.; Ślachciński, M. *Microchem. J.* **2012**, *102*, 61−67.
(114) Matusiewicz, H.; Ślachciński, M. *J. Anal. At. Spectrom.* **2010**, *25*, 1324−1333.
(115) Zhang, J.; Zhang, G.; Zhao, C.; Quan, X.; Jia, Q. *Microchem. J.* **2012**, *100*, 95−99.
(116) Frentiu, T.; Ponta, M.; Senila, M.; Mihalton, A. I.; Darvasi, E.; Frentiu, M.; Cordos, E. *J. Anal. At. Spectrom.* **2010**, *25*, 739−742.
(117) Stacewicz, T.; Bulska, E.; Ruszczyńska. *Spectrochim. Acta, Part B* **2010**, *65*, 306−310.
(118) Xing, Z.; Kuermaiti, B.; Wang, J.; Han, G.; Zhang, S.; Zhang, X. *Spectrochim. Acta, Part B* **2010**, *65*, 1056−1060.
(119) Wu, Q.; Zhu, Z.; Liu, Z.; Zheng, H.; Hu, S.; Li, L. *J. Anal. At. Spectrom.* **2012**, *27*, 496−500.
(120) Li, W.; Jiang, X.; Xu, K.; Hou, X.; Zheng, C. *Microchem. J.* **2011**, *99*, 114−117.
(121) Krähling, T.; Müller, S.; Meyer, C.; Stark, A. K.; Franzke, J. *J. Anal. At. Spectrom.* **2011**, *26*, 1974−1978.
(122) He, Q.; Zhu, Z.; Hu, S.; Zheng, H.; Jin, L. *Anal. Chem.* **2012**, *84*, 4179−4184.
(123) Vanderwal, R. L.; Fujiyama-Noval, J. H.; Kumar, C.; Das, G. D.; Hariharan, A.; Ward, B. *Appl. Spectrosc.* **2011**, *65*, 1073−1082.
(124) Novosád, L.; Hrdlička, A.; Slavíček; Otruba, V.; Kanický, V. *J. Anal. At. Spectrom.* **2012**, *27*, 305−309.
(125) Weagant, S.; Chen, V.; Karanassios, V. *Anal. Bioanal. Chem.* **2011**, *401*, 2865−2880.
(126) Kadenkin, A.; Broekaert, J. A. C. *J. Anal. At. Spectrom.* **2011**, *26*, 1481−1487.
(127) Frentiu, T.; Petreus, D.; Senila, M.; Mihaltan, A. I.; Darvasi, E.; Ponta, E.; Plaian, E.; Cordos, E. A. *Microchem. J.* **2011**, *97*, 188−195.
(128) Tung, N. H.; Chikae, M.; Ukita, Y.; Viet, P. H.; Takamura, Y. *Anal. Chem.* **2012**, *84*, 1210−1213.
(129) Kitano, A.; Iiduka, A.; Yamamoto, T.; Ukita, Y.; Tamiya, E.; Takamura, Y. *Anal. Chem.* **2011**, *83*, 9424−9430.
(130) Wagie, H. E.; Geissinger, P. *Appl. Spectrosc.* **2012**, *66*, 609−627.
(131) Heywood, M. S.; Taylor, N.; Farnsworth, P. B. *Anal. Chem.* **2011**, *83*, 6493−6499.
(132) Hahn, D. W.; Omenetto, N. *Appl. Spectrosc.* **2010**, *64*, 335A−366A.
(133) Hahn, D. W.; Omenetto, N. *Appl. Spectrosc.* **2012**, *66*, 347−419.
(134) Russo, R. E.; Suen, T. W.; Bolshakov, A. A.; Yoo, J.; Sorkhabi, O.; Mao, X.; Gonzalez, J.; Oropeza, D.; Zorba, V. *J. Anal. At. Spectrom.* **2011**, *26*, 1596−1603.
(135) Mendys, A.; Dzierżęga, K.; Grabiec, M.; Pellerin, S.; Pokrzywka, B.; Travaillé, G.; Bousquet, B. *Spectrochim. Acta, Part B* **2011**, *66*, 691−697.
(136) Kumar, A.; Singh, R. K.; Joshi, H. *Spectrochim. Acta, Part B* **2011**, *66*, 444−450.

(137) Ribière, M.; Chéron, B. G. *Spectrochim. Acta, Part B* **2010**, *65*, 524−532.
(138) Gornushkin, I. G.; Panne, U. *Spectrochim. Acta, Part B* **2010**, *65*, 345−359.
(139) Diwakar, P. K.; Groh, S.; Niemax, K.; Hahn, D. W. *J. Anal. At. Spectrom.* **2010**, *25*, 1921−1930.
(140) Holá, M.; Konečná, V.; Mikuška, P.; Kaiser, J.; Kanický, V. *Spectrochim. Acta, Part B* **2010**, *65*, 51−60.
(141) Lindner, H.; Autrique, D.; Pisonero, J.; Günther, D.; Bogaerts, A. *J. Anal. At. Spectrom.* **2010**, *25*, 295−304.
(142) Werheit, P.; Fricke-Begemann, C.; Gesing, M.; Noll, R. *J. Anal. At. Spectrom.* **2011**, *26*, 2166−2174.
(143) Ruiz, J.; González, A.; Cabalín; Laserna, J. J. *Appl. Spectrosc.* **2010**, *64*, 1342−1349.
(144) Matiaske, A. M.; Gornushkin, I. B.; Panne, U. *Anal. Bioanal. Chem.* **2012**, *402*, 2597−2606.
(145) Kexue, L. I.; Zhou, W.; Shen, Q.; Shao, J.; Qian, H. *Spectrochim. Acta, Part B* **2010**, *65*, 420−424.
(146) Multarie, R. A.; Cremers, D. A.; Dupre, J. M.; Gustafson, J. E. *Appl. Spectrosc.* **2010**, *64*, 750−759.
(147) Abdelhamid, M.; Fortes, F. J.; Harith, M. A.; Laserna, J. J. *J. Anal. At. Spectrom.* **2011**, *26*, 1445−1450.
(148) Latkoczy, C.; Kägi, R.; Fierz, M.; Ritzmann, M.; Günther, D.; Boller, M. *J. Environ. Monit.* **2010**, *12*, 1422−1429.
(149) Dyar, M. D.; Tucker, J. M.; Humphries, S.; Clegg, S. M. *Spectrochim. Acta, Part B* **2011**, *66*, 39−56.
(150) Douglas, D. N.; Crisp, J. L.; Reid, H. J.; Sharp, B. L. *J. Anal. At. Spectrom.* **2011**, *26*, 1294−1301.
(151) Dikshit, V.; Yueh, F. Y.; Singh, J. P.; McIntyre, D. L.; Jain, J. C.; Melikechi, N. *Spectrochim. Acta, Part B* **2012**, *68*, 65−70.
(152) Michel, A. P. M. *Spectrochim. Acta, Part B* **2010**, *65*, 185−191.
(153) Hoehse, M.; Gornushkin, I.; Merk, S.; Panne, U. *J. Anal. At. Spectrom.* **2011**, *26*, 414−424.
(154) Popov, A. M.; Colao, F.; Fantoni, R. *J. Anal. At. Spectrom.* **2010**, *25*, 837−848.
(155) Russo, R. E.; Boĺshakov, A. A.; Mao, X.; McKay, C. P.; Perry, D. L.; Sorkhabi, O. *Spectrochim. Acta, Part B* **2011**, *66*, 99−104.
(156) Cahoon, E. M.; Almirall, J. R. *Anal. Chem.* **2012**, *84*, 2239−2244.
(157) Wagatsuma, K. *Anal. Sci.* **2010**, *26*, 303−309.
(158) Matsuura, M.; Wagatsuma, K. *Anal. Sci.* **2011**, *27*, 231−235.
(159) Zhang, L.; Kashiwakura, S.; Wagatsuma, K. *Spectrochim. Acta, Part B* **2011**, *66*, 785−792.
(160) Zhang, L.; Kashiwakura, S.; Wagatsuma, K. *Spectrochim. Acta, Part B* **2012**, *67*, 24−31.
(161) Weinstein, V.; Steers, E. B. M.; Smid, P.; Pickering, J. C.; Mushtaq, S. *J. Anal. At. Spectrom.* **2010**, *25*, 1283−1289.
(162) Mushtaq, S.; Steers, E. B. M.; Pickering, J. C.; Gusarov, T.; Smid, P.; Weinstein, V. *J. Anal. At. Spectrom.* **2011**, *26*, 766−775.
(163) Mushtaq, S.; Pickering, J. C.; Steers, E. B. M.; Horvath, P.; Whitby, J. A.; Michler, J. *J. Anal. At. Spectrom.* **2011**, *26*, 1746−1755.
(164) Mushtaq, S.; Steers, E. B. M.; Pickering, J. C.; Weinstein, V. *J. Anal. At. Spectrom.* **2012**, *27*, 1264−1273.
(165) Korolov, I.; Bano, G.; Donko, Z.; Derzsi, A.; Hartmann, P. *J. Chem. Phys.* **2011**, *134*, 064308/1−6.
(166) Korolov, I.; Bano, G.; Donko, Z. *Spectrochim. Acta, Part B* **2011**, *66*, 706−711.
(167) Simon, P.; Bogaerts, A. *J. Anal. At. Spectrom.* **2011**, *26*, 804−810.
(168) Derzsi, A.; Donko, Z. *J. Anal. At. Spectrom.* **2011**, *26*, 792−797.
(169) Voronov, M.; Smid, P.; Hoffmann, V.; Hofmann, Th.; Venzago, C. *J. Anal. At. Spectrom.* **2010**, *25*, 511−518.
(170) Voronov, M.; Hoffmann, V.; Buscher, W.; Engelhard, C.; Ray, S. J.; Hieftje, G. M. *J. Anal. At. Spectrom.* **2011**, *26*, 811−815.
(171) Voronov, M.; Hoffmann, V.; Buscher, W.; Engelhard, C.; Ray, S. J.; Hieftje, G. M. *J. Anal. At. Spectrom.* **2012**, *27*, 1225−1233.
(172) Efimova, V.; Derzsi, A.; Zlotorowicz, A.; Hoffmann, V.; Donko, Z.; Eckert, J. *Spectrochim. Acta, Part B* **2010**, *65*, 311−315.
(173) Lotito, G.; Nelis, T.; Guillot, Ph.; Günther, D. *Spectrochim. Acta, Part B* **2011**, *66*, 619−626.
(174) Fliegel, D.; Günther, D. *J. Anal. At. Spectrom.* **2011**, *26*, 2052−2057.
(175) Yan, X.; Lin, Y.; Huang, R.; Hang, W.; Harrison, W. W. *J. Anal. At. Spectrom.* **2010**, *25*, 534−543.
(176) Alberts, D.; Horvath, R.; Nelis, Th.; Pereiro, R.; Bordel, N.; Michler, J.; Sanz-Medel, A *Spectrochim. Acta, Part B* **2010**, *65*, 533−541.
(177) Valledor, R.; Pisonero, J.; Nelis, Th.; Bordel, N. *Spectrochim. Acta, Part B* **2012**, *68*, 24−33.
(178) Efimova, V.; Hoffmann, V.; Eckert, J. *J. Anal. At. Spectrom.* **2011**, *26*, 784−791.
(179) DeJesus, M. R.; Gu, G.; King, F. L.; Barnes, J. H., IV; Lewis, C. L. *J. Anal. At. Spectrom.* **2011**, *26*, 2206−2215.
(180) Rubinshtein, A. A.; Schilling, G. D.; Ray, S. J.; Sperline, P. P.; Denton, M. B.; Barinaga, Ch. J.; Koppenaal, D. W.; Hieftje, G. M. *J. Anal. At. Spectrom.* **2010**, *25*, 735−738.
(181) Churchill, G.; Putyera, K.; Weinstein, V.; Wang, X.; Steers, E. B. M. *J. Anal. At. Spectrom.* **2011**, *26*, 2263−2273.
(182) Wagatsuma, K.; Urushibata, S. *Microchem. J.* **2010**, *95*, 107−112.
(183) Gusarova, T.; Hofmann, T.; Kipphardt, H.; Vernzago, C.; Matschat, R.; Panne, U. *J. Anal. At. Spectrom.* **2010**, *25*, 314−321.
(184) Gusarova, T.; Methven, B.; Kipphardt, H.; Sturgeon, R.; Matschat, R.; Panne, U. *Spectrochim. Acta, Part B* **2011**, *66*, 847−854.
(185) Di Sabatino, M.; Dons, A. L.; Hinrichs, J.; Arnberg, L. *Spectrochim. Acta, Part B* **2011**, *66*, 144−148.
(186) Weyler, S.; Bengtson, A. *J. Anal. At. Spectrom.* **2010**, *25*, 849−855.
(187) Engelhard, C.; Ray, S. J.; Buscher, W.; Hoffmann, V.; Hieftje, G. M. *J. Anal. At. Spectrom.* **2010**, *25*, 1874−1881.
(188) Gamez, G.; Frey, D.; Michler, J. *J. Anal. At. Spectrom.* **2012**, *27*, 50−55.
(189) Voronov, M.; Hoffmann, V.; Wallendorf, T.; Marke, S.; Mönch, J.; Engelhard, C.; Buscher, W.; Ray, S. J.; Hieftje, G. M. *J. Anal. At. Spectrom.* **2012**, *27*, 419−425.
(190) Gamez, G.; Voronov, M.; Ray, S. J.; Hoffmann, V.; Hieftje, G. M.; Michler, J. *Spectrochim. Acta, Part B* **2012**, *70*, 1−9.
(191) Fernandez, B.; Costa, J. M.; Pereiro, R.; Sanz-Medel, A. *Anal. Bioanal. Chem.* **2010**, *396*, 15−29.
(192) Fernandez, B.; Pereiro, R.; Sanz-Medel, A. *Anal. Chim. Acta* **2010**, *679*, 7−16.
(193) Pereiro, R.; Sola-Vazquez, A.; Lobo, L.; Pisonero, J.; Bordel, N.; Costa, J. M.; Sanz-Medel, A. *Spectrochim. Acta, Part B* **2011**, *66*, 399−412.
(194) Gonzalez Gago, C.; Pisonero, J.; Pereiro, R.; Bordel, N.; Mazon Ramos, P.; Sanz-Medel, A. *J. Anal. At. Spectrom.* **2010**, *25*, 1612−1617.
(195) Lobo, L.; Bordel, N.; Pereiro, R.; Tempez, A.; Chapon, P.; Sanz-Medel, A. *J. Anal. At. Spectrom.* **2011**, *26*, 798−803.
(196) Valledor, R.; Pisonero, J.; Bordel, N.; Martin, J. I.; Quiros, C.; Tempez, A.; Sanz-Medel, A. *Anal. Bioanal. Chem.* **3010**, *396*, 2881−2887.
(197) Lobo, L.; Fernandez, B.; Pereiro, R.; Bordel, N.; Demenev, E.; Giubertoni, D.; Bersani, M.; Hönicke, P.; Beckhoff, B.; Sanz-Medel, A. *J. Anal. At. Spectrom.* **2011**, *26*, 542−549.
(198) Pisonero, J.; Licciardello, A.; Hierro-Rodriguez, A.; Quiros, C.; Sanz-Medel, A.; Bordel, N. *J. Anal. At. Spectrom.* **2011**, *26*, 1604−1609.
(199) Bustelo, M.; Fernandez, B.; Pisonero, J.; Pereiro, R.; Bordel, N.; Vega, V.; Pridan, V. M.; Sanz-Medel, A. *Anal. Chem.* **2011**, *83*, 329−337.
(200) Pisonero, J.; Valledor, R.; Licciardello, A.; Quiros, C.; Martin, J. I.; Sanz-Medel, A.; Bordel, N. *Anal. Bioanal. Chem.* **2012**, *403*, 2437−2448.
(201) Lobo, L.; Tuccitto, N.; Bordel, N.; Pereiro, R.; Pisonero, J.; Licciardello, A.; Tempez, A.; Chapon, P.; Sanz-Medel, A. *Anal. Bioanal. Chem.* **2010**, *396*, 2863−2869.
(202) Gonzalez de Vega, C.; Lobo, L.; Fernandez, B.; Bordel, N.; Pereiro, P.; Sanz-Medel, A. *J. Anal. At. Spectrom.* **2012**, *27*, 318−326.
(203) Sola-Vazquez, A.; Costa-Fernandez, J. M.; Pereiro, R.; Sanz-Medel, A. *Anal. Bioanal. Chem.* **2011**, *401*, 2771−2777.
(204) Compernolle, S.; Pisonero, J.; Bordel, N.; Wambeke, D.; De Raedt, I.; Kimpe, K.; Sanz-Medel, A.; Vanhaecke, F. *Anal. Chim. Acta* **2011**, *701*, 129−133.

(205) Sanchez, P.; Alberts, D.; Fernandez, B.; Menendez, A.; Pereiro, R.; Sanz-Medel, A. *J. Anal. At. Spectrom.* **2012**, *27*, 71−79.
(206) Sanchez, P.; Fernandez, B.; Menendez, A.; Pereiro, R.; Sanz-Medel, A. *J. Anal. At. Spectrom.* **2010**, *25*, 370−377.
(207) Sanchez, P.; Alberts, D.; Fernandez, B.; Menendez, A.; Pereiro, R.; Sanz-Medel, A. *Anal. Chim. Acta* **2012**, *714*, 1−7.
(208) Sanchez, P.; Fernandez, B.; Menendez, A.; Orejas, J.; Pereiro, R.; Sanz-Medel, A. *Anal. Chim. Acta* **2011**, *684*, 47−53.
(209) Alberts, D.; Fernandez, B.; Pereiro, R.; Sanz-Medel, A. *J. Anal. At. Spectrom.* **2011**, *26*, 776−783.
(210) Alberts, D.; Vega, V.; Pereiro, R.; Bordel, N.; Prida, V. M.; Bengtson, A.; Sanz-Medel, A. *Anal. Bioanal. Chem.* **2010**, *396*, 2833−2840.
(211) Alberts, D.; Therese, L.; Guillot, P.; Pereiro, R.; Sanz-Medel, A.; Belenger, P.; Ganciu, M. *J. Anal. At. Spectrom.* **2010**, *25*, 1247−1252.
(212) Valledor, R.; Pisonero, J.; Nelis, T.; Bordel, N. *J. Anal. At. Spectrom.* **2011**, *26*, 758−765.
(213) Canulescu, S.; Molchan, I. S.; Tauziede, C.; Tempez, A.; Whitby, J. A.; Thompson, G. E.; Skeldon, P.; Chapon, P.; Michler, J. *Anal. Bioanal. Chem.* **2010**, *396*, 2871−2879.
(214) Gu, G.; DeJesus, M.; King, F. L. *J. Anal. At. Spectrom.* **2011**, *26*, 816−821.
(215) Galindo, R. E.; Gago, R.; Duday, D.; Palacio, C. *Anal. Bioanal. Chem.* **2010**, *396*, 2725−2740.
(216) Schmitt, S. W.; Gamez, G.; Sivakov, V.; Schubert, M.; Christiansen, S. H.; Michler, J. *J. Anal. At. Spectrom.* **2011**, *26*, 822−827.
(217) Hoffmann, V.; Steinert, M.; Acker, J. *J. Anal. At. Spectrom.* **2011**, *26*, 1990−1996.
(218) Chen, H.-L.; Li, N.; Klostermeier, A.; Schmid-Fetzer, R. *J. Anal. At. Spectrom.* **2011**, *26*, 2189−2196.
(219) Gielniak, B.; Fiedler, T.; Broekaert, J. A. C. *Spectrochim. Acta, Part B* **2011**, *66*, 21−27.
(220) Olenici-Craciunescu, S. B.; Müller, S.; Michels, A.; Horvatic, V.; Vadla, C.; Franzke, J. *Spectrochim. Acta, Part B* **2011**, *66*, 268−273.
(221) Mezei, P.; Cserfalvi, T.; Hartmann, P.; Bencs, L. *Spectrochim. Acta, Part B* **2010**, *65*, 218−224.
(222) Shekhar, R.; Karunasagar, D.; Dash, K.; Ranjit, M. *J. Anal. At. Spectrom.* **2010**, *25*, 875−879.
(223) Jamroz, P.; Pohl, P.; Zyrnicki, W. *J. Anal. At. Spectrom.* **2012**, *27*, 1032−1037.
(224) Tombrink, S.; Mueller, S.; Heming, R.; Michels, A.; Lampen, P.; Franzke, J. *Anal. Bioanal. Chem.* **2010**, *397*, 2917−2922.
(225) Quarles, C. D., Jr.; Niemann, S.; Marcus, R. K. *J. Anal. At. Spectrom.* **2010**, *25*, 1780−1786.
(226) Castro, J.; Krishna, M. V. B.; Choiniere, J. R.; Marcus, R. K. *Anal. Bioanal. Chem.* **2010**, *397*, 1259−1271.
(227) Marcus, R. K.; Quarles, C. D., Jr.; Barringa, C. J.; Carado, A. J.; Koppenaal, D. W. *Anal. Chem.* **2011**, *83*, 2425−2429.
(228) Quarles, C. D., Jr.; Carado, A. J.; Barringa, C. J.; Koppenaal, D. W.; Marcus, R. K. *Anal. Bioanal. Chem.* **2012**, *402*, 261−268.
(229) Li, W.; Zheng, C.; Fan, G.; Tang, L.; Xu, K.; Lv, Y.; Hou, X. *Anal. Chem.* **2010**, *83*, 5050−5055.
(230) Meyer, C.; Heming, R.; Gurevich, E. L.; Marggraf, U.; Okruss, M.; Florek, S.; Franzke, J. *J. Anal. At. Spectrom.* **2011**, *26*, 505−510.
(231) Meyer, C.; Demecz, D.; Gurevich, E. L.; Marggraf, U.; Jestel, G.; Franzke, J. *J. Anal. At. Spectrom.* **2012**, *27*, 677−681.
(232) Shelley, J. T.; Hieftje, G. M. *J. Anal. At. Spectrom.* **2011**, *26*, 2153−2159.
(233) Shelley, J. T.; Hieftje, G. M. *J. Anal. At. Spectrom.* **2010**, *25*, 345−350.
(234) Kratzer, J.; Mester, Z.; Sturgeon, R. E. *Spectrochim. Acta, Part B* **2011**, *66*, 594−603.
(235) Chen, G. C.-I.; Shelley, J. T.; Jackson, A. U.; Wiley, J. S.; Engelhard, C.; Cooks, R. G.; Hieftje, G. M. *J. Anal. At. Spectrom.* **2011**, *26*, 1434−1444.
(236) Xing, Z.; Wang, J. A.; Han, G. J.; Kuermaiti, B.; Zhang, S. C.; Zhang, X. R. *Anal. Chem.* **2010**, *82*, 5872−5877.
(237) Carado, A. J.; Quarles, C. D., Jr.; Duffin, A. M.; Barringa, C. J.; Russo, R. E.; Marcus, R. K.; Eiden, G. C.; Koppenaal, D. W. *J. Anal. At. Spectrom.* **2012**, *27*, 385−389.
(238) Tarik, M.; Günther, D. *J. Anal. At. Spectrom.* **2010**, *25*, 1416−1423.
(239) Lotito, G.; Günther, D. *Anal. Bioanal. Chem.* **2012**, *402*, 2565−2576.
(240) Beauchemin, D. *Anal. Chem.* **2010**, *82*, 4786−4810.
(241) Engelhard, C. *Anal. Bioanal. Chem.* **2011**, *399*, 213−219.
(242) Jakubowski, N.; Prohaska, T.; Rottmann, L.; Vanhaecke, F. *J. Anal. At. Spectrom.* **2011**, *26*, 693−726.
(243) Jakubowski, N.; Prohaska, T.; Vanhaecke, F.; Roos, P. H.; Lindemann, T. *J. Anal. At. Spectrom.* **2011**, *26*, 727−757.
(244) Beauchemin, D. *Mass Spectrom. Rev.* **2010**, *29*, 560−592.
(245) Pröfrock, D.; Prange, A. *Appl. Spectrosc.* **2012**, *66*, 843−868.
(246) Agatemor, C.; Beauchemin, D. *Anal. Chim. Acta* **2011**, *706*, 66−83.
(247) Balcaen, L.; Moens, L.; Vanhaecke, F. *Spectrochim. Acta, Part B* **2010**, *65*, 769−786.
(248) Rodriguez-Gonzalez, P.; Epov, V. N.; Pecheyran, C.; Amouroux, D.; Donard, O. F. X. *Mass Spectrom. Rev.* **2012**, *31*, 504−521.
(249) Easter, R. N.; Caruso, J. A.; Vonderheide, A. P. *J. Anal. At. Spectrom.* **2010**, *25*, 493−502.
(250) Haider, S. R.; Sharp, B. L.; Reid, H. J. *TrAC, Trends Anal. Chem.* **2011**, *30*, 1793−1808.
(251) Bettmer, J. *Anal. Bioanal. Chem.* **2010**, *397*, 3495−3502.
(252) McIntyre, S. M.; Ferguson, J. W.; Houk, R. S. *Spectrochim. Acta, Part B* **2011**, *66*, 581−587.
(253) McIntyre, S. M.; Ferguson, J. W.; Witte, T. M.; Houk, R. S. *Spectrochim. Acta, Part B* **2011**, *66*, 248−254.
(254) Witte, T. M.; Houk, R. S. *Spectrochim. Acta, Part B* **2012**, *69*, 25−31.
(255) Witte, T. M.; Houk, R. S. *Spectrochim. Acta, Part B* **2012**, *69*, 9−19.
(256) Taylor, N.; Farnsworth, P. B. *Spectrochim. Acta, Part B* **2012**, *69*, 2−8.
(257) Aghaei, M.; Lindner, H.; Bogaerts, A. *J. Anal. At. Spectrom.* **2012**, *27*, 604−610.
(258) Agatemor, C.; Beauchemin, D. *Spectrochim. Acta, Part B* **2011**, *66*, 1−11.
(259) Gackle, M.; Merten, D. *Spectrochim. Acta, Part B* **2010**, *65*, 991−1001.
(260) Geertsen, V.; Lemaitre, P.; Tabarant, M.; Chartier, F. *J. Anal. At. Spectrom.* **2012**, *27*, 146−158.
(261) Paredes, E.; Bosque, J.; Mermet, J. M.; Todoli, J. L. *Spectrochim. Acta, Part B* **2010**, *65*, 908−917.
(262) Asogan, D.; Sharp, B. L.; O'Connor, C. J. P.; Green, D. A.; Wilkins, J. *J. Anal. At. Spectrom.* **2011**, *26*, 631−634.
(263) Frick, D. A.; Günther, D. *J. Anal. At. Spectrom.* **2012**, *27*, 1294−1303.
(264) Olesik, J. W.; Gray, P. J. *J. Anal. At. Spectrom.* **2012**, *27*, 1143−1155.
(265) Flamigni, L.; Koch, J.; Wiltsche, H.; Brogioli, R.; Gschwind, S.; Günther, D. *J. Anal. At. Spectrom.* **2012**, *27*, 619−625.
(266) Graham, A. W. G.; Ray, S. J.; Enke, C. G.; Barinaga, C. J.; Koppenaal, D. W.; Hieftje, G. M. *J. Am. Soc. Mass Spectrom.* **2011**, *22*, 110−117.
(267) Graham, A. W. G.; Ray, S. J.; Enke, C. G.; Felton, J. A.; Carado, A. J.; Barinaga, C. J.; Koppenaal, D. W.; Hieftje, G. M. *Anal. Chem.* **2011**, *83*, 8552−8559.
(268) Fernandez, S. D.; Sugishama, N.; Encinar, J. R.; Sanz-Medel, A. *Anal. Chem.* **2012**, *84*, 5851−5857.
(269) Rappel, C.; Schaumloffel, D. *J. Anal. At. Spectrom.* **2010**, *25*, 1963−1968.
(270) Orlandini, v.; Niessen, J. O.; Petersen, J. H.; Schaper, J. N.; Bings, N. H. *J. Anal. At. Spectrom.* **2012**, *27*, 1234−1244.
(271) Foltynova, P.; Kanicky, V.; Preisler, J. *Anal. Chem.* **2012**, *84*, 2268−2274.

(272) Popp, M.; Hann, S.; Koellensperger, G. *Anal. Chim. Acta* **2010**, *668*, 114−129.
(273) Mesko, M. F.; Hartwig, C. A.; Bizzi, C. A.; Pereira, J. S. F.; Mello, P. A.; Flores, E. M. M. *Int. J. Mass Spectrom.* **2011**, *307*, 123−136.
(274) Sola-Vazquez, A.; Costa-Fernandez, J. M.; Pereiro, R.; Sanz-Medel, A. *Analyst* **2011**, *136*, 246−256.
(275) Dressler, V. L.; Antes, F. G.; Moreira, C. M.; Pozebon, D.; Duarte, F. A. *Int. J. Mass Spectrom.* **2011**, *307*, 149−162.
(276) Horner, N. S.; Beauchemin, D. *Anal. Chim. Acta* **2012**, *717*, 1−6.
(277) Ito, K.; Palmer, C. D.; Steuerwald, A. J.; Parsons, P. J. *J. Anal. At. Spectrom.* **2010**, *25*, 1334−1342.
(278) Garcia-Sartal, C.; Taebunpakul, S.; Stokes, E.; Barciela-Alonso, M. D.; Bermejo-Barrera, P.; Goenaga-Infante, H. *Anal. Bioanal. Chem.* **2012**, *402*, 3359−3369.
(279) Xing, L. Y.; Beauchemin, D. *J. Anal. At. Spectrom.* **2011**, *26*, 2006−2011.
(280) Albert, A.; Brauckmann, C.; Blaske, F.; Sperling, M.; Engelhard, C.; Karst, U. *J. Anal. At. Spectrom.* **2012**, *27*, 975−981.
(281) Raju, C. S. K.; Cossmer, A.; Scharf, H.; Panne, U.; Luck, D. *J. Anal. At. Spectrom.* **2010**, *25*, 55−61.
(282) Jia, X. Y.; Han, Y.; Wei, C.; Duan, T. C.; Chen, H. T. *J. Anal. At. Spectrom.* **2011**, *26*, 1380−1386.
(283) Falta, T.; Heffeter, P.; Mohamed, A.; Berger, W.; Hann, S.; Koellensperger, G. *J. Anal. At. Spectrom.* **2011**, *26*, 109−115.
(284) Caumette, G.; Lienemann, C. P.; Merdrignac, I.; Bouyssiere, B.; Lobinski, R. *J. Anal. At. Spectrom.* **2010**, *25*, 1123−1129.
(285) Bierla, K.; Riu, A.; Debrauwer, L.; Zalko, D.; Bouyssiere, B.; Szpunar, J. *J. Anal. At. Spectrom.* **2010**, *25*, 889−892.
(286) Meermann, B.; Bockx, M.; Laenen, A.; Van Looveren, C.; Cuyckens, F.; Vanhaecke, F. *Anal. Bioanal. Chem.* **2012**, *402*, 439−448.
(287) Meermann, B.; Hulstaert, A.; Laenen, A.; Van Looveren, C.; Vliegen, M.; Cuyckens, F.; Vanhaecke, F. *Anal. Chem.* **2012**, *84*, 2395−2401.
(288) Kundel, M.; Thorenz, U. R.; Petersen, J. H.; Huang, R. J.; Bings, N. H.; Hoffmann, T. *Anal. Bioanal. Chem.* **2012**, *402*, 3345−3357.
(289) Martinez-Sierra, J. G.; Sanz, F. M.; Espilez, P. H.; Santamaria-Fernandez, R.; Gayon, J. M. M.; Alonso, J. I. G. *J. Anal. At. Spectrom.* **2010**, *25*, 989−997.
(290) Gammelgaard, B.; Sturup, S.; Christensen, M. V. *Metallomics* **2012**, *4*, 149−155.
(291) Wang, M.; Feng, W. Y.; Zhao, Y. L.; Chai, Z. F. *Mass Spectrom. Rev.* **2010**, *29*, 326−348.
(292) Esteban-Fernandez, D.; Ahrends, R.; Linscheid, M. W. *J. Mass Spectrom.* **2012**, *47*, 760−768.
(293) Sanz-Medel, A. *Anal. Bioanal. Chem.* **2010**, *398*, 1853−1859.
(294) Tholey, A.; Schaumloffel, D. *TrAC, Trends Anal. Chem.* **2010**, *29*, 399−408.
(295) Grebe, M.; Profrock, D.; Kakuschke, A.; Busto, M. E. D.; Montes-Bayon, M.; Sanz-Medel, A.; Broekaert, J. A. C.; Prange, A. *J. Anal. At. Spectrom.* **2012**, *27*, 440−448.
(296) Hann, S.; Falta, T.; Boeck, K.; Sulyok, M.; Koellensperger, G. *J. Anal. At. Spectrom.* **2010**, *25*, 861−866.
(297) Crotti, S.; Granzotto, C.; Cairns, W. R. L.; Cescon, P.; Barbante, C. *J. Mass Spectrom.* **2011**, *46*, 1297−1303.
(298) Jimenez, M. S.; Gomez, M. T.; Bolea, E.; Laborda, F.; Castillo, J. *Int. J. Mass Spectrom.* **2011**, *307*, 99−104.
(299) Helfrich, A.; Bettmer, J. *Int. J. Mass Spectrom.* **2011**, *307*, 92−98.
(300) Dubascoux, S.; Le Hecho, I.; Hassellov, M.; Von der Kammer, F.; Gautier, M. P.; Lespes, G. *J. Anal. At. Spectrom.* **2010**, *25*, 613−623.
(301) Schmidt, B.; Loeschner, K.; Hadrup, N.; Mortensen, A.; Sloth, J. J.; Koch, C. B.; Larsen, E. H. *Anal. Chem.* **2011**, *83*, 2461−2468.
(302) Nischwitz, V.; Goenaga-Infante, H. *J. Anal. At. Spectrom.* **2012**, *27*, 1084−1092.
(303) Mitrano, D. M.; Barber, A.; Bednar, A.; Westerhoff, P.; Higgins, C. P.; Ranville, J. F. *J. Anal. At. Spectrom.* **2012**, *27*, 1131−1142.
(304) Tiede, K.; Boxall, A. B. A.; Wang, X. M.; Gore, D.; Tiede, D.; Baxter, M.; David, H.; Tear, S. P.; Lewis, J. *J. Anal. At. Spectrom.* **2010**, *25*, 1149−1154.
(305) Pergantis, S. A.; Jones-Lepp, T. L.; Heithmar, E. M. *Anal. Chem.* **2012**, *84*, 6454−6462.
(306) Tuoriniemi, J.; Cornelis, G.; Hassellov, M. *Anal. Chem.* **2012**, *84*, 3965−3972.
(307) Reed, R. B.; Higgins, C. P.; Westerhoff, P.; Tadjiki, S.; Ranville, J. F. *J. Anal. At. Spectrom.* **2012**, *27*, 1093−1100.
(308) Gschwind, S.; Flamigni, L.; Koch, J.; Borovinskaya, O.; Groh, S.; Niemax, K.; Günther, D. *J. Anal. At. Spectrom.* **2011**, *26*, 1166−1174.
(309) Franze, B.; Strenge, I.; Engelhard, C. *J. Anal. At. Spectrom.* **2012**, *27*, 1074−1083.
(310) Kapellios, E. A.; Pergantis, S. A. *J. Anal. At. Spectrom.* **2012**, *27*, 21−24.
(311) Koch, J.; Günther, D. *Appl. Spectrosc.* **2011**, *65*, 155a−162a.
(312) Resano, M.; Garcia-Ruiz, E.; Vanhaecke, F. *Mass Spectrom. Rev.* **2010**, *29*, 55−78.
(313) Wiltsche, H.; Günther, D. *Anal. Bioanal. Chem.* **2011**, *399*, 2167−2174.
(314) Vanhaecke, F.; Resano, M.; Koch, J.; McIntosh, K.; Günther, D. *J. Anal. At. Spectrom.* **2010**, *25*, 1259−1267.
(315) Walle, M.; Koch, J.; Tabersky, D.; Hametner, K.; Zhigadlo, N. D.; Katrych, S.; Karpinski, J.; Günther, D. *J. Anal. At. Spectrom.* **2010**, *25*, 193−195.
(316) Koch, J.; Heiroth, S.; Lippert, T.; Günther, D. *Spectrochim. Acta, Part B* **2010**, *65*, 943−949.
(317) Fliegel, D.; Frei, C.; Fontaine, G.; Hu, Z. C.; Gao, S.; Günther, D. *Analyst* **2011**, *136*, 4925−4934.
(318) Glaus, R.; Kaegi, R.; Krumeich, F.; Günther, D. *Spectrochim. Acta, Part B* **2010**, *65*, 812−822.
(319) Brogioli, R.; Hattendorf, B.; Koch, J.; Wiltsche, H.; Flamigni, L.; Günther, D. *Anal. Bioanal. Chem.* **2011**, *399*, 2201−2209.
(320) Stark, H. J.; Wennrich, R. *Anal. Bioanal. Chem.* **2011**, *399*, 2211−2217.
(321) Traub, H.; Czerwensky, M.; Matschat, R.; Kipphardt, H.; Panne, U. *J. Anal. At. Spectrom.* **2010**, *25*, 690−696.
(322) Compernolle, S.; Wambeke, D.; De Raedt, I.; Vanhaecke, F. *Spectrochim. Acta, Part B* **2012**, *67*, 50−56.
(323) Pugh, J. A. T.; Cox, A. G.; McLeod, C. W.; Bunch, J.; Whitby, B.; Gordon, B.; Kalber, T.; White, E. *J. Anal. At. Spectrom.* **2011**, *26*, 1667−1673.
(324) Fittschen, U. E. A.; Bings, N. H.; Hauschild, S.; Forster, S.; Kiera, A. F.; Karavani, E.; Fromsdorf, A.; Thiele, J. *Anal. Chem.* **2008**, *80*, 1967−1977.
(325) Do, T. M.; Hsieh, H. F.; Chang, W. C.; Chang, E. E.; Wang, C. F. *Spectrochim. Acta, Part B* **2011**, *66*, 610−618.
(326) Kumtabtim, U.; Siripinyanond, A.; Auray-Blais, C.; Ntwari, A.; Becker, J. S. *Int. J. Mass Spectrom.* **2011**, *307*, 174−181.
(327) Kovacs, R.; Nishiguchi, K.; Utani, K.; Günther, D. *J. Anal. At. Spectrom.* **2010**, *25*, 142−147.
(328) Asogan, D.; Sharp, B. L.; O'Connor, C. J. P.; Green, D. A.; Wilkins, J. *J. Anal. At. Spectrom.* **2011**, *26*, 631−634.
(329) Wagner, B.; Jedral, W. *J. Anal. At. Spectrom.* **2011**, *26*, 2058−2063.
(330) Fricker, M. B.; Kutscher, D.; Aeschlimann, B.; Frommer, J.; Dietiker, R.; Bettmer, J.; Günther, D. *Int. J. Mass Spectrom.* **2011**, *307*, 39−45.
(331) Glaus, R.; Koch, J.; Günther, D. *Anal. Chem.* **2012**, *84*, 5358−5364.
(332) Resano, M.; McIntosh, K. S.; Vanhaecke, F. *J. Anal. At. Spectrom.* **2012**, *27*, 165−173.
(333) Bohme, M.; Hohn, P.; Günther, D.; Kniep, R.; Auffermann, G. *J. Anal. At. Spectrom.* **2010**, *25*, 856−860.
(334) Martinez, M.; Arnaudguilhem, C.; Lobinski, R.; Bouyssiere, B.; Caetano, M.; Chirinos, J. *J. Anal. At. Spectrom.* **2012**, *27*, 1007−1011.
(335) Abrego, Z.; Ugarte, A.; Unceta, N.; Fernandez-Isla, A.; Goicolea, M. A.; Barrio, R. J. *Anal. Chem.* **2012**, *84*, 2402−2409.
(336) Kumtabtim, U.; Matusch, A.; Dani, S. U.; Siripinyanond, A.; Becker, J. S. *Int. J. Mass Spectrom.* **2011**, *307*, 185−191.
(337) Becker, J. S. *Int. J. Mass Spectrom.* **2010**, *289*, 65−75.

(338) Becker, J. S.; Zoriy, M.; Matusch, A.; Wu, B.; Salber, D.; Palm, C.; Becker, J. S. *Mass Spectrom. Rev.* **2010**, *29*, 156−175.
(339) Hare, D.; Austin, C.; Doble, P. *Analyst* **2012**, *137*, 1527−1537.
(340) Konz, I.; Fernandez, B.; Fernandez, M. L.; Pereiro, R.; Sanz-Medel, A. *Anal. Bioanal. Chem.* **2012**, *403*, 2113−2125.
(341) Urgast, D. S.; Ou, O.; Gordon, M. J.; Raab, A.; Nixon, G. F.; Kwun, I. S.; Beattie, J. H.; Feldmann, J. *Anal. Bioanal. Chem.* **2012**, *402*, 287−297.
(342) Becker, J. S.; Kumtabtim, U.; Wu, B.; Steinacker, P.; Otto, M.; Matusch, A. *Metallomics* **2012**, *4*, 284−288.
(343) Becker, J. S.; Niehren, S.; Matusch, A.; Wu, B.; Hsieh, H. F.; Kumtabtim, U.; Hamester, M.; Plaschke-Schlutter, A.; Salber, D. *Int. J. Mass Spectrom.* **2010**, *294*, 1−6.
(344) Pugh, J. A. T.; Cox, A. G.; McLeod, C. W.; Bunch, J.; Writer, M. J.; Hart, S. L.; Bienemann, A.; White, E.; Bell, J. *Anal. Bioanal. Chem.* **2012**, *403*, 1641−1649.
(345) Giesen, C.; Waentig, L.; Mairinger, T.; Drescher, D.; Kneipp, J.; Roos, P. H.; Panne, U.; Jakubowski, N. *J. Anal. At. Spectrom.* **2011**, *26*, 2160−2165.
(346) Giesen, C.; Mairinger, T.; Khoury, L.; Waentig, L.; Jakubowski, N.; Panne, U. *Anal. Chem.* **2011**, *83*, 8177−8183.
(347) Gholap, D. S.; Izmer, A.; De Samber, B.; van Elteren, J. T.; Selih, V. S.; Evens, R.; De Schamphelaere, K.; Janssen, C.; Balcaen, L.; Lindemann, I.; Vincze, L.; Vanhaecke, F. *Anal. Chim. Acta* **2010**, *664*, 19−26.
(348) D'Ilio, S.; Violante, N.; Majorani, C.; Petrucci, F. *Anal. Chim. Acta* **2011**, *698*, 6−13.
(349) Donati, G. L.; Amais, R. S.; Nobrega, J. A. *J. Anal. At. Spectrom.* **2011**, *26*, 1827−1832.
(350) Ardini, F.; Soggia, F.; Rugi, F.; Udisti, R.; Grotti, M. *J. Anal. At. Spectrom.* **2010**, *25*, 1588−1597.
(351) Gueguen, F.; Nonell, A.; Granet, M.; Favre, G.; Isnard, H.; Chartier, F. *J. Anal. At. Spectrom.* **2010**, *25*, 201−205.
(352) Gourgiotis, A.; Granet, M.; Isnard, H.; Nonell, A.; Gautier, C.; Stadelmann, G.; Aubert, M.; Durand, D.; Legand, S.; Chartier, F. *J. Anal. At. Spectrom.* **2010**, *25*, 1939−1945.
(353) Tam, T. T. N. N.; Sturup, S.; Ostergaard, J.; Franzen, U.; Gammelgaard, B. *J. Anal. At. Spectrom.* **2011**, *26*, 1466−1473.
(354) Nguyen, T. T. T. N.; Ostergaard, J.; Sturup, S.; Gammelgaard, B. *Anal. Bioanal. Chem.* **2012**, *402*, 2131−2139.
(355) Rogers, D. A.; Ray, S. J.; Hieftje, G. M. *Metallomics* **2010**, *2*, 271−279.
(356) Rogers, D. A.; Ray, S. J.; Hieftje, G. M. *Metallomics* **2010**, *2*, 280−288.
(357) Rogers, D. A.; Ray, S. J.; Hieftje, G. M. *J. Anal. At. Spectrom.* **2010**, *25*, 62−73.
(358) Arnquist, I. J.; Kreschollek, T. E.; Holcombe, J. A. *Spectrochim. Acta, Part B* **2011**, *66*, 255−260.
(359) Husakova, L.; Urbanova, I.; Audrlicka-Vavrusova, L.; Sramkova, J.; Cernohorsky, T.; Bednarikova, M.; Pilarova, L. *Microchim. Acta* **2011**, *173*, 173−181.
(360) Krejcova, A.; Cernohorsky, T.; Pouzar, M. *Int. J. Environ. Anal. Chem.* **2012**, *92*, 620−635.
(361) Santamaria-Fernandez, R. *Anal. Bioanal. Chem.* **2010**, *397*, 973−978.
(362) Pramann, A.; Rienitz, O.; Schiel, D.; Guttler, B. *Int. J. Mass Spectrom.* **2011**, *299*, 78−86.
(363) Yang, L.; Meija, J. *Anal. Chem.* **2010**, *82*, 4188−4193.
(364) Wang, J.; Ren, T. X.; Lu, H.; Zhou, T.; Zhao, M. T. *Int. J. Mass Spectrom.* **2011**, *308*, 65−70.
(365) Yang, L.; Sturgeon, R. E.; Mester, Z.; Meija, J. *Anal. Chem.* **2010**, *82*, 8978−8982.
(366) Malinovsky, D.; Vanhaecke, F. *Anal. Bioanal. Chem.* **2011**, *400*, 1619−1624.
(367) Newman, K. *J. Anal. At. Spectrom.* **2012**, *27*, 63−70.
(368) Barling, J.; Weis, D. *J. Anal. At. Spectrom.* **2012**, *27*, 653−662.
(369) Mason, A. J.; Henderson, G. M. *Int. J. Mass Spectrom.* **2010**, *295*, 26−35.
(370) Pointurier, F.; Hubert, A.; Faure, A. L.; Hemet, P.; Pottin, A. C. *J. Anal. At. Spectrom.* **2011**, *26*, 1474−1480.
(371) Szeles, E.; Varga, Z.; Stefanka, Z. *J. Anal. At. Spectrom.* **2010**, *25*, 1014−1018.
(372) Lindahl, P.; Keith-Roach, M.; Worsfold, P.; Choi, M. S.; Shin, H. S.; Lee, S. H. *Anal. Chim. Acta* **2010**, *671*, 61−69.
(373) Fontaine, G. H.; Hametner, K.; Peretti, A.; Günther, D. *Anal. Bioanal. Chem.* **2010**, *398*, 2915−2928.
(374) Vio, L.; Cretier, G.; Chartier, F.; Geertsen, V.; Gourgiotis, A.; Isnard, H.; Morin, P.; Rocca, J. L. *J. Anal. At. Spectrom.* **2012**, *27*, 850−856.